GOCE Data for Ocean Modelling

Herceg, Matija; Tscherning, Carl Christian ; Knudsen, Per

Publication date:
2012

Document Version
Publisher's PDF, also known as Version of record

GOCE DATA FOR OCEAN MODELLING

MATIJA HERCEG

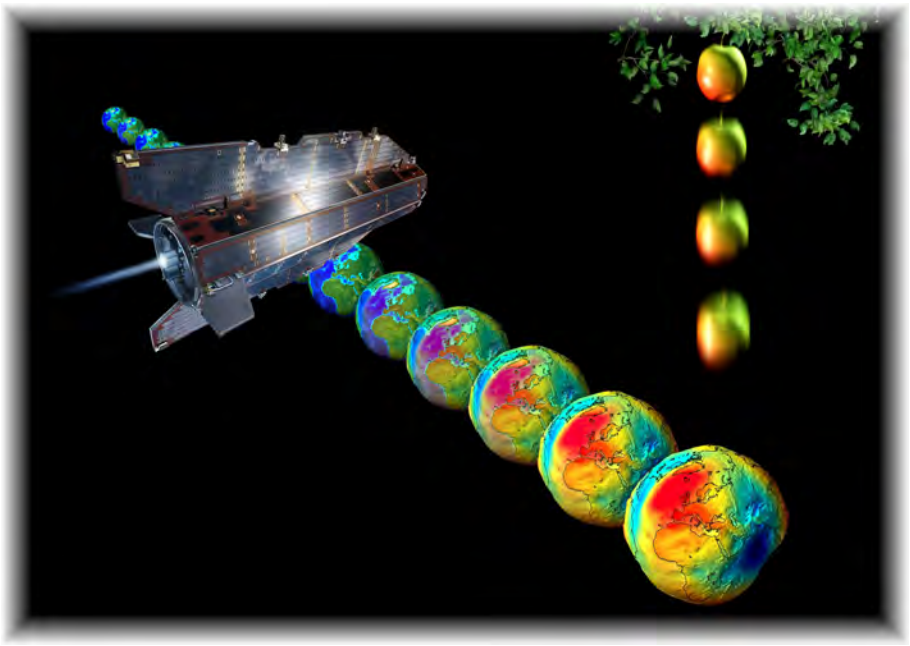

Thesis submitted for the degree of philosophiae doctor

January 31, 2012

DTU Space
National Space Institute

Cover image: Illustration of the GOCE satellite
Credits: ESA-AOES Medialab
From: http://www.esa.int/esaLP/ESA1XK1VMOC_LPgoce_1.html

SUPERVISOR:
Per Knudsen

COSUPERVISOR:
Carl Christian Tscherning

LOCATION:
DTU Space
National Space Institute
Technical University of Denmark
Juliane Maries Vej 30
DK - 2100 Copenhagen
Tel (+45) 3532 5700
Fax (+45) 3536 2475

Matija Herceg: *GOCE data for Ocean Modelling*, PhD thesis, © January 31, 2012

ABSTRACT

As the most advanced gravity space mission to date, The Gravity Field and Steady State Ocean Circulation Explorer (GOCE) mapped global variations in the gravity field with remarkable detail and accuracy. Variations are mapped by observing second order derivatives (gradients) of the Earth gravitational potential. The results are Earth geopotential models and the geoid. An important use of GOCE is in oceanography, where an improved understanding of Earth's gravitational field contributes to an improved description of the ocean circulation.

The GOCE gradients, having a spatially dense data distribution, may potentially provide better predictions of the regional gravity field than those obtained using a spherical harmonic Earth Geopotential Model (EGM). Thus, the success of GOCE is depending on adequate methodologies for extracting the gravity field from its observations as well as on the combination of the gravity field with information from other sources.

The aim of this PhD study is to develop a methodology to improve the use of GOCE gradients and to determine the Earth's gravity field with better accuracy than by using global models, which have been truncated at a specific harmonic degree and order. The method makes use of all available GOCE gradient data in addition to the global models and aims at improving the determination of Earth's gravitational field in regional areas. Subsequently, the calculated equipotential surface, known as the geoid, is used together with measurements of sea surface height in a calculation of the Mean Dynamic Topography (MDT). This reflects the geostrophic ocean currents and leads to a better understanding of ocean mass and heat transfer.

In regional geoid recovery from GOCE gradients, two methods are used, one of them being Least-Squares Collocation (LSC). The second method is developed as a part of this study, and it is based on the reduced point mass responses. Such functions are harmonic and may be used to represent the (anomalous) gravity potential globally or locally.

Since the LSC method requires the solution of as many linear equations as the number of data, GOCE gradient data needs to be thinned prior to applying the method. This is not case for the Reduced Point Mass (RPM), where the number of equations we want to solve depends on the number of point masses. The method is tested in a region in the North Atlantic called the Geoid and Ocean Circulation in the North

Atlantic (GOCINA) area, *i.e.* 58.0N to 70.0N latitude, and $-30.0W$ to 10.0E longitude.

The results show that the RPM method and LSC method gives very similar results, *i.e.* the difference is insignificant when compared to the Earth's Gravitational Model 2008 (EGM2008) results. However, when all the GOCE gradient data are used with the RPM method, an improvement in the gravitational field determination is achieved.

The enhanced geoid by the RPM method is then used for the improvement of the MDT in the GOCINA region. For the validation of the MDT, comparisons with DTU10 MDT, Maximenko MDT and GOCINA project MDT is made.

The results presented here are based on only 18 months of GOCE data, and they show that GOCE data provides better estimation of the MDT and ocean's geostrophic circulation in GOCINA region than any previously obtained using only satellite observations. However, it could not be documented in this study whether the regionally enhanced geoid models by the use of GOCE gradients, in addition to the global models, contribute to a further improvement of the determination of the MDT in the GOCINA area.

RESUMÉ

Formå let med dette ph.d.-studie er at udvikle en metode til at forbedre anvendelsen af GOCE og bestemme jordens tyngdefelt med større nøjagtighed end de globale modeller, som beregnes rutinemæssigt. Metoden gør brug af alle tilgængelige GOCE gradiometer data i tilknytning til de globale modeller og forbedrer bestemmelsen af jordens tyngdefelt i regionale områder. Efterfølgende beregnes equipotentialfladen kaldet geoiden, som anvendes sammen med højdemålinger af havoverfladen i en beregning at den dynamiske havtopografi, som afspejler de geostrofe havestrømme og føre til en bedre forståelse for oceanernes masse- og varmetransport.

I bestemmelsen af de regionale geoidemodeller ud fra GOCE gradiometer data anvendes to metoder, hvoraf den ene er Mindste Kvadraters Kollokation (MKK). Den anden methode er udviklet som en del af dette studie og er baseret på reducerede punktmasse-respons (RPM). Sådanne funktioner kan anvendes til at repræsentere tyngdefeltet både globalt og regionalt. Af beregningsmæssige hensyn kan kun RPM-metoden udnytte alle data-værdier i den pågældende region. Metoden er afprøvet i et område i Nordatlanten kaldet GOCINA-området.

Resultaterne viser, at RPM-metoden sammenlignet med MKK - metoden, giver meget ensartede resultater. Når alle data-værdier anvendes med RPM-metoden opnås en forbedret bestemmelse af tyngdefeltet. Resultaterne af de indledende analyser af havets topografi viser, at GOCE forbedrer bestemmelsen af denne topografi sammenlignet med tidligere modeller af tyngdefeltet. Det kunne ikke dokumenteres i dette studie, hvorvidt de regionalt forbedrede geoidemodeller bidrager til en yderligere forbedring af bestemmelsen af havet topografi i GOCINA-området.

PUBLICATIONS

The research presented here was carried out within the Division of Geodesy, at the Denmark Technical University. Some ideas and figures appeared previously in the following publications:

C.C. Tscherning, M. Veicherts, and M. Herceg: *Reduced point mass or multipole base functions*. In the Honor of Proffessor emeritus Demetrius N. Arbelos, 2010.

Point-mass functions or multipole base-functions are harmonic functions, which may be used to represent the (anomalous) gravity potential T globally or locally. The functions may be expressed by closed expressions or as sums of Legendre series. In both cases at least the two first terms must be removed since they are not present in T. For local applications the effect of a global gravity model is generally removed (and later restored). Then more terms need to be removed or substituted by terms similar to error-degree variances. We have done some calculations to illustrate the effect of reducing the point mass or multipole functions, i.e. showing how the first zero-crossing as a function of spherical distance comes closer to zero when more terms are removed.

Matija Herceg and Per Knudsen: *Full resolution geoid from GOCE gradients for ocean modeling*. ESA Living Symposium proceedings, Bergen, 2010.

The main objective of the study is to improve the methodology for combining GOCE gravity field models with satellite altimetry to derive optimal dynamic ocean topography models for oceanography. Since dynamic ocean topography determination is the difference between the sea surface and the geoid, the definition of both surfaces is of great significance. Here a method for geoid determination, using simulated GOCE gradients and the point mass method, is used for the regional determination of the gravity field that is not recovered by the global GOCE gravity model of spherical harmonic coefficients up to degree and order 200. Comparisons with the GOCINA mean dynamic topography show that the GOCE gradients enhance the determination of the mean dynamic topography at wavelength not recovered by the planned global GOCE gravity field model.

All of old. Nothing else ever.
Ever tried. Ever failed.
No matter.
Try again. Fail again.
Fail better.

— Samuel Beckett

ACKNOWLEDGMENTS

This thesis presents a work that has been done during 39 months of my Ph.D. and it is submitted in fulfillment of the requirements for obtaining a *degree of philosophiae doctor* at the Denmark Technical University. The research presented was carried out within the Division of Geodesy, DTU Space, under supervision of Per Knudsen at DTU Space and C. C. Tscherning at University of Copenhagen.

During, and as a part of the Ph.D. education, I have had the opportunity to to participate in many conferences, meetings and workshops. I appreciate all the experiences that I have gained during my Ph.D. program, and I am happy and proud because I had an opportunity to get to know a lot of nice, smart and inspiring people.

As a part of my Ph.D. I have been working with Dr. Mirko Reguzzoni and professor Fernando Sansò at Politecnico di Milano over a period of about 4 months. The optimal combination of GOCE grids routine that I have developed there has been included in the Space wise processing line of GOCE data. I am very grateful to Mirko and professor Sansò for all the help and knowledge I acquired there.

I am thankful to the two main people behind this thesis, namely my supervisors, Per and Christian, who were always fair and patient.

I am grateful for the help of my friends and colleagues who made my stay in Denmark interesting and pleasant: Yongcun, Olivier, Deniz, Nicolai, Riccardo and my best skydiver friend Stavros. A special thanks goes to Joanna, since she is the reason why this thesis is readable.

Finally, I need to mention my family, because this thesis is theirs as much as it is mine. Even though far away, my father Ljudevit and my mother Snježana were always in some sense with me. And my brother Antun and sisters Iva and Dragica, who were always ready to cheer me up with some jokes that only we can understand.

CONTENTS

I THESIS BACKGROUND 21

1 INTRODUCTION 23
- 1.1 Motivation . . . 23
- 1.2 Objectives . . . 24
- 1.3 Scope of this thesis . . . 25
- 1.4 Outline of this thesis . . . 27

2 GRAVITY AND GEOID 29
- 2.1 The Earth's gravity field . . . 29
- 2.2 Geoid . . . 32
- 2.3 Gravimetry . . . 32
- 2.4 Satellite gradiometry . . . 33
- 2.5 The Earth's gravity models . . . 39

3 GRAVITY FIELD AND STEADY-STATE OCEAN CIRCULATION EXPLORER (GOCE) MISSION 41
- 3.1 Introduction . . . 41
- 3.2 The GOCE products . . . 44
- 3.3 The GOCE applications . . . 48

4 OCEAN MODELLING 51
- 4.1 Satellite altimetry . . . 51
  - 4.1.1 Satellite altimetry principle . . . 51
  - 4.1.2 The repeat track method . . . 53
  - 4.1.3 Satellite altimetry applications . . . 54
- 4.2 Mean sea surface and dynamic topography . . . 55
  - 4.2.1 The geostrophic surface currents . . . 56
  - 4.2.2 Reference ellipsoid, tide system and spectral content . . . 57

II METHODOLOGY 59

5 METHODS USED FOR DATA PROCESSING 61
- 5.1 Least squares collocation . . . 61
- 5.2 Reduced point mass method . . . 62
  - 5.2.1 Closed expressions for gravity gradients when using point masses . . . 65
  - 5.2.2 Expressions for gravity gradients when using reduced point masses . . . 65
  - 5.2.3 Least Squares estimation and regularization . . . 68
- 5.3 Combination of geoid and mean sea surface . . . 69

6 PREPROCESSING AND DATA USAGE 71
- 6.1 Test area; Geoid and Ocean Circulation in the North Atlantic (GOCINA region) . . . 71
- 6.2 GOCINA gravity data . . . 72

6.3 Gravity anomaly and geoid heights from EGM2008 . . 72
6.4 GOCE gravity gradients 73
6.5 Mean see surface data 76
6.6 Mean dynamic topography data 76

III APPLICATION OF METHODS AND VALIDATION 79

7 RESULTS AND ANALYSIS 81
7.1 Truncation of the long wavelength part of the gravity field quantities 82
7.1.1 Gravity anomaly and gravity anomaly residuals derived from different gravitational models . . 84
7.1.2 Geoid height and geoid height anomaly derived from different gravitational models 86
7.1.3 GOCE gradients and gradient anomaly 88
7.2 Empirical covariance function estimation 91
7.3 Collocation results 96
7.3.1 Collocation prediction of gravity anomaly in GOCINA region 96
7.3.2 Collocation prediction of geoid height anomaly in GOCINA region 99
7.4 Reduced point mass results 101
7.4.1 Regularization of reduced point mass solution . 103
7.4.2 Prediction of the gravity gradients using the reduced point mass method 106
7.4.3 Prediction of the gravity anomaly residuals using the reduced point mass method 107
7.4.4 Prediction of the geoid height anomaly using the reduced point mass method 108
7.5 Comparison of the used methods 110
7.6 Enhancing geoid heights with GOCE gradients 117
7.7 Merging enhanced geoid heights with Mean Sea Surface 122
8 CONCLUSIONS AND FUTURE WORK 129
8.1 Conclusions 129
8.2 Implications 130
8.3 Improvements with respect to the existing methods . . 130
8.4 Future work and recommendations 131

IV APPENDIX 133

A EXPRESSIONS FOR THE FIRST AND SECOND ORDER DERIVATIVES OF THE POTENTIAL IN THE LOCAL-NORTH-EAST UP COORDINATE SYSTEM 135
A.1 Transformation between Coordinate systems 135
B PUBLICATIONS 149

BIBLIOGRAPHY 167

LIST OF FIGURES

Figure 1.1 Basic principle of Reduced Point Mass method 25
Figure 1.2 Concept of mean dynamic topography (MDT) calculation from DTU10 mean sea surface (MSS) and EGM2008 geoid [m]. MDT=MSS-geoid . . . 26
Figure 2.1 Gravitational attraction 30
Figure 3.1 GOCE flying 42
Figure 3.2 Notation and location of the 6 accelerometers of the GOCE gradiometer in the Gradiometer Reference Frame (GRF) and with all 6 Accelerometer Reference Frame's (ARF) 42
Figure 3.3 GOCE accelerometer 43
Figure 3.4 GOCE SST and gradiometry principle 43
Figure 3.5 GOCE sensor system 44
Figure 3.6 Error degree variances of GOCE releases compared to EGM2008 as a reference model 47
Figure 3.7 Coefficients error variances (log10 scale) 48
Figure 4.1 Concept of satellite altimetry 52
Figure 4.2 Global sea level has a rise of about 3 millimeters per year since Topex/Poseidon (on the left) began its precise measurement of sea surface height in 1993 and was followed by Jason-1 in 2001. (Credit: University of Colorado) 54
Figure 5.1 Concept of deriving mean dynamic topography (MDT) from geoid and mean sea surface (MSS). GOCINA region MDT, based on DTU10 MSS and EGM2008 geoid [m] 69
Figure 6.1 Gravity anomaly data in the GOCINA region [mgal] 72
Figure 6.2 Global gravity based on the EGM2008 up to degree 2190 [mgal] 72
Figure 6.3 Global geoid height based on the EGM2008 up to degree 2190 [m] 73
Figure 6.4 GOCE T_{zz} gradient component [E] 74
Figure 6.5 Global vertical gradient at mean GOCE altitude (260km), based on the EGM2008 up to degree 2190 [E] 74
Figure 6.6 GOCE T_{zz} dataset with associated errors throughout the mission span 75
Figure 6.7 DTU10 Mean Sea Surface [m] 76
Figure 6.8 DTU10 Mean Dynamic Topography [m] 77
Figure 6.9 GOCINA Mean Dynamic Topography (meters) 77

Figure 6.10 Maximenko Mean Dynamic Topography (meters) 78
Figure 7.1 EGM2008 based global gravity anomaly residuals, when EGM2008 up to harmonic degree and order 100 is subtracted [mGal] 83
Figure 7.2 EGM2008 based global geoid height anomaly, when EGM2008 up to harmonic degree and order 100 is subtracted [m] 83
Figure 7.3 Global T_{zz} GOCE gradient anomalies at flight altitude, when EGM2008 up to harmonic degree and order 100 is subtracted[E] 84
Figure 7.4 Gravity anomaly based on EGM2008 (up to harmonic degree and order 2190), GOCE Direct release 2 (up to harmonic degree and order 240), GOCE Space Wise release 1 (up to harmonic degree and order 210) and GOCE Time Wise release 2 (up to harmonic degree and order 250) global models (up to harmonic degree and order 2190) models 84
Figure 7.5 Geoid heights based on EGM2008 (up to harmonic degree and order 2190), GOCE Direct release 3 (up to harmonic degree and order 240), GOCE Space Wise release 2 (up to harmonic degree and order 210) and GOCE Time Wise release 3 (up to harmonic degree and order 250) global models (up to harmonic 2190) models . . 86
Figure 7.6 Geoid height anomalies when the EGM2008 based geoid up to harmonic degree 100 is subtracted . 87
Figure 7.7 GOCE T_{yy} gradient at satellite altitude (a), GOCE T_{zz} gradient at satellite altitude (219.038 observation) (b) 88
Figure 7.8 GOCE T_{yy} and T_{zz} gradient anomaly when the EGM2008 up to harmonic degree and order 100 is subtracted 90
Figure 7.9 GOCINA observed gravity anomaly residuals (subtracted EGM2008 up to harmonic degree and order 100) 93
Figure 7.10 Empirical covariance estimations based on all gravity anomaly (ground and marine) in the GOCINA region 93
Figure 7.11 Empirical covariance estimations based on just marine gravity anomaly in the GOCINA region 94
Figure 7.12 Empirical covariance estimations based on GOCE T_{zz} gradient anomalies (EGM2008 up to degree and order 100 is subtracted) available in the GOCINA region 94

Figure 7.13 Gravity anomaly residuals based on the EGM2008 [*mGal*](a), predicted gravity anomaly residuals by collocation from selected $0.1^\circ \times 0.2^\circ$ GOCE T_{zz} gradient anomaly [*mGal*] (b) and the difference between the two [*mGal*] (c) 98
Figure 7.14 Geoid height anomaly based on EGM2008 [*mGal*] (a), predicted geoid height anomaly by collocation from selected $0.1^\circ \times 0.2^\circ$ GOCE T_{zz} gradient anomaly [*mGal*] (b) and the difference between the two [*mGal*] (c) 99
Figure 7.15 Function of the different gravity field quantities in respect to the spherical distance ψ: the gravitational potential $[\frac{m^2}{s^2}]$, the gravity anomaly $[\frac{m}{s^2}]$ and the gravity gradients $[\frac{m^2}{s^2}]$. Function shows the quantities when using point masses solution for the closed expression, for the contribution up to harmonic degree and order 100, and for the reduced point masses. 102
Figure 7.16 Regularization tests - prediction of the residual geoid (degree 100 and up) 104
Figure 7.17 Regularization tests - difference between the prediction of the residual geoid (degree 100 and up) and the EGM2008 residual geoid 105
Figure 7.18 T_{zz} gradient anomaly [*E*], where the contribution from the EGM2008 up to harmonic degree and order 100 is subtracted (a), predicted T_{zz} gradient anomaly by reduced point masses from selected $0.1^\circ \times 0.2^\circ$ GOCE T_{zz} gradient anomaly (b) and the difference between the two (c) . . . 106
Figure 7.19 GOCINA gravity anomaly residuals [*mGal*] (contribution from the EGM2008 up to harmonic degree and order 100 is subtracted) (a), predicted GOCINA gravity anomaly residuals by reduced point mass method from selected $0.1^\circ \times 0.2^\circ$ GOCE T_{zz} gradient anomaly (b) and the difference between the two (c) 107
Figure 7.20 GOCINA geoid height anomaly [*m*] (contribution from the EGM2008 up to harmonic degree and order 100 is subtracted) (a), predicted GOCINA geoid height anomaly by reduced point mass method from selected $0.1^\circ \times 0.2^\circ$ GOCE T_{zz} gradient anomaly (b) and the difference between the two (c) 108
Figure 7.21 Comparison between the gravity anomaly residuals [*mgal*] predicted using the LSC and the RPM method 110

Figure 7.22 Comparison between geoid height anomaly [m] predicted using the LSC and the RPM method . . 111
Figure 7.23 Comparison between geoid height anomaly [$mgal$] predicted by collocation (when using selected $0.1° \times 0.2°$ GOCE T_{zz} gradient anomaly), and by reduced point masses (when using all the T_{zz} gradients anomaly available in the GOCINA region) 113
Figure 7.24 Power spectrum of the geoid height anomaly prediction when EGM2008 up to harmonic degree and order 100 is subtracted. The prediction is done by the LSC and the RPM methods with different datasets 115
Figure 7.25 Power spectrum of the difference between geoid height anomaly prediction (when EGM2008 up to harmonic degree and order 100 is subtracted) and EGM2008 based geoid height anomaly. Prediction is done by the LSC and the RPM methods with different datasets used. 116
Figure 7.26 Comparison between geoid height anomalies from complete EGM2008 model, predicted by collocation and predicted reduced point masses. Long wavelength part up to harmonic degree and order 240 (based on GOCE Direct r3) is subtracted 118
Figure 7.27 Power spectrum of the geoid height anomaly residuals, when Direct release 3 up to harmonic degree and order 240 is subtracted 119
Figure 7.28 Power spectrum of the differences between geoid height anomaly residuals based on the EGM2008 and the geoid height anomaly predicted by different methods (when Direct release 3 up to harmonic degree and order 240 is subtracted) . . . 120
Figure 7.29 The enhanced geoid heights by reduced point mass method when the gradient signal higher than harmonic degree and order 240 is used . . 120
Figure 7.30 DTU10 Mean Sea Surface in GOCINA region . 122
Figure 7.31 GOCE Direct enhanced MDT, *i.e.* the difference between the DTU10 Mean Sea Surface and GOCE Direct r3 full geoid enhanced with gradients. The mean of 0.50m is subtracted. 123
Figure 7.32 Different mean dynamic topography in GOCINA region [m]) 124
Figure 7.33 Power spectra of different MDT estimates . . . 125
Figure 7.34 Current speed calculated from different mean dynamic topography in the GOCINA region [$\frac{m}{s}$] 126

Figure A.1 Coordinate systems and basis vectors 136

LIST OF TABLES

Table 3.1 GOCE Geophysical, *i.e.* Level 2, products (Flobergha-gen et al. 2010 [13]) 46
Table 7.1 Statistics of the gravity anomaly [mGal] and the gravity anomaly residuals [mGal] in GOCINA region based on observations and different global models (up to maximum harmonic degree of each model: EGM2008 is 2190, GOCE Direct 3 is 240, GOCE Space wise 2 is 210 and GOCE Time wise 250) 85
Table 7.2 Statistics of the geoid height [m] and the geoid height anomaly [m] in GOCINA region based on observations and different global models (up to maximum harmonic degree of each model: EGM2008 is 2190, GOCE Direct 3 is 240, GOCE Space wise 2 is 210 and GOCE Time wise 250) . 87
Table 7.3 GOCE Tyy and Tzz gradient statistics in the GOCINA region 88
Table 7.4 GOCE T_{yy} and T_{zz} gradient anomaly statistics when the contribution from different models up to harmonic degree and order 100 are subtracted 89
Table 7.5 Parameters for fitting of the covariance functions in GOCINA region using different datasets. The parameters are: scaling factor a, constant in units of $\frac{m}{s^4}$ A, depth of Bjerhammar sphere ($R_E - R_B$) in meters, variance σ^2, and correlation length in degrees 95
Table 7.6 Statistics for prediction of gravity anomaly residuals and geoid height anomaly by collocation . 97
Table 7.7 Statistics on the prediction of gradient anomaly [*E*], gravity anomaly residuals [*mGal*] and geoid height anomaly [*m*] using the reduced point mass method 109
Table 7.8 Statistics of gravity anomaly residuals [*mGal*] and geoid height anomaly [*m*] prediction by RPM and LSC (when selected $0.1° \times 0.2°$ T_{zz} dataset is used), and by RPM (when all T_{zz} gradient anomalies are used) 112

Table 7.9 Gravity anomaly residuals [*mGal*] and geoid height anomaly [*m*] prediction comparison by RPM and LSC (when selected $0.1° \times 0.2°$ GOCE T_{zz} dateset is used), and by RPM (when all T_{zz} gradient anomalies are used) 112
Table 7.10 Gravity anomaly residuals [*mGal*] and geoid height anomaly [*m*] prediction difference by RPM and LSC (when selected $0.1° \times 0.2°$ GOCE T_{zz} dateset is used), and by RPM (when all T_{zz} gradient anomalies are used) 112
Table 7.11 Statistics of the geoid height anomaly prediction by the LSC and RPM method when the GOCE Direct release 3 model up to harmonic degree and order 240 is subtracted 117

ACRONYMS

DIR Direct

DORIS Doppler Orbitography and Radiopositioning Integrated by Satellite

EEF Earth Explorers File Format Standards

EGG-C European GOCE Gravity Consortium

EGM Earth Geopotential Model

EGM2008 Earth's Gravitational Model 2008

ENVISAT Environmental Satellite

ESA European Space Agency

FOS Flight Operations Segment

GOCE The Gravity Field and Steady State Ocean Circulation Explorer

GOCINA Geoid and Ocean Circulation in the North Atlantic

GPS Global Positioning System

GRACE Gravity Recovery and Climate Experiment

GRF Gradiometer Reference Frame

GRS80 Geodetic Reference System 1980

GUT GOCE User Toolbox

HPF High-Level Processing Facility

ICESat Ice, Cloud, and land Elevation Satellite

ICM Interative Combination Method

IRF Inertial Reference Frame

LSC Least-Squares Collocation

MBW Measurement Bandwidth

MDT Mean Dynamic Topography

MSL Mean Sea Level

MSS Mean Sea Surface

NASA National Aeronautics and Space Administration

RPM Reduced Point Mass

RTM Residual Terrain Modeling

SGG Satellite Gravity Gradiometer

SLA Sea Level anomaly

SPW Space-wise

SSH Sea Surface Height

SST Satellite to Satellite Tracking

TIM Time-wise

TRF Terrestrial Reference Frame

XML Extensible Markup Language

Part I

THESIS BACKGROUND

1

INTRODUCTION

This chapter will provide a short introduction to the work done in this thesis, and a motivation for the idea of improving ocean modelling with GOCE gradients.

The aim of this work will be described in the objectives section, followed by the more detailed explanation in the outline section.

1.1 MOTIVATION

As the most advanced gravity space mission to date, GOCE mapped global variations in the gravity field with remarkable detail and accuracy. One of the results are the models of the geoid, *i.e.* the surface of equal gravitational potential defined by the gravity field. This is crucial for deriving accurate measurements of ocean circulation.

GOCE derived data is much needed to understand more about the physical processes occurring inside the Earth and for use in practical applications such as surveying and levelling. Also, GOCE has a broad range of fascinating new possibilities for the fields of oceanography, solid Earth physics, geodesy and sea-level research.

To facilitate the easy use of GOCE products for oceanographers and to support the needs of specific applications, the GOCE User Toolbox (GUT) was developed. Such a toolbox is required to guarantee optimal use of the existing and future gravity data acquired from the Gravity Recovery and Climate Experiment (GRACE) as well as GOCE. The GUT contains software packages that allow the gravity field data, in conjunction and consistency with any other auxiliary data sets, to be pre-processed by users not familiar with gravity field processing procedures, for oceanographic and hydrologic applications both on a regional and global scale.

The success of GOCE is depending on adequate methodologies for extracting the gravity field from its observations and for combining the gravity field, *i.e.* GUT applications, with information from other sources. The aim of this study is to improve the methodology for using GOCE gradients and to possibly extract more signal in local areas than the one produced by GOCE global models. In such a way, improvements in ocean modelling can be made. A better determination of the ocean

mean circulation will advance the understanding of the ocean mass and heat transport role in a climate changes.

1.2 OBJECTIVES

GOCE is the first satellite mission to observes gravity gradients in space; these are primarily to be used for the determination of high precision global gravity field models. The advantage of the GOCE gradients, a dense data distribution, may potentially provide better predictions of the regional gravity field than those obtained using a global spherical harmonic EGM.

Gravity field recovery from GOCE gradient data using Least-Squares Collocation (LSC) in different areas of the Earth was recently investigated by Tscherning and Arabelos 2011 [48] and Yildiz 2011 [61]. This LSC investigation confirm that short wavelength of the gravity field, beyond maximal degree of the global GOCE EGM, is present in the GOCE gradient measurements.

Initially, GOCE spherical harmonic models are combined with high resolution mean sea surface models for deriving global MDT models. Then, GOCE gradient data is used for regional enhancements of the geoid and the MDT.

The main objective of the project is to study how gradients can be used to extract more short wavelength information of the gravity field and to use this enhancement to improve modelling of ocean circulation, *i.e.* MDT in regional area. This is done by development of a method for regional gravity field recovery by using GOCE gradients in addition to the global models. In regional gravity field recovery from GOCE gradients, the LSC method can be used. However, the LSC method requires the solution of as many linear equations as the number of data, so GOCE gradient data needs to be thinned prior to applying the method. To overcome this thinning, a Reduced Point Mass (RPM) method is developed as a part of this study. The RPM is based on the reduced point mass response. Such functions are harmonic and may be used to represent the (anomalous) gravity potential globally or locally. Another advantage of the RPM method is that the computation time is shorter compared to the LSC method. The results presented in this study are based on all available GOCE gradient data in the GOCINA region, *i.e.* 18 months of observations.

The resulting technique can supplement the available collection of tools for the MDT determination, and can be applied to other regions of the world oceans where gravity data of high quality and spatial distribution is not available.

1.3 SCOPE OF THIS THESIS

The scope of this thesis is given in the following section. The main objective of the project is to study how gradients can be used to extract more short wavelength information of the gravity field in local regions. The principle of the method based on the reduced point mass response for the use of the GOCE gradients, is presented on the figure 1.1, where it is shown how each GOCE observations contribute to the solution of the point mass response.

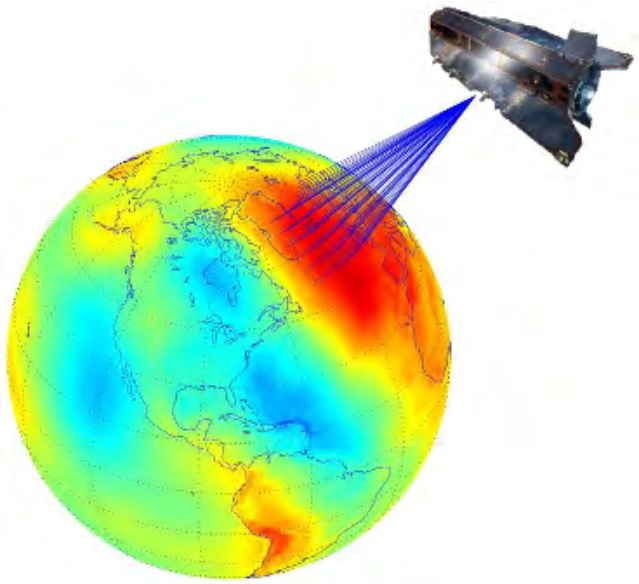

Figure 1.1: Basic principle of Reduced Point Mass method

The Earth anomalous gravity field, at each point is modelled by the set of base functions, obtained as the anomalous gravity potential from each point mass located at the position 20km below the surface of the ellipsoid. The recovered enhanced geoid by the RPM method is then used for the improvement of the MDT in the GOCINA region.

The sea surface does not coincide with a level surface, *i.e.* geoid, of the Earth's gravity field; the deviations are called MDT. The figure 1.2 shows how the MDT is determined. Such a new estimate of the geoid and MDT can then be used for better modelling of the ocean circulation.

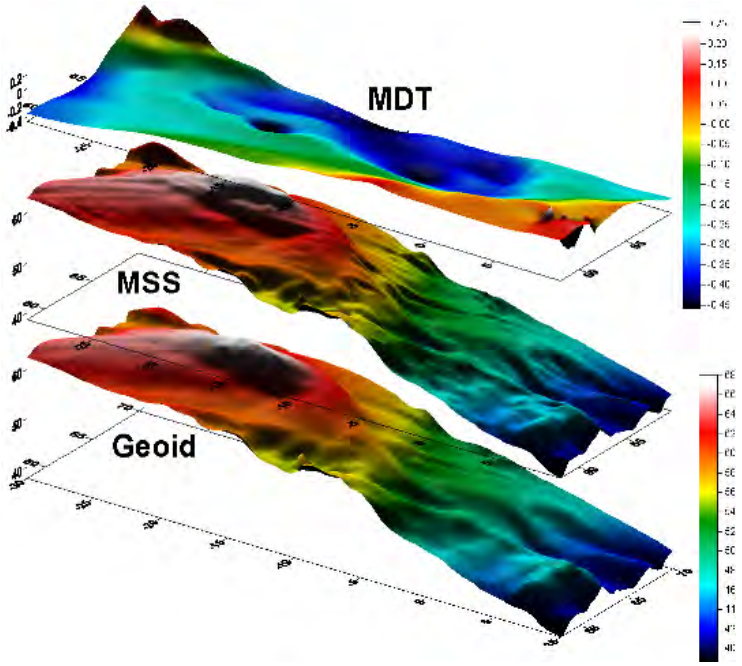

Figure 1.2: Concept of mean dynamic topography (MDT) calculation from DTU10 mean sea surface (MSS) and EGM2008 geoid [m]. MDT=MSS-geoid

1.4 OUTLINE OF THIS THESIS

This thesis structure is based on three main parts: Thesis background, Methodology, and Application of methods and validation. The first part introduces the reader to the motivation behind the idea and to the objectives, which show what needs to be done in order to identify and possibly solve the problem (chapter 1). Chapter 2 provides a short but concise explanation of the fundamental theory of the gravity field, geoid, gravitational potential and its quantities. It also describes the method behind the measurement and provides a representation of the gravitational field of the Earth. Since the main source of the input data used in this thesis is GOCE data, the GOCE mission and its products are also described in this part (chapter 3). Furthermore, chapter 4 explains the theory behind ocean modelling and satellite altimetry.

The second part of the thesis explains the methods and data that are used in the calculations. It presents the development of the RPM method for regional gravity potential determination and its derivatives by using all GOCE gradient data. Chapter 5 explains the LSC and the RPM methods, which is done by referencing the formulas from appendix A. For comparison and validation of the RPM method, the LSC method for regional gravity field modeling from satellite gravity gradiometer is applied. In chapter 6, the test area, *i.e.* the GOCINA region, is introduced.

Gravity data acquired in the GOCINA project is shown because it is used for fitting the empirical covariance function estimation in the test area. The EGM2008 (Pavlis et al. 2008 [36]) up to degree and order 2160 is presented, since it is the reference for all gravity anomaly residuals and geoid height anomalies. Furthermore, filtered GOCE gravity gradients are presented: the global and extracted datasets over the GOCINA region, which contains 237.897 observations for the T_{xx}, T_{yy} and T_{zz} components. In this study, the DTU10 Mean Sea Surface (MSS) was used, which is an update of the DNSC08 MSS model. The DTU10 MSS (Andersen 2011 [1]) is the time averaged ellipsoidal height of the ocean surface computed from a combination of satellite altimetry using a total of 8 different satellite missions. From here, the DTU10 MDT was derived by differencing the DNSC08 MSS and the EGM2008 based geoid.

The third and last part of this thesis shows the work that has been done on modelling the gravity anomalies and geoid heights using the GOCE gravity gradients. Firstly, in chapter 7, the tests are shown where the long wavelength part of gravity field up to harmonic degree and order 100 is subtracted from gravity gradients. Then, modelling of the residual geoid heights when a complete GOCE model up to harmonic degree and order 240 is subtracted from gravity gradients is presented. The recovered residual geoid heights are then used to produce enhanced GOCE based geoid and MDT in GOCINA

region. From the enhanced GOCE based MDT, the current speeds are calculated and analyzed. Following the results and analysis, in chapter 8, the conclusions, implications and the future development ideas are described.

2

GRAVITY AND GEOID

In this chapter, the fundamental theory of the gravity field, geoid, gravitational potential and its quantities are presented. It shows different methods for the measurement and representation of the gravitational potential quantities with the focus on satellite gradiometry.

2.1 THE EARTH'S GRAVITY FIELD

A fundamental Earth-fixed rectangular coordinate system xyz is usually defined with origin in the Earth's center of mass; the z-axis coincides with the mean axis of rotation; the x-axis lies in the mean Greenwich meridian plane and is normal to the z-axis; the y-axis is normal to the xz-plane and directed so that xyz system is right-handed; the xy-plane is thus the mean equatorial plane.

According to Newton's law of Gravitation (*1687*), two point masses m_1 and m_2 attract each other with the gravitational force:

$$K = -G\frac{m_1 m_2}{l^2}\frac{\mathbf{l}}{l} \tag{2.1}$$

where G is the gravitational constant, $6.673 \cdot 10^{-11} m^3 kg^{-1} s^{-2}$, and l the distance between the masses.

By setting the mass at the attracted point P to unity, (2.1) transforms into the gravitational acceleration:

$$B = -G\frac{m}{l^2}\frac{\mathbf{l}}{l} \tag{2.2}$$

Where b originates at P and is directed towards the source point P'. The vector l may be expressed by the position vectors r and r' (Fig. 2.1) in the global Cartesian xyz-sistem:

$$l = r - r', \qquad r^T = (x, y, z), \qquad r'^T = (x', y', z'), \tag{2.3}$$

where

$$l = |l| = \sqrt{(x - x')^2 + (y - y')^2 + (z - z')^2}. \tag{2.4}$$

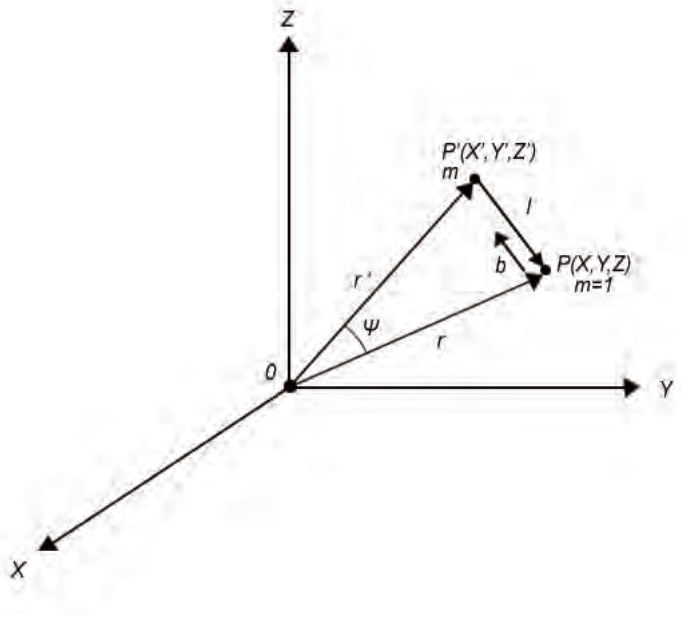

Figure 2.1: Gravitational attraction

The Earth is composed of an infinite number of differential mass elements dm. The gravitation on the unit mass at P results from the integral over the individual contribution:

$$b = b(r) = -G \iiint_{earth} \frac{r - r'}{|r - r'|} dm \tag{2.5}$$

The mass element dm can be expressed by the volume density $\rho = \rho(r')$ and the volume element dv, $dm = \rho dv$.

Because the gravitational filed is invariant to rotation, $curl b = 0$, the vector b may be represented as the gradient of potential V, $b = grad V$ Torge 2001 [45].

The gravitational potential V may be expressed by the formula

$$V(P) = V(x, y, z) = G \iiint_{earth} \frac{\rho(Q)}{l} dv_Q, \tag{2.6}$$

where P is a point having the coordinates (x,y,z), Q is a point variable within the Earth's body, which forms the center of the volume element dv_Q, l is the distance between P and Q, and $\rho(Q)$ is the mass density at Q.

The integral is to be extended over the whole Earth's body, which includes the solid and liquid parts, effects of the atmosphere and temporal variations.

As a result of the Earth's rotation about its axes, the centrifugal force acts on an object of mass on the Earth's surface. With assumption of a

rotation has a constant velocity ω, about the rotational axis, with the axis assumed fixed with the Earth, the centrifugal acceleration is:

$$z = (\omega \times r) \times \omega = \omega^2 p, \tag{2.7}$$

Centrifugal acceleration acting on a unit mass is directed outward and is perpendicular to the spin axis with the geocentric latitude $p = r\cos\bar{\varphi}$, and the magnitude is:

$$z = |z| = \omega^2 r\cos\bar{\varphi}. \tag{2.8}$$

with the centrifugal potential defined as:

$$Z(P) = \frac{\omega^2}{2}p^2, \qquad \lim_{n\to\infty} Z = 0 \tag{2.9}$$

Having a definition of gravitation and centrifugal acceleration, one can define the gravity acceleration or *gravity g*, as a resultant of *b* and *z*, $g = b + z$. Following the same logic, the *gravity potential W* is expressed as a sum of gravitational potential *V* and potential of centrifugal force *Z*:

$$W(x,y,z) = G\iiint_{earth}\frac{\rho(Q)}{l}dv_Q + \frac{\omega^2}{2}p^2. \tag{2.10}$$

The field of the potential *V* is called the *gravitational field*, and the field of the potential *W* is the *gravity field*.

The *gravity vector g* is the gradient of *W*, and in a Cartesian system we have

$$g = gradW = \begin{bmatrix} W_x \\ W_y \\ W_z \end{bmatrix}; \tag{2.11}$$

its components are the partial derivatives of *W* with respect to *x*, *y*, *z*.

The second-order partial derivatives of V form a symmetric matrix

$$V_{ij} = \begin{bmatrix} V_{xx} & V_{xy} & V_{xz} \\ V_{yx} & V_{yy} & V_{yz} \\ V_{zx} & V_{zy} & V_{zz} \end{bmatrix} \tag{2.12}$$

which is called the (second order) *gravitational gradient matrix*. Similarly, the second-order derivatives of W form the *gravity gradient matrix*, also called the *Eötvös tensor*.

$$W_{ij} = gradg = grad(gradW) = \begin{bmatrix} W_{xx} & W_{xy} & W_{xz} \\ W_{yx} & W_{yy} & W_{yz} \\ W_{zx} & W_{zy} & W_{zz} \end{bmatrix} \quad (2.13)$$

The trace of the matrix (2.12) is the *Laplacian* of V:

$$\Delta V = V_{xx} + V_{yy} + V_{zz} \quad (2.14)$$

Outside of attracting masses, above the Earth's surface S, V satisfies the *Laplace's equation*

$$\Delta V = 0; \quad (2.15)$$

the solutions to this equation are called *harmonic functions*, Moritz 1980 [33]. In the Earth's interior, the potential surface V satisfies *Poisson's equation*

$$\Delta V = -4\pi G\rho, \quad (2.16)$$

where ΔV and ρ refer to the same point inside Earth's interior.
The corresponding relations for the gravity potential W are

$$\Delta W = 2\omega^2 \quad \text{outside S}, \quad \Delta W = -4\pi G\rho + 2\omega^2 \quad \text{inside S}. \quad (2.17)$$

2.2 GEOID

The geoid is of fundamental importance for geodesy, oceanography and the physics of the solid Earth. In geodesy and oceanography, the geoid serves as a height reference surface for describing continental and sea surface topography.

The geoid is that equipotential surface which would coincide with the mean ocean surface of the Earth, if the oceans were in equilibrium, at rest (relative to the rotating Earth), and extended through the continents.

2.3 GRAVIMETRY

Gravimetry is the measurement of gravitational field's strength. There are two basic principles of gravity measurements; absolute and relative

gravity measurements. Absolute gravity measurements refer to the determination of g from the fundamental acceleration quantities, length and time. The free-fall and the rise-and-fall methods, as well as the pendulum methods are significant in this respect. The measurements of a difference in gravity Δg by the direct or indirect observation of one of the two acceleration quantities, length or time, keeping the other one fixed, is known as a relative gravity measurement. Relative gravity measurements can be performed with considerably more ease than absolute measurements of g, and there are three measurement types, pendulum measurements, spring gravimeter measurements and lever torsion spring balance (Torge 2001 [45]). Instruments for performing measurements of gravity field are called *gravimeters*.

Gravity gradiometer determines either all, several or linear combinations of the components of the gradient matrix by the methods described above and by exploiting the different reactions of neighboring proof masses to the gravity field. On the Earth's surface, gravimeters can be used to approximate the components of *grad g* by measuring gravity differences between adjacent stations.

Continuous gravity measurements contain information on Earth's tides and ocean tidal loading, free oscillations and the nearly diurnal free wobble of the Earth, inner core translation, polar motion, and volcanic and earthquake activity.

2.4 SATELLITE GRADIOMETRY

Current knowledge of the Earth's global gravitational field is mainly derived from analysis of the motion of artificial satellites (Satellite to Satellite Tracking (SST)), measurements of second order derivatives of gravitational potential V (Satellite Gravity Gradiometer (SGG)) or by combination of these two methods. In a mission combining these, a spacecraft equipped with a Global Positioning System (GPS) receiver and a gradiometer is flown around the Earth in a low and nearly polar orbit. The GPS receiver is used for the determination of the long spatial wavelengths of Earth's gravitational field and the gradiometer for the short wavelengths. As such the two techniques are complementary (Koop 1993 [26]).

The gravity gradients are determined by a technique called differential accelerometry in which the outputs of any combination of two out of nine accelerometers are differenced.

By measuring the distance components and forces it should be feasible to derive the gravitational matrix, V_{ij}. Components of the gravitational tensor are also called gravity gradients, and these components or linear combinations of them are measured by gravity gradiometer instrument.

The basic properties of the gravitational field, namely the Laplace equation $\Delta V = \nabla^2 V = -4\pi G\rho$ (G being a gravitational constant and ρ

Earth's mean density), which becomes zero outside a mass distribution, and $\nabla \times \nabla V = 0$ (conservative field) can be translated into (Rummel 1986 [39]):

$$\sum_{i=1}^{3} V_{ii} = 0, \qquad \text{and } V_{ij} = V_{ji} \tag{2.18}$$

It can be seen that V_{ij} is symmetric and has only five independent components.

For the purpose of gravity field determination one is interested in the deviations of the actual field from an ellipsoidal model called the anomalous potential.

There are two basic techniques for gravity field determination from satellite; SST and satellite gradiometry, Rummel and Colombo 1985 [40]. Major differences between these two concepts are the following: two satellites in the same orbit, such as GRACE, of SST can be viewed as two point masses in free fall, subject only to the influence of the gravitational field, their relative movement is being measured, and the gravity field is sensed only in this direction. On the other hand, satellite gradiometer, in a case of a full gradiometer, *i.e.* senses the gravitational field simultaneously in all directions, can measure the complete curvature structure of the local gravitational field. By a full tensor gradiometer it is assumed that six second order derivatives of the gravitational potential V are determined.

$$V_{ij} = \frac{\delta^2 V}{\delta x^i \delta x^j} \tag{2.19}$$

As a part of instrument calibration, surface forces can be eliminated and changes in the measurements due to rotation and orientation can be corrected for.

The observable V_{ij} is split into a normal, or reference part U_{ij}, computed from a chosen reference potential U (without centrifugal force), *e.g.* from a known set of potential coefficients, and into an unknown disturbance part T_{ij}, belonging to the disturbing potential T:

$$V_{ij}(P) = U_{ij}(P) + T_{ij}(P) \tag{2.20}$$

The disturbing potential is the fundamental quantity of the residual gravity field. It is closely related to the height anomaly and the geoid height. From equation 2.20 and assuming that the centrifugal parts of W and U are identical, the disturbing potential is formed by the difference of the gravitation of the Earth and of the level ellipsoid, and it is thus a harmonic function outside the Earth's masses. Hence,

it obeys *Laplace's* differential equation $\Delta T = 0$, where Δ is Laplace operator Torge 2001 [45].

T can be expanded into spherical harmonics by:

$$T = \frac{GM}{r} \sum_{l=2}^{\infty} \left(\frac{a}{r}\right)^{l} \sum_{m=0}^{l} (\Delta\bar{C}_{lm} \cos m\lambda + \Delta\bar{S}_{lm} \sin m\lambda)\bar{P}_{lm}(\cos\vartheta) \tag{2.21}$$

where

GM	is the gravitational constant times mean mass of the Earth,
r	is the radial distance of the computation point from the geocenter,
a	is a scaling factor approximately equal to the equatorial radius of the Earth ellipsoid used for the determination of the harmonic coefficients,
l	is the degree of the spherical harmonic coefficient,
m	is the order of the spherical harmonic coefficient,
ϑ	is the geocentric co-latitude of the computation point,
λ	is the longitude of the computation point,
$\bar{P}_{lm}$	is the normalized associated Legendre functions of degree n and order m, and
$\Delta\bar{C}_{lm}, \Delta\bar{S}_{lm}$	is the residual coefficients of the spherical harmonic series after subtracting the coefficients of the normal potential from the gravitational potential.

The series expansion can be also represented by:

$$T(r,\vartheta,\lambda) = \sum_{l=2}^{\infty} \frac{r}{l-1} \left(\frac{a}{r}\right)^{l+1} \delta g_l(\vartheta,\lambda) \tag{2.22}$$

As known from potential theory, the surface spherical harmonics δg_l are derived by inversion as a surface integral of the gravity anomalies over the unit sphere σ:

$$\Delta g_l = \frac{2l+1}{4\pi} \iint_{\sigma} \Delta g P_l(\cos\psi)\, d\sigma \tag{2.23}$$

where $P_l(\cos\psi)$ are the Legendre polynomials. Inserting into 2.22 yields the disturbing potential on the geoid in spherical approximation:

$$T(\vartheta,\lambda) = \frac{R}{4\pi}\int\int_{\sigma} S(\psi)\Delta g\, d\sigma \tag{2.24}$$

where the integral kernel is:

$$S(\psi) = \sum_{l=2}^{\infty} \frac{2l+1}{l-1} P_l(\cos\psi). \tag{2.25}$$

This integral has been derived by Stokes (1849), and it is called *Stokes' formula*. *Stokes's function* $S(\psi)$ acts as a weighting function on the gravity anomalies. It depends on the spherical distance ψ between the point of computation and the surface element $d\sigma$ with the gravity anomaly Δg (Torge 2001 [45]).

In order to obtain gravity field quantities like geoid heights and gravity anomalies from the GOCE gravity potential harmonic series some approximations are introduced. The geoid height is defined as the distance between the ellipsoid and the geoid. The geoid is defined by the condition that its potential equals the constant normal potential of the corresponding point on the reference ellipsoid. By applying Bruns formula to equation 2.21 we get the relation between geoid heights and the disturbing potential Torge 2001 [45].

$$N = \frac{T}{\gamma_0} \tag{2.26}$$

where N is the geoid height, T the disturbing potential on the geoid and γ_0 the normal gravity at the reference ellipsoid.

The normal gravity at the reference ellipsoid is computed by the formula of Somigliana (see Torge 2001 [45]):

$$\begin{aligned} \gamma_0(\varphi') &= \gamma_a \frac{1 + k\sin^2\varphi'}{\sqrt{1 - e^2\sin^2\varphi'}} \\ k &= \frac{b\gamma_b}{a\gamma_a} - 1 \end{aligned} \tag{2.27}$$

with γ_a being the normal gravity at the equator and γ_b the normal gravity at the pole.

By applying equation 2.26 to equation 2.21, the geoid heights as defined above can be written as a spherical harmonic series:

$$N(r,\vartheta,\lambda) = \frac{GM}{r}\sum_{l=2}^{\infty}\left(\frac{a}{r\gamma_0}\right)^l \sum_{m=0}^{l} (\Delta\bar{C}_{lm}\cos m\lambda + \Delta\bar{S}_{lm}\sin m\lambda)\bar{P}_{lm}(\cos\vartheta)$$

(2.28)

Gravity anomalies are derived from the fundamental equation of physical geodesy by introducing the derivatives along the plumb line of the disturbing potential and the normal gravity (Heiskanen and Moritz 1967 [18]).

$$\Delta g = g_P - \gamma_0 = -\frac{\partial T}{\partial h} + \frac{1}{\gamma_0}\frac{\partial \gamma}{\partial h}T \tag{2.29}$$

with g_P being the magnitude of the gravity at the geoid.

In spherical approximation (by approximating the real plumb line with the geocentric vector) it becomes (Heiskanen and Moritz 1967 [18]):

$$\Delta g = -\frac{\partial T}{\partial r} - \frac{2}{a}T \tag{2.30}$$

By applying the spherical approximation of 2.30 to equation 2.21 we get the spherical harmonic series for the gravity anomalies:

$$\Delta g(r,\vartheta,\lambda) = \frac{GM}{r^2}\sum_{l=2}^{\infty}(l-1)\left(\frac{a}{r}\right)^l \sum_{m=0}^{l}(\Delta\bar{C}_{lm}\cos m\lambda + \Delta\bar{S}_{lm}\sin m\lambda)\bar{P}_{lm}(\cos\vartheta) \tag{2.31}$$

The above formulas are given in spherical approximation.

If we assume that the mean value of the gravity anomalies Δg over the Earth are is zero, and the surface element is described in spherical coordinates ϑ, λ, we have:

$$d\sigma = \sin\vartheta d\vartheta d\lambda \tag{2.32}$$

And statistical behavior of Δg is described by the covariance function:

$$C(\psi) = cov(\Delta g, \Delta g', \psi) = \frac{1}{4\pi}\int\int_{\sigma}\Delta g \Delta g' d\sigma \tag{2.33}$$

where ψ is spherical distance. Covariance function is calculated as the mean value of all products of gravity anomalies at the points P and P', having constant spherical distance ψ on the unit sphere. $C(\psi)$ is only dependent on the spherical distance and not on the position (Torge 2001 [45]). For the $\psi = 0$, $\Delta g = \Delta g$, and the covariance transforms to variance.

$$\sigma^2(\Delta g) = \frac{1}{4\pi}\int\int_{\sigma}\Delta g^2 d\sigma \tag{2.34}$$

Spherical harmonic coefficients can be used for definition of the signal degree variances of T as:

$$c_n(T) = \sum_m T_{lm}^2 \tag{2.35}$$

Similarly, the error degree variances of T are:

$$\epsilon_n(T) = \sum_m E\left\{\varepsilon_{lm}^2\right\} \tag{2.36}$$

To come back to gradiometry and gradiometer principles; a gradiometer could be based on a variety of principles and operated in various environments. It could for example be placed on Earth or orbit in a free fall around the Earth, it could be rotating or space fixed, while measuring forces or torques. The forces could be either solely the gravitational force, $F_i = G_i$ or, for example, atmospheric drag and solar radiation in the case of a free falling proof mass.

Important is that only the motion of the proof mass relative to the measurement frame is observable, and the observables can be divided into two main classes: kinematical and dynamical. Under kinematical measurements we understand observations of positions and position changes. In the dynamical case certain controlled forces are applied to the proof mass in order to constrain its motion.

For a spherical harmonic expansion of the gravity field the number of unknown coefficients becomes $(l+1)^2$, where l is the order of spherical harmonic expansion. A system of normal equations of this size can only be solved if some favorably sparse structure, such as block diagonal, is present. In a case of least squares method for determination of the coefficients, the arrangement of cell averages in an equi-angular grid and proper grouping of the unknown coefficients $\Delta\bar{C}_{nma}$ causes the normal matrix of the adjustment to the block diagonal.

In gravity field global model estimation and covariance propagation sometimes a block diagonal *approximation* of the normal matrix N is used (e.g. in SST). Block diagonal normal matrices arise only under *regularity conditions* (Colombo 1981 [9], Sansó and Tscherning 2003 [42]) which are hardly exactly met. The item of approximating a given symmetric positive definite matrix by a block diagonal one is then interesting. Therefore criteria for the approximation is needed, so that the computation of the block diagonal matrix B approximating the inverse N^{-1} requires an effort smaller than for the direct computation of N^{-1}. Solutions and simulated scenarios are proposed in Herceg et al. 2011 [19].

The improved knowledge of the Earth's gravitational field, resulting from such a mission, can contribute to many Earth related sciences, such as geodesy (levelling with GPS), satellite orbit determination, solid Earth physics (continental lithosphere, polar regions) and

oceanography, the latter not only for topics like ocean circulation but also for studies of climate changes.

2.5 THE EARTH'S GRAVITY MODELS

Global gravity field modeling is required for large-scale problems including the determination of satellite orbits, inertial navigation, and development of geophysical and geodynamic models. The geoid is required for establishing a global vertical reference system and for deriving sea surface topography.

Global gravity models are based on spherical harmonic expansion (equation 2.26). The low frequency part of these series expansions comes from the analysis of satellite orbits, while higher degrees of expansion are achieved by combining low-degree models with results of terrestrial, shipborne and airborne gravimetry, satellite altimetry and satellite gradiometry.

The global models used in this thesis are EGM2008 to degree 2160 (developed by Pavlis et al. 2008 [36]), and a third generation GOCE-only gravity field solution based on the so-called Direct (DIR) and Time-wise (TIM) methodology (a part from first generation of Space-wise (SPW) solution) using GOCE measurements from 1 November 2009 until 17 April 2011.

3

GRAVITY FIELD AND STEADY-STATE OCEAN CIRCULATION EXPLORER (GOCE) MISSION

As the most advanced gravity space mission to date, GOCE mapped global variations in the gravity field with extreme detail and accuracy. This chapter will give an overview of the GOCE mission. It will briefly describe GOCE products, with the focus on the GOCE gravity gradient observations in Terrestrial Reference Frame (TRF), and it will present possible application of the GOCE data.

3.1 INTRODUCTION

GOCE is a European Space Agency (ESA) satellite that was launched on March 17, 2009 from Plesetsk, Russia. GOCE is the first satellite mission that observes second order derivatives, *i.e.* gradients, of the Earth gravitational potential from space over short baselines within a platform flying in drag-free mode (Figure 3.1).

GOCE gradient measurements are primarily used for the determination of high precision global gravity field models. These measurements enables the determination of the gravity anomalies at *1 mgal* and gravimetric geoid models at *1 cm* level accuracies at wavelengths of a few hundred kilometers and longer Pail et al. 2011 [35]. GOCE is flying in drag-free mode, which implies cancelling non-gravitational forces and all torques, leaving the satellite to free fall subject only to gravity. It has sun-synchronous, near-circular, dusk-dawn, low-Earth orbit, with an inclination angle of 96.7°. The measurement altitude is about 250km, while the hibernation altitude is 270km. GOCE is a slim, octagonal spacecraft approximately 5m long and 1m in diameter. It is a rigid structure weighing about 1050 kg. Flight operations are monitored and controlled by ESA-ESOC via the Kiruna ground station in Sweden and secondary ground station in Svalbard, Norway. The satellite payload contains a gradiometer, a 12-channel dual-frequency GPS receiver with geodetic quality and a laser retroreflector, which enables tracking by ground-based lasers, *cf.* Floberghagen et al. 2010 [13].

The satellite's primary instrument is three pairs of 3-axis highly sensitive capacitive accelerometers on orthogonal axes (Figure 3.2).

The ccelerometers are servo-controlled and each pair is separated by a distance of about 0.5 m. They measure gravitational gradients along

Figure 3.1: GOCE flying

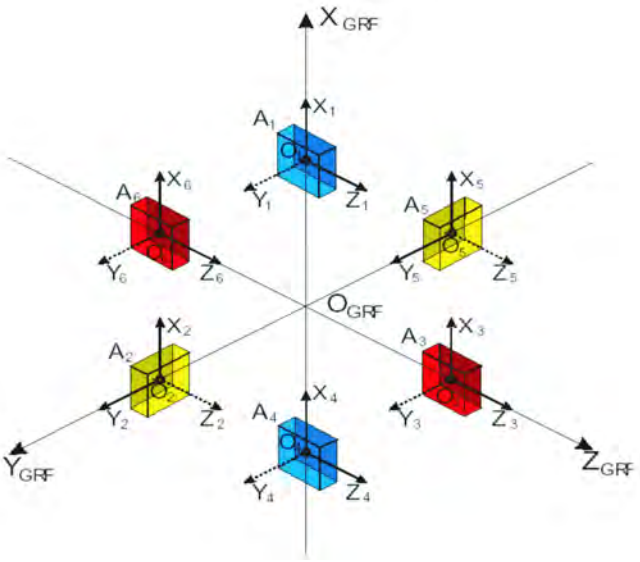

Figure 3.2: Notation and location of the 6 accelerometers of the GOCE gradiometer in the Gradiometer Reference Frame (GRF) and with all 6 Accelerometer Reference Frame's (ARF)

three different axes by the differences in acceleration between pairs of test-masses of an ensemble of 6 accelerometers inside a satellite, see figure 3.3.

The GOCE gradiometer will observe local satellite gravity gradients with high precision in a Measurement Bandwidth (MBW) of 0.005 – 0.1Hz (Visser 2008 [58]).

The measured signal is the difference in gravitational acceleration at the proof-mass locations inside the spacecraft, where of course the gravitational signal reflects the various attracting masses of the Earth. Sources of uneven mass distribution include amongst others the relative distribution of oceans, land and ice, ocean mass exchange by

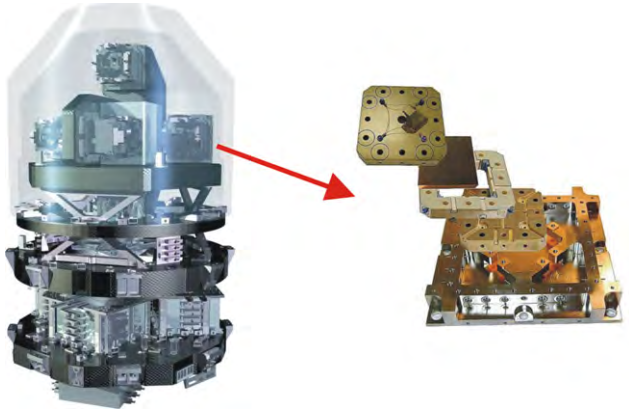

Figure 3.3: GOCE accelerometer

circulation, mountains and valleys, lithospheric subduction zones and mantle inhomogeneities down to the mantle boundary and beyond.

Non-gravitational acceleration of the spacecraft, *i.e.* due to air drag and radiation pressure, affects all accelerometers inside the satellite in the same manner. The non-gravitational accelerations, ideally, cancel when differencing two accelerometers along a gradiometer arm. Rotational motion of the satellite is addressed by correcting for the centrifugal accelerations. Due to the r^{-2} dependency of gravitational forces, a low orbit implies stronger signals and a greater accuracy.

The gradiometer measurements are supplemented by exploiting the concept of SST in the high-low mode (figure 3.4). Taking GPS distance measurements from GPS satellites to the low-earth orbiting GOCE platform, long wavelength distortions in the orbit due to the effects of the gravity field are detected (Drinkwater et al. 2007 [10]).

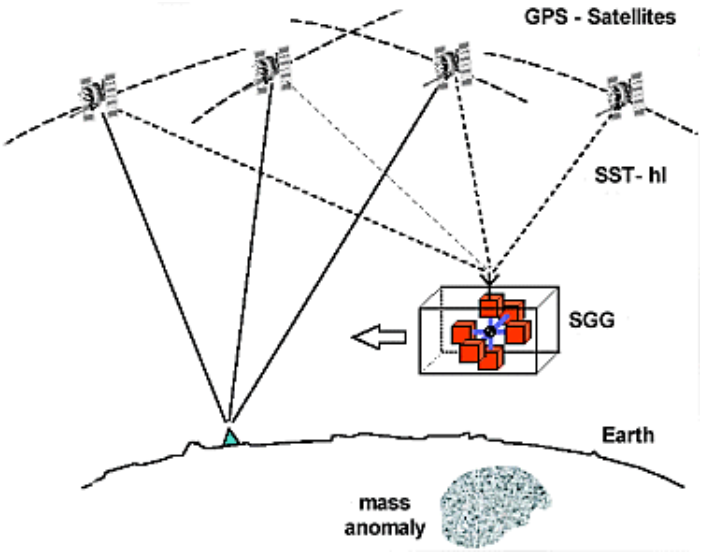

Figure 3.4: GOCE SST and gradiometry principle

Gravity gradients acquired by GOCE do not cover the entire Earth because of its sun-synchronous orbit leaving data gaps with a radius of about 6.5° in the polar regions.

During operations, the satellite is continuously monitored and controlled by the Flight Operations Segment (FOS) in Darmstadt. The FOS generates and uplinks commands to programme the GOCE satellite operations, and meanwhile processes instrument data to monitor the health status and performance of the platform and the instruments.

On figure 3.5, the GOCE sensor system is presented: star sensors, which measure high rate and high precision inertial orientation, GPS receiver, which measures orbit trajectory with centimeter precision, laser retro reflector for orbit validation, ion thrusters for drag control and to control the signal from common mode accelerations from gradiometer, magneto-torquers for angular control based on angular rates from star sensors and gradiometer and cold gas thrusters, which are used for gradiometer in-flight calibration with cold gas thrusters (Floberghagen et al. 2010 [13]).

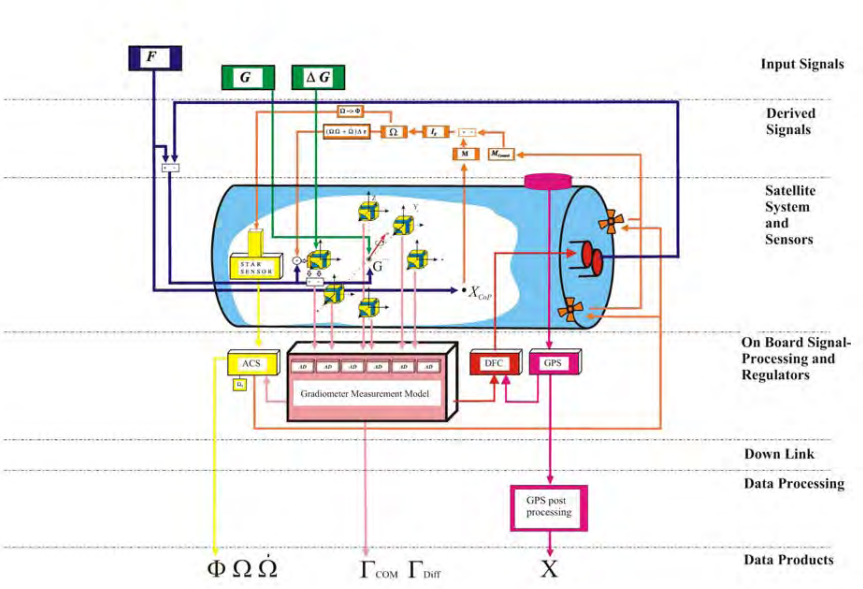

Figure 3.5: GOCE sensor system

3.2 THE GOCE PRODUCTS

There are three basic levels of data products to be produced by the ground segment, *Level 0*, *Level 1b* and *Level 2*.

Level 0 products include satellite and instrument housekeeping data and ancillary data, output of the 6 accelerometers along their 3 measurement axes at 1 Hz.

Level 1b products include gravity gradients in Gradiometer Reference Frame (GRF) together with the GRF to Inertial Reference Frame (IRF), frame transformation matrices, linear accelerations and angular rates and accelerations, SST measurements and derived positions and reconstructed satellite orbits in Earth-Fixed Reference Frame, attitude and orbit data (position, velocity and time).

Level 2 products are generated by the High-Level Processing Facility (HPF), a distributed system developed and operated by the European GOCE Gravity Consortium (EGG-C). GOCE *Level 2* products (Table 3.1) include gravity gradients, precise orbit solutions, as well as the GOCE-only gravity field models including supporting information. These *Level 2* data products will be generated by the HPF. The HPF is a distributed processing chain being developed by a group of 10 European Institutes known as the EGG-C, see Floberghagen et al. 2010 [13].

A first generation of GOCE gravity field models, based on 2 months of data, *i.e.* from 1. Nov 2009 to 31. Dec 2009, had already been released at ESA's Living Planet symposium in Bergen, Norway, July 2010, for Direct (DIR), Time-wise (TIM) and Space-wise (SPW) solutions. The second generation gravity field solutions have been released on March 11, 2011, but just for Direct and Time-wise models. These solutions are based on 8 months of data, November 2009 to July 2010 (effectively 6 months after reduction of data gaps and calibration phases). In the same, time Variance-Covariance matrices for the first release of the Direct and Space Wise solutions were updated. The third generation gravity field solutions have been released on November 2011, containing gravity gradient data from 1 November 2009 until 17 April 2011.

Three different solutions for the gravity field are being released by ESA, representing the DIR, TIM and SPW.

The time-wise solution is inferred from GOCE data exclusively, *i.e.* it does not contain gravity field information through a background reference model. Therefore, it is representative of the GOCE mission performance and constitutes an independent means of comparison to other models, see Pail et al. 2010 [34].

The direct numerical solution, in contrast with the time-wise one, has been constructed taking prior gravity field information through a background reference model. As such, it incorporates data from other satellite missions such as GRACE. The low degrees of the direct solution are consequently more accurate than those of the time-wise solution, Bruinsma et al. 2010 [7].

None of these two new solutions incorporate surface data or airborne data in any way, but gravity gradients acquired do not cover the entire Earth. This is due to the previously mentioned data gap of approximately 6.5° found in the polar regions.

PRODUCT NAME	PRODUCT DEFINITION	LATENCY
Gravity Gradients		
EGG_NOM_2	Level 2 gravity gradients in GRF with corrections: - Externally calibrated and corrected gravity gradients - Corrections to gravity gradients due to temporal gravity variations - Flags for outliers, fill-in gravity gradients for data gaps with flags - Statistical information	2 weeks
EGG_TRF_2	L2 gravity gradients in EFRF with corrections: - Externally calibrated gravity gradients in Earth fixed reference frame including error estimates for transformed gradients - Transformation parameters to Earth fixed reference frame	6 months
GOCE Orbits		
SST_PSO_2	Precise science orbits: - Reduced-dynamic and kinematic precise science orbits - Rotation matrices between IRF and EFRF - Quality report for precise orbits	2 weeks
GOCE Gravity Fields		
EGM_GOC_2	Final GOCE gravity field model: - Spherical harmonic series including error estimates - Grids of geoid heights, gravity anomalies and deflections of the vertical - Propagated error estimates in terms of geoid heights - Quality report for gravity field model	9 months
EGM_GVC_2	Variance-covariance matrix for the final gravity field in terms of spherical harmonic series	9 months

Table 3.1: GOCE Geophysical, *i.e.* Level 2, products (Floberghagen et al. 2010 [13])

The space-wise model makes use of both satellite tracking data, derived from the on-board GPS receiver, and gravity gradients observed by the on-board electrostatic gradiometer, see Migliaccio et al. 2010 [32] Reduced dynamic orbits are used for geo-locating gravity gradients. EGM2008 is used for degree variance modelling and for error calibration of the estimated gravitational potential along track, thus affecting the low degrees of the solution. The Space-wise model is available just in the first release of the the gravity field.

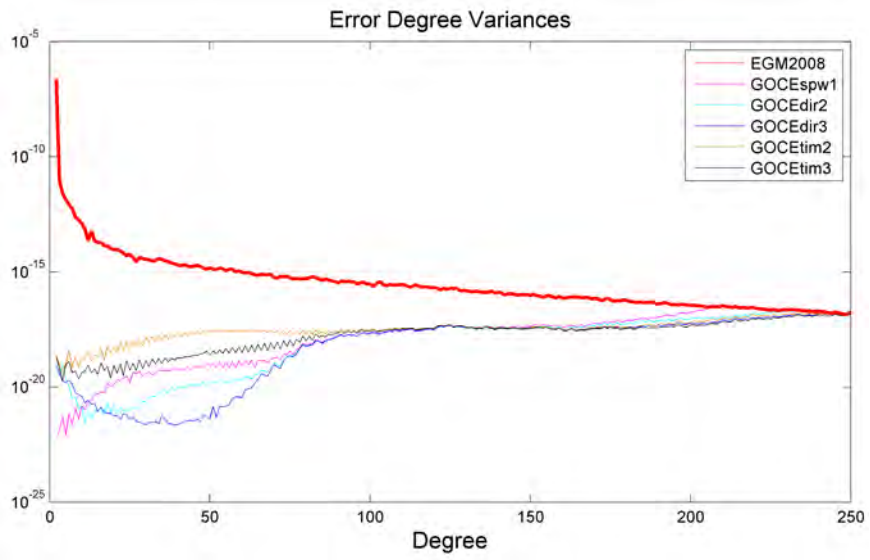

Figure 3.6: Error degree variances of GOCE releases compared to EGM2008 as a reference model

Error degree variances of GOCE releases compared to EGM2008 as a reference model are shown on figure 3.6, while coefficients error variances (log10 scale) are shown in figure 3.7.

During the extended mission, the processing team behind the Space-wise solution plans to deliver gridded data in a local geographical reference frame. Grids may either be referred at mean satellite altitude, returning the gravitational potential and its second order derivatives thus representing the original information from Mission data, or, through downward continuation, at ground level, returning the diagonal component of the gravity gradient tensor. External information, such as other independent global models based on satellite and/or ground data, may be easily integrated in gridded representations. It will also result in an easier integration in geophysical applications, ESA 2011 [11].

Calibration of GOCE gradiometer data in the measurements bandwidth using ground data was performed by Tscherning and Veicherts 2006 [50], and calibration of GOCE SGG data was performed using high-low SST, terrestrial gravity data and global gravity field models Bouman et al. 2004 [5].

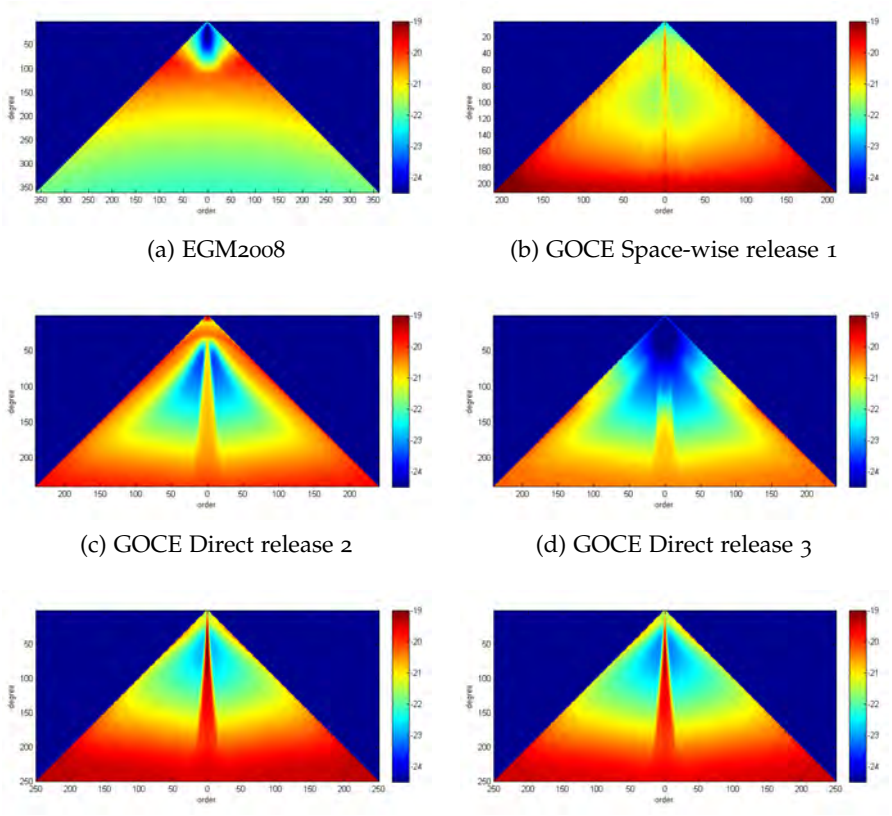

(a) EGM2008 (b) GOCE Space-wise release 1

(c) GOCE Direct release 2 (d) GOCE Direct release 3

(e) GOCE Time-wise release 2 (f) GOCE Time-wise release 3

Figure 3.7: Coefficients error variances (log10 scale)

In this thesis, EGG_TRF_2, *Level 2* gravity gradients were used in period from 31th of October 2009 to 30th of April 2011. Dataset contains 31.042.201 gradient observations before removing flagged records (see chapter 6).

3.3 THE GOCE APPLICATIONS

Since the gravity gradient measurements taken by GOCE reflect density variations in the Earth's interior, the resulting data will lead to new insights into processes occurring in the lithosphere and upper mantle down to a depth of about 200 km (Rio 2009 [38]). It will also further our knowledge of the crustal uplift occurring due to post-glacial rebound. With a better understanding of these processes, GOCE indirectly helps assessing the potential dangers of the current sea-level change.

In respect to geodetic applications, data from GOCE will lead to a global unification of height systems and will help facilitate a global system for tide-gauge records.

With the detailed GOCE global geoid, satellite-altimetry data records, spanning almost 20 years, can be used to provide a detailed picture of ocean circulation patterns and variations.

For geoid applications, e.g. for Mean Dynamic Topography estimation, the current GOCE models do not handle the polar gaps well enough, and in polar regions will be important to use combination models ideally including both surface data and GRACE.

4

OCEAN MODELLING

Ocean circulation plays a crucial role in climate regulation by transporting heat from low to high latitudes in surface waters, while currents cooled at high latitudes flow back toward the Equator as deep water (Rio 2009 [38]). Through its accurate measurements of Earth's gravity field at short scales, GOCE promises significant advancement in our ability to determine the ocean's general circulation. In the next sections, the basic principle of satellite altimetry its products will be presented, *i.e.* mean sea surface (MSS) and mean dynamic topography (MDT).

4.1 SATELLITE ALTIMETRY

Satellite altimetry measures the time taken by a radar pulse to travel from a satellite antenna to the surface and back to the satellite receiver. The combined knowledge of the satellite's orbit relative to a reference ellipsoid and the altimetric range, which is the distance between the satellite and the ocean surface, gives the sea level above the reference ellipsoide, *i.e.* Sea Surface Height (SSH).

The shape of the sea level results from different forcings. Effects, which give shape to the ocean at rest (Earth rotation and gravity) and external that generate the motions of the ocean resulting in a sea level shape that differs from its shape at rest. The external forces are gravitational effects from the Moon and the Sun (tides) as well as forcing from the atmosphere (winds, solar heating, precipitation...).

A key instruments on board satellites for altimetry purposes are the radar and laser altimeters. Purpose of radar altimeter is measuring the height of the satellite above the ocean surface. From this range measurement, the absolute sea level or the variations in sea level can be inferred. In order to do so, the range measurements must be subtracted from the altitude of the satellite, defined in a well-determined reference frame.

4.1.1 *Satellite altimetry principle*

The simple explanation of satellite altimetry is that the height of the satellite above the closest ocean surface h is measured with a mi-

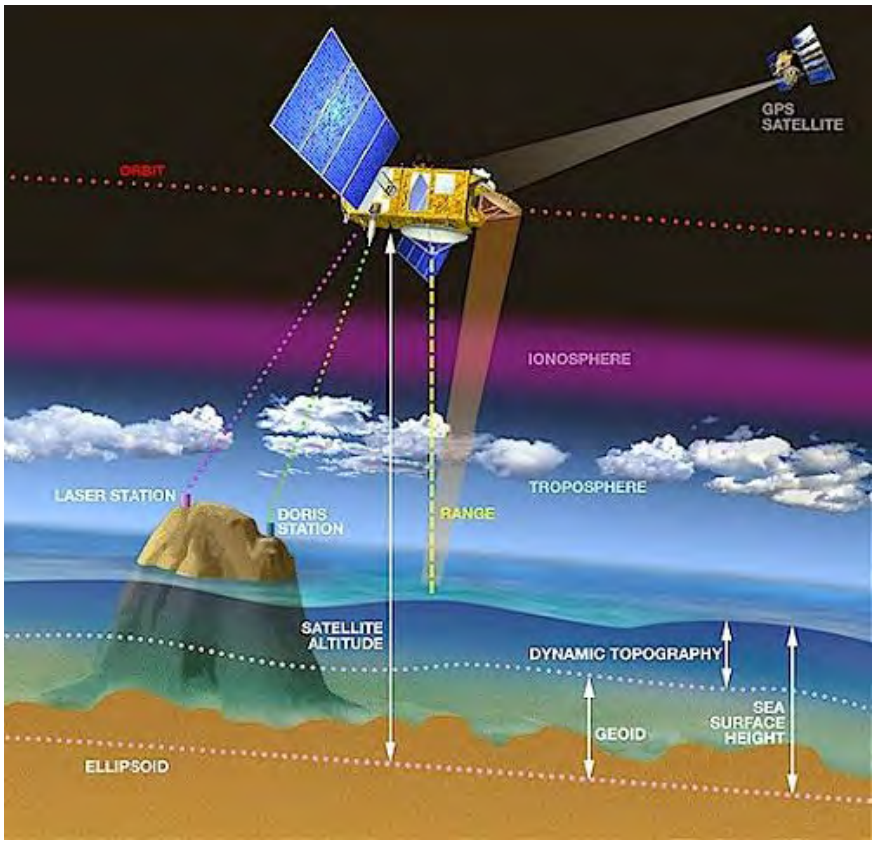

Figure 4.1: Concept of satellite altimetry

crowave radar operating in a pulse-limited mode. The radar signal spreads on a large spot on the ocean surface (about 45 km in diameter) and than a smaller effective footprint (1-5 km in diameter) is formed with a sharp radar pulse and accurately recording its two way travel time. The wavefront of the pulse ensures that the altitude is measured to the closest ocean surface (with 1700 pulses per second). Then, the corrections for the ionospheric and atmospheric delays are implemented to get the correct distance from the satellite to the ocean surface. To get the height of the ocean surface, it is also necessary to have the accurate position of the radar altimeter satellite. This height of the satellite above the ellipsoid h' is measured by tracking the satellite from a globally-distributed network of lasers and/or Doppler stations, Doppler Orbitography and Radiopositioning Integrated by Satellite (DORIS), and GPS. The trajectory and height of the satellite are then corrected by dynamic orbit calculations. The difference between the height of the satellite above the ellipsoid (h_S) and the satellite altitude above the ocean surface (h_R) is equal to the sea surface height (η):

$$\eta = h_S - h_R \tag{4.1}$$

The SSH integrates effects such as sea surface height without any perturbing factors (wind, currents, tides, etc.), *i.e.* geoid, ocean circulation, or dynamic topography, which includes permanent circulation and a variable component due to wind, eddies, seasonal variations, etc.

Based on the above, the use of altimetric data for oceanographic applications depends on the capacity to separate the geoid height, that ranges between ± 100 m, from the dynamic topography, that ranges between ± 1m. Although the centimeter accuracy of the geoid height, for scales greater than 100 km, is now reached with GOCE, it is still insufficient to directly apply equation 4.1 along altimetric tracks.

4.1.2 *The repeat track method*

Satellite altimetry directly provides sea surface topography with respect to an ellipsoidal reference surface. With the exception of the polar regions, satellite altimeters cover oceans with repeated tracks. Because measurements are only available on the satellite ground tracks, the data still has to be processed to form a regularly spaced grid, Zandbergen 1990 [62].

To make the best possible use of altimetric data, the *repetitive tracks* method was applied on the altimetric heights. If η is the height of the mean sea surface above the reference ellipsoid and N is the geoid height, then mean dynamic topography MDT is expressed by:

$$h = \eta - N \tag{4.2}$$

Assuming a stationary geoid, the average of M altimetric measurements $\{\eta_i\}_{i=1,M}$, at a geographical position (x, y), is the sum of the geoid height (N) and the average of the dynamic topography at that location for the time period (P) covering the M measurements, $\overline{h}_P(x, y)$, (Rio 2009 [38]).

$$\begin{aligned}
\overline{\eta_P}(x, y) &= \frac{1}{M}\sum_{i=1}^{M}\eta_i(t, x, y) = \\
&= \frac{1}{M}\sum_{i=1}^{M}(N(x, y) + h_i(t, x, y)) = \\
&= N(x, y) + \frac{1}{M}\sum_{i=1}^{M}h_i(t, x, y) = \\
&= N(x, y) + \overline{h}_P(x, y)
\end{aligned} \tag{4.3}$$

This mean altimetric height $\overline{\eta_P}(x, y)$ can be subtracted from any instantaneous altimetric height $\eta(t, x, y)$. The resulting value is the

variable part of the ocean dynamic topography also called the Sea Level anomaly (SLA):

$$\begin{aligned}\eta(t,x,y) - \overline{\eta_P}(x,y) &= N(x,y) + h(t,x,y) - N(x,y) - \overline{h}_P(x,y) = \\ &= h(t,x,y) - \overline{h}_P(x,y) \\ &= h'_P(t,x,y)\end{aligned} \tag{4.4}$$

The SLA is always referenced to a given period, and the time t at which the SLA is computed needs not to fall inside the chosen period P.

4.1.3 *Satellite altimetry applications*

Since 1986, satellite altimetry missions have been providing vital information for an international user community. That high-quality altimetry measurements are merged with other data to obtain the broadest picture of the ocean and to be used in climate prediction models.

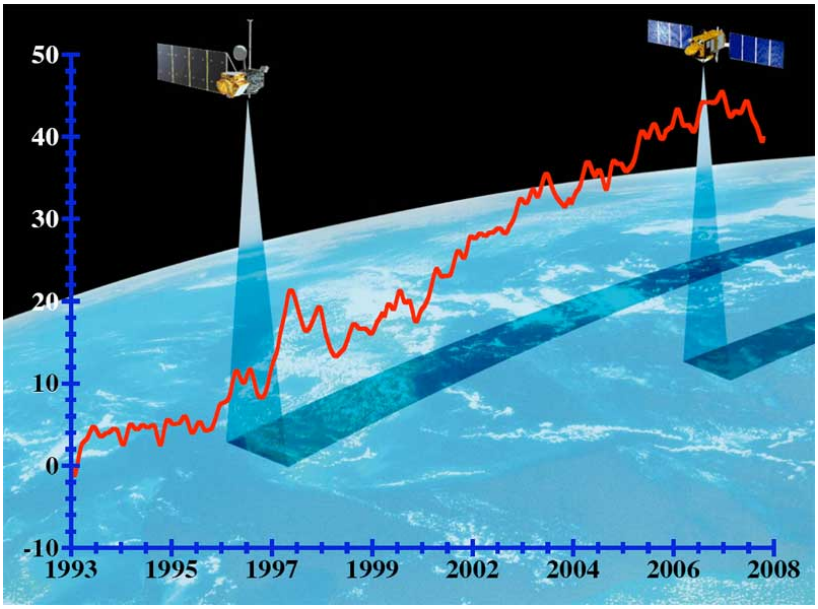

Figure 4.2: Global sea level has a rise of about 3 millimeters per year since Topex/Poseidon (on the left) began its precise measurement of sea surface height in 1993 and was followed by Jason-1 in 2001. (Credit: University of Colorado)

External forces such as the wind cause the sea surface to deviate from the geoid. Existing ESA ocean altimeters measure sea-surface height and typically show $\pm$ 1 meter variations relative to the geoid (ERS and Envisat, Rio 2009 [38]). The large-scale current systems flow along the lines of equal topography and are focused around the strongest gradients in sea surface height.

Presently, the degree to which altimetry data can be used to make precise estimates of the transport of heat, salt and freshwater, is limited by the quality of the geoid at short length scales.

There are many applications of satellite altimetry, such as geoid and mean sea surface determination, prediction of seafloor depth, planning shipboard surveys, petroleum exploration (locate offshore sedimentary basins in remote areas), research of plate tectonics, lithospheric structure and undersea volcanoes.

4.2 MEAN SEA SURFACE AND DYNAMIC TOPOGRAPHY

The averaged sea surface height above a certain reference ellipsoid based on the measurements over several years is called MSS. This can be derived from tide gauge records, satellite altimetry and oceanographic methods, *i.e.* steric and geostrophic levelling, Torge 2001 [45]. Data that represent mean sea surface are usually corrected for the effects of ocean and solid earth tides, and for the variation of the sea surface due to atmospheric pressure loading.

Sea surface height is mostly affected by the tidal forces of the Moon and the Sun acting on the Earth. Sea surface height is influenced by ocean circulation, which is very nearly in geostrophics balance. Sea surface height has a span range of about 120m and it is composed of mean sea surface height and sea surface height variability.

The sea surface does not coincide with a level surface, *i.e.* geoid, of the Earth's gravity field; the deviations are called MDT. MDT is affected by temporal variations of long-term, annual, seasonal and short-term character, occurring at different scales. Averaging the ocean surface over time or modeling ocean tides provides Mean Sea Level (MSL) for the corresponding time interval. In the equation 4.4, the $\overline{h}_P$ term is the MDT for the time period P. It is the missing quantity needed to recover absolute dynamic topography value from sea level anomalies $h'_P(t, x, y)$ (Rio 2009 [38]):

$$h(t, x, y) = \overline{h}_P(x, y) + h'_P(t, x, y) \tag{4.5}$$

MDT is the small residual of two much larger fields (equation 4.2), and typical variations in between the MSS and the geoid are up to 100 m, whereas for the MDT they are around 1m. Thus, a small error in MSS or geoid leads to an order of magnitude error in the MDT. If we accept that the errors in the MSS are small relative to those in the geoid, we can focus just on the geoid errors.

One type of geoid error that impacts the MDT calculations is the *omission error*, which arises from the unmodelled parts of the geoid associated with harmonic degree and order above L (where L represents the lower spatial limit captured by the gravity model of roughly 20,000/L km). This MDT error decreases with increasing L. In addition,

there is another error which shares the same characteristics and dependence on L. This is the act of truncating the spherical harmonic model of the gravity model to obtain the geoid as a spatially gridded field, which leads to *Gibbs* type numerical artefacts in the gridded geoid that radiate away from strong gravity field gradients. This is usually produced by features such as mountains, subduction trenches and sea mounts (Knudsen et al. 2011 [25]).

Another type of error, that propagates in to the MDT estimate, is the commission error. In spherical harmonic terms, such errors are defined for a given gravity field model, and tend to grow with increasing degree and order.

The MDT error decreases with an increasing L due to geoid omission errors and increases due to the accumulated geoid commission error. This results in a trade-off when it comes to choosing the value of L, where any decrease in omission error is offset by the increase in commission error.

Taking into account both geoid omission and commission error, we see that the estimated MDT is:

$$h' = \eta - N_L = h + \Delta N_L + \delta_L \tag{4.6}$$

where h' is the true MDT, ΔN_L is the geoid ommission error and δ_L is the geoid commission error.

Both errors produce small scale noise in the MDT, which can be handled in different ways. First approach is based on neglecting the distinction between the two error sources and apply a spatial filter directly to the MDT. In second approach, one can first apply a spectral filter to MSS, and in that way almost eliminate the geoid omission error component. It is still necessary to apply a spatial filter to the MDT.

The best estimate is obtained when the filtering minimizes the attenuation and distortion of the MDT, while adequately suppressing the noise due to geoid omission and commission errors. Choosing the correct filter radius, *i.e.* the degree of smoothing, is crucial for minimizing the degree of attenuation of the MDT.

The filtered MDT estimate is expressed by applying a filter F to the height residuals in equation 4.6.

$$h' = F \circ (h + \Delta N_L + \delta_L) \tag{4.7}$$

4.2.1 *The geostrophic surface currents*

Under a number of hypotheses, absolute dynamic heights are related to ocean surface currents through the geostrophic equations. Geostrophic equations are described by the zonal u and meridional v

geostrophic velocity components, which are proportional to height gradients. u and v components can be expressed in a Cartesian coordinate system fixed to the Earth (Rio 2009 [38]):

$$u(t,x,y) = -\frac{\gamma}{f}\frac{\partial h(t,x,y)}{\partial y}$$
$$v(t,x,y) = \frac{\gamma}{f}\frac{\partial h(t,x,y)}{\partial x} \tag{4.8}$$

where $f = 2\omega_e \sin\varphi$ is the Coriolis force coefficient, ω_e is the anglar velocity of the Earth and γ is the normal gravity. Because f approaches zero at the equator, noise will be further amplified at low latitudes.

4.2.2 *Reference ellipsoid, tide system and spectral content*

Both altimetric mean sea surface heights and geoid heights are given relative to a reference ellipsoid, which corresponds to a theoretical shape of the Earth. Before subtracting a geoid from a MSS, both fields have to be expressed relative to the same reference ellipsoid. Altimetric MSS are most commonly computed relative to the TOPEX ellipsoid, while the GOCE geoid heights are computed relative to the Geodetic Reference System 1980 (GRS80) reference ellipsoid.

Geoid heights and MSS heights differ depending on what tidal system is implemented to deal with the permanent tide effects. Three different tidal systems are accepted: the *mean tide*, *zero tide* and *tide free* systems (Rio 2009 [38]). In the *mean tide* system, the effects of the permanent tides are included in the definition of the geoid. In the *zero tide* system, the effects of the permanent tides are removed from the gravity field definition. In the latter system not only the effects of the permanent tides are removed but the Earth's response to this removal is also taken into account. Altimetric MSS are usually expressed in the *mean tide* system.

Altimetric mean sea surfaces and geoid models don't have the same spectral content. Mean sea surfaces are usually known with a centimetric accuracy at spatial scales down to a few kilometres, while the same accuracy on the geoid is achieved using GOCE data at scales down to around 100 km. With this in mind, before subtracting a geoid from a MSS, the two fields have to be filtered in order to achieve similar spectral content. The filtering can be done either in geographical or spectral, *i.e.* spherical harmonic, space. In the latter case, the MSS needs to be completed over the continents in order to obtain a global field.

The results of preliminary analysis (Knudsen et al. 2011 [25]), using Direct (release 1) GOCE gravity field model, clearly demonstrate the potential of the GOCE mission. From the two months based model, the resolution of the MDT has been improved and the estimated surface

current speeds have been increased compared with a GRACE satellite-only MDT. Calculation of the geostrophic surface currents from the MDT reveals improvements for all of the ocean's major current systems.

Part II

METHODOLOGY

5

METHODS USED FOR DATA PROCESSING

In this chapter, the theory behind the development methodology of the Reduced Point Mass (RPM) is described. Furthermore, the gravity potential determination and its derivatives will be presented using the RPM. This is done by using the expressions for the second order derivatives of the potential in the local North-East-Up coordinate system (see appendix A). For comparison and validation of the RPM method, the Least-Squares Collocation (LSC) method for regional gravity field modeling from satellite gravity gradiometer is applied. Initially this method is described.

5.1 LEAST SQUARES COLLOCATION

LSC combines the calculation of station coordinates and other deterministic unknowns, *i.e.* harmonic coefficients, Earth ellipsoid and Earth orientation parameters, with the estimation of gravity field quantities of unsurveyed points by utilizing many types of observables Krarup 1969 [27].

The basic observation equation for LSC is

$$y_i = L_i T_{LSC} + e_i + A_i^T X \tag{5.1}$$

where X are contingent parameters, A_i is a vector connecting parameters and the observations and e_i the error contribution.

Here the contribution from a contingent datum transformation and a EGM must have been subtracted.

LSC is an overdetermined problem with respect to the parameters, *i.e.* number of observations exceeds the number of parameters, and an undetermined problem with respect to the gravity field signal, *i.e.* more signal have to be predicted than have been observed. It is solved by applying a least squares minimum condition on the weighted quadratic sum of the signal part and the noise, thus combining least squares adjustment with least squares prediction, Moritz 1980 [33].

The estimate of T_{LSC} is obtained by

$$\tilde{T}_{LSC}(P) = \{C_{Pi}\}^T \bar{C}^{-1} \{y - A^T X\} \tag{5.2}$$

where $\bar{C} = \left\{C_{ij} + \sigma_{ij}\right\}$, and σ_{ij} is the variance-covariance of the errors.

The estimates of the (M) parameters are obtained by

$$\tilde{X} = (A^T C^{-1} A + W)^{-1} (A^T C^{-1} y) \tag{5.3}$$

The error-estimates and error-covariances, ec_{kl} are found with:

$$H = \{COV(L_k, L_i)\}^T \bar{C}^{-1}, \text{ MxN matrix} \tag{5.4}$$

$$M_x^2 = (A^T \bar{C}^{-1} A + W)^{-1} \tag{5.5}$$

$$\{ec_{kl})\} = \{\sigma_{kl})\} - H\left\{cov(L_j, L_l)\right\} + HAM_X(HA)^T \tag{5.6}$$

W is the matrix of contributions from observations only related to parameters such as the differences between geodetic coordinates in a geocentric and non-geocentric datum Tscherning and Veicherts 2007 [51].

5.2 REDUCED POINT MASS METHOD

There are different implementations of the point mass methodology for geoid determination, and they are already described in many publications, see Vermeer 1995 [57].

Point-mass functions or multipole base-functions are harmonic functions, which may be used to represent the (anomalous) gravity potential T either globally or locally. The functions may be expressed by closed expressions or as sums of Legendre series. In both cases at least the two first terms must be removed since they are not present in T. For local applications the effect of a global gravity model is generally removed. This is later on restored. Then, more terms need to be removed or substituted by terms similar to the error-degree variances.

Linear combinations from the point masses functions or mass multipoles have been used for the representation of the global (W) or regional anomalous gravity potential, T, see e.g. Hauck and Lelgemann 1985 [17], Vermeer 1982 [52], 1989 [53], 1990 [54], 1992 [55], 1993 [56], Marchenko et al. 2001 [30], Wu 1984 [59], Chanfang et al. 2011 [8].

The Earth anomalous gravity field, T, at point Q is modeled by a set of base functions, each obtained as the anomalous gravity potential from each point mass m_i located at the position P_i on the surface of

the ellipsoid with radius R_M. This radius is smaller than that of the Earth, R_E.

$$T(Q) = \sum_i T_i(Q) \tag{5.7}$$

where

$$T_i(Q) = Gm_i \frac{1}{|P_i - Q|} = Gm_i \frac{1}{\sqrt{s_i^2 + z_i^2}} \tag{5.8}$$

where s is the horizontal distance and z is the height difference between the points. In this case, Cartesian coordinates are used for simplicity.

Now, any quantity associated with the gravity field may be obtained by applying a linear functional to T, *i.e.*

$$y(Q) = L(T(Q)). \tag{5.9}$$

For geoid heights the relation is simply obtained using Bruns formula:

$$N(Q) = \frac{T(Q)}{\gamma} \tag{5.10}$$

where γ is the normal gravity.

The first order derivative of the gravity potential along the z direction is:

$$\frac{\partial}{\partial z} T_i(Q) = -Gm_i \frac{z_i}{(s_i^2 + z_i^2)^{\frac{3}{2}}} \tag{5.11}$$

The vertical component of the gradients are then computed as the second order derivative of the gravity potential along z direction, *i.e.*

$$\frac{\partial^2}{\partial z^2} T_i(Q) = -Gm_i \frac{1}{(s_i^2 + z_i^2)^{\frac{3}{2}}} + 3Gm_i \frac{z_i^2}{(s_i^2 + z_i^2)^{\frac{5}{2}}} \tag{5.12}$$

Formulas shown here can be used for regional anomalous potential representation only when radial gradient component is used for gravitational potential recovery. These formulas were used as the first step in the development of the RPM method. For the use of all symmetric second order derivatives of the potential, following approach is used.

Normally a gravitational potential function is related to the position in terms of spherical coordinates (ϕ, λ, r). The spatial derivatives of interest in connection with the output from a satellite gradiometer

are all second partial derivatives with respect to a local Cartesian coordinate system at an arbitrary point in the near Earth space. As the derivatives of the potential have tensorial properties, the required transformations are conveniently derived by the methods of tensor calculus.

A geocentric system is presented by $x^p = (x, y, z)$ and in spherical coordinates by $u^p = (\lambda, \phi, r)$. The local coordinate system is described by the basis e_p with vectors in triad (e_1, e_2, e_3) that are not unit vectors. Here, a local rectangular coordinate system (η, ξ, ζ) is defined by the e_p basis, Reed 1973 [37].

The position vector of an arbitrary point P in space is given in terms of the geocentric Cartesian coordinates by:

$$r = x^P i_P = x\hat{i}_1 + y\hat{i}_2 + z\hat{i}_3 \tag{5.13}$$

Geocentric coordinates are functionally related to the spherical coordinates by:

$$x^P = x^P(u^P) \tag{5.14}$$

which is given by:

$$\begin{aligned} x &= r\cos\varphi\cos\lambda \\ y &= r\cos\varphi\sin\lambda \\ z &= r\sin\varphi \end{aligned} \tag{5.15}$$

If the potential is considered, $V = V(u^P) = V(\lambda, \varphi, r)$, the gradient of V is defined in the (x, y, z) or (η, ξ, ζ) Cartesian coordinate system in the normalized basis as (see appendix A):

$$\nabla V = \frac{1}{r\cos\varphi} V_\lambda \hat{e}_1 + \frac{1}{r} V_\varphi \hat{e}_2 + V_r \hat{e}_3 \tag{5.16}$$

First order derivatives in the local (η, ξ, ζ) system are:

$$\begin{aligned} V_\eta &= \frac{1}{r\cos\varphi}\frac{\partial V}{\partial \lambda} \\ V_\xi &= \frac{1}{r}\frac{\partial V}{\partial \varphi} \\ V_\zeta &= \frac{\partial V}{\partial r} \end{aligned} \tag{5.17}$$

And the symmetric second order derivatives of the potential, or the gravitational gradients, in the (η, ξ, ζ) system are:

$$\begin{aligned} V_{\eta\eta} &= \frac{1}{r^2 \cos^2\varphi}\frac{\partial^2 V}{\partial \lambda^2} - \frac{\tan\varphi}{r^2}\frac{\partial V}{\partial \varphi} + \frac{1}{r}\frac{\partial V}{\partial r} \\ V_{\xi\xi} &= \frac{1}{r^2}\frac{\partial^2 V}{\partial \varphi^2} + \frac{1}{r}\frac{\partial V}{\partial r} \\ V_{\zeta\zeta} &= \frac{\partial^2 V}{\partial r^2} \end{aligned} \tag{5.18}$$

5.2.1 *Closed expressions for gravity gradients when using point masses*

To expand equation 5.18 completely, a derivation of the cosine of the spherical distance with respect to the longitude and latitude needs to be carried out. Finally, expressions for the second order derivatives of the potential (and closed expressions for gravity gradients when using point masses) in the (η, ξ, ζ) system, are (see appendix A for complete derivations and simplification):

$$V_{\eta\eta} = 3\frac{r_q^2}{l^5}\cos^2\varphi_q \sin^2(\Delta\lambda) - \frac{1}{l^3} \tag{5.19}$$

$$\begin{aligned} V_{\xi\xi} = 3\frac{r_q^2}{l^5}\left(\cos\varphi_P \sin\varphi_q - \sin\varphi_P \cos\varphi_q \cos(\Delta\lambda)\right)^2 - \\ - \frac{1}{l^3} \end{aligned} \tag{5.20}$$

$$V_{\zeta\zeta} = \frac{\partial^2 V}{\partial r_P^2} = -\frac{1}{l^3} + 3\frac{(r_P - r_q t)^2}{l^5} \tag{5.21}$$

Where partial differential equation of second order satisfies *Laplacian differential equation*:

$$\begin{aligned} \Delta V &= V_{\eta\eta} + V_{\xi\xi} + V_{\zeta\zeta} \\ \Delta V &= 0 \end{aligned} \tag{5.22}$$

5.2.2 *Expressions for gravity gradients when using reduced point masses*

For the expressions of gravity gradients, when using reduced point masses, the derivative of the sum of a finite Legendre series is used:

$$S = \sum_{l=0}^{n} a_l s^{l+1} P_l(t) \tag{5.23}$$

which can be computed easily using a recursion algorithm (Tscherning and Rapp 1974 [49]). For

$$\begin{aligned} e_l &= \frac{2l+1}{l+1}s \\ f_{l+1} &= -\frac{l+1}{l+2}s^2 \end{aligned} \tag{5.24}$$

and

$$b_l = e_l t b_{l+1} + f_{l+1} b_{l+2} + a_l \tag{5.25}$$

with $b_{n+1} = b_{n+2} = 0$, we have

$$S = b_0 s \tag{5.26}$$

The derivatives of S with respect to t are then computed by a recursion algorithm obtained by equation 5.25 (Tscherning 1976 [46]):

$$b_l^1 = e_l(b_{l+1}^1 + t b_{l+1}^1) + f_{l+1} b_{l+2}^1 \tag{5.27}$$

$$b_l^2 = e_l(2b_{l+1}^2 + t b_{l+1}^2) + f_{l+1} b_{l+2}^2 \tag{5.28}$$

In this case, the expressions for the second order derivatives of the gravitational potential in η, ξ, and ζ direction are:

$$\begin{aligned} V_{\eta\eta} &= \frac{1}{r_P^2 \cos^2\varphi_P}\frac{\partial^2 V}{\partial\lambda_P^2} - \frac{\tan\varphi_P}{r_P^2}\frac{\partial V}{\partial\varphi_P} + \frac{1}{r_P}\frac{\partial V}{\partial r_P} = \\ &= \frac{1}{r_P^2 \cos^2\varphi_P}\left[\frac{\partial V}{\partial t}\frac{\partial^2 t}{\partial\lambda_P^2} + \frac{\partial^2 V}{\partial t^2}\left(\frac{\partial t}{\partial\lambda_P}\right)^2\right] - \\ &- \frac{\tan\varphi_P}{r_P^2}\frac{\partial t}{\partial\varphi_P}\frac{\partial V}{\partial t} + \frac{1}{r_P}\frac{\partial V}{\partial r_P} \end{aligned} \tag{5.29}$$

$$\begin{aligned} V_{\xi\xi} &= \frac{1}{r_P^2}\frac{\partial^2 V}{\partial\varphi_P^2} + \frac{1}{r_P}\frac{\partial V}{\partial r_P} = \\ &= \frac{1}{r_P^2}\left[\frac{\partial V}{\partial t}\frac{\partial^2 t}{\partial\varphi_P^2} + \frac{\partial^2 V}{\partial t^2}\left(\frac{\partial t}{\partial\varphi_P}\right)^2\right] + \frac{1}{r_P}\frac{\partial V}{\partial r_P} \end{aligned} \tag{5.30}$$

$$V_{\zeta\zeta} = \frac{\partial^2 V}{\partial r_P^2} \tag{5.31}$$

where partial derivatives of the spherical distance with respect to the latitude are expressed as t are(see appendix A):

$$\frac{\partial t}{\partial \varphi_P} = \cos\varphi_P \sin\varphi_q - \sin\varphi_P \cos\varphi_q \cos(\Delta\lambda)$$
$$\frac{\partial t}{\partial \lambda_P} = -\cos\varphi_P \cos\varphi_q \sin(\Delta\lambda) \tag{5.32}$$

and partial derivatives of spherical distance with respect to the longitude as:

$$\frac{\partial^2 t}{\partial \varphi_P^2} = -t$$
$$\frac{\partial^2 t}{\partial \lambda_P^2} = -\cos\varphi_P \cos\varphi_q \cos(\Delta\lambda) \tag{5.33}$$

Once the gravity field is known on the geoid or the physical surface of the Earth, an evaluation of the base function in the point at altitude provides gravity field quantities in space.

This approach is able to tailor the algorithm for point mass depth and grid spacing relations. The method provides the calculation of full gravity field quantities or reduced by using either full or reduced point masses.

Gravity and geoid determination by means of the reduced point masses can be used as an alternative method to the conventional ones for geoid determination, and they can be used to cross check the results.

5.2.3 *Least Squares estimation and regularization*

The method of least squares is a standard approach to the approximate solution of overdetermined systems, *i.e.* sets of equations in which there are more equations than unknowns. Linear relations between the GOCE gradient observations l and the unknowns expressed in terms of the point masses m, including an error, can be defined is following:

$$l_i = a^T \underline{m} + v_i \tag{5.34}$$

Using matrix notation that is:

$$l = Am + v \tag{5.35}$$

with v representing the residual vector and A being the design matrix.

Converting this system of observation equations to normal equations yields expression for the estimation of unknown point masses from the set of observations:

$$m = (A^T C_v^{-1} A + C_m^{-1})^{-1} A^T C_v^{-1} l \tag{5.36}$$

Where C_v is the covariance matrix of the observation errors and C_m is the a priori covariance matrix of the point masses associated with the parameters m.

The a posteriori error covariance matrix associated with the estimated point masses is:

$$C = (A^T C_v^{-1} A + C_m^{-1})^{-1} \tag{5.37}$$

If the covariance matrix C_m in equation 5.36 is disregarded, it can cause problems due to singularities in an estimation of a detailed model from potential field functional observations, since such an estimation typically involves a downward continuation. In that case a regularization of the equation system is required, Rummel et al. 1979 [41]. So far, various algorithms for computing a regularized solution and various methods for choosing the regularization parameter have been proposed. Usually, a diagonal matrix is added to the normal equations matrix. The matrix elements are either one, degree-dependent factors, or degree variances of the Earth's gravity field according to Kaula's rule of thumb (Kaula 1966 [21]). This diagonal matrix is scaled by a regularization parameter. In practice, the value of this scaling parameter is determined by a parameter choice rule, as explained in the chapter 7.

5.3 COMBINATION OF GEOID AND MEAN SEA SURFACE

To calculate the MDT, the GOCE direct gravity field model, release 3, was used to define the geoid to the maximum degree and order of 240. From the GOCE gradients, where long wavelength part of the gravity field up to degree and order 240 is subtracted, the geoid height anomaly was recovered. The GOCE direct based geoid was then enhanced by the geoid height anomaly recovered from the GOCE gradients. This was then subtracted from the MSS to give the unfiltered MDT.

To make a meaningful assessment of the geodetic MDT, filtering must be made.

However, because spatial filtering also attenuates MDT gradients associated with ocean currents to a degree that is proportional to the filter width, it is important to find the minimum filter radius that will adequately remove the noise, thus preserving, as far as possible, the oceanographic content of the MDT (Knudsen et al. 2011 [25]).

Finding the minimum sufficient radius can be done by repeated filtering of the MDT while gradually increasing the filter radius to find the radius at which, by visual inspection, the unrealistic short scales have been removed from the MDT. Another way is to take the non-GOCE MDT as the truth, and compare it with the resulting enhanced GOCE MDT. To perform the assessment and validation, the residuals were determined by the simple formula $r = MSS - geoid - MDT$.

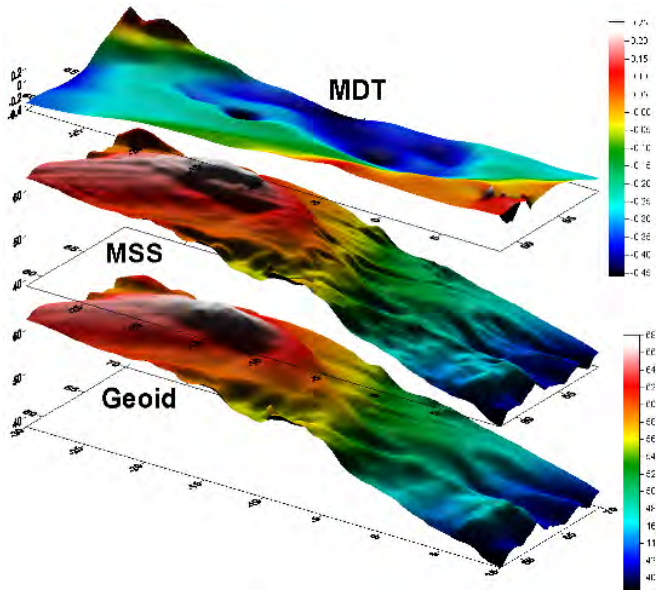

Figure 5.1: Concept of deriving mean dynamic topography (MDT) from geoid and mean sea surface (MSS). GOCINA region MDT, based on DTU10 MSS and EGM2008 geoid [m]

6

PREPROCESSING AND DATA USAGE

In this chapter, the preprocessing of the data will be explained, *i.e.* choice of the test region, explanation of the different gravity field datasets and sea surface models used throughout this work. Main focus will be on the GOCE gravity gradient data and its residuals when contribution of the long wavelength part of the global spherical harmonic models is subtracted.

6.1 TEST AREA; GEOID AND OCEAN CIRCULATION IN THE NORTH ATLANTIC (GOCINA REGION)

In the context of ocean monitoring, a major task is to determine an accurate geoid and, thereby, to create a platform for validation of future GOCE *Level 2* data and higher order scientific products. This was done in the GOCINA project in the region between Greenland and the United Kingdom, see Knudsen et al. 2006 [24]. A new and accurate geoid is used in conjunction with an accurate MSS to determine the MDT. The central quantity bridging the geoid and the ocean circulation is the MDT. The MDT provides the absolute reference surface for the ocean circulation and is, in particular, expected to improve the determination of the mean ocean circulation.

Up to the launch of GOCE, the gravimetric geoid was in general not known with sufficient accuracy to allow full use of the massive sea surface height information, which several satellite altimetry missions have regularly provided since the early 90'ies, in global analyses of the ocean circulation. However, in a few marine regions in the world, sufficient in situ information about the Earth's gravity field exists to compute a more accurate geoid. The region covering the Northern Atlantic and the Nordic seas between Greenland, Iceland, Norway, and the United Kingdom is one of those regions, *i.e.* the Northern Atlantic Ocean between Europe and Greenland from about 58N to 70N.

6.2 GOCINA GRAVITY DATA

The final gravity data consists of the shipborne and airborne data. From adjusted and combined data, an optimal solution is obtained for the complete region.

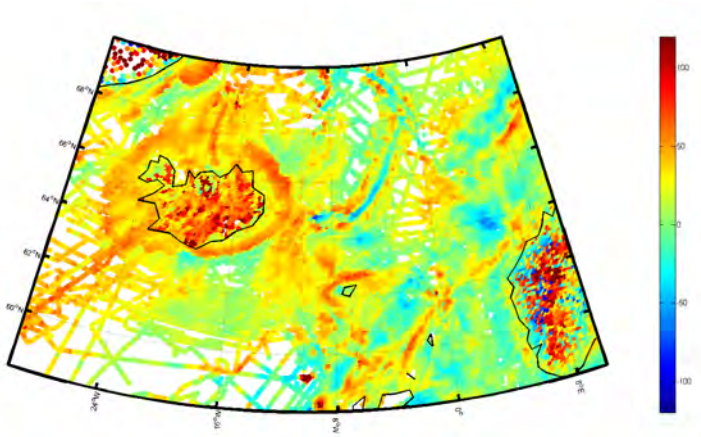

Figure 6.1: Gravity anomaly data in the GOCINA region [mgal]

GOCINA gravity data was used for a fitting of the empirical covariance function estimation.

6.3 GRAVITY ANOMALY AND GEOID HEIGHTS FROM EGM2008

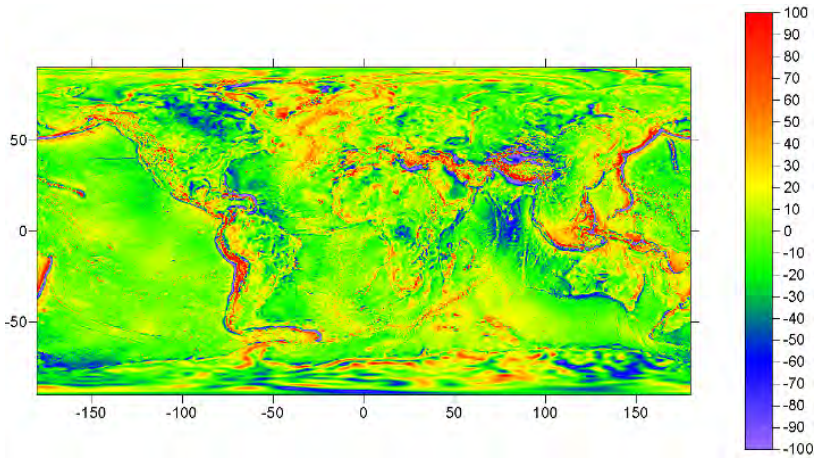

Figure 6.2: Global gravity based on the EGM2008 up to degree 2190 [mgal]

A new EGM2008 to degree 2160 has been developed by Pavlis et al. 2008 [36]. EGM2008 incorporates shipborne, airborne, and satellite altimetry derived gravity anomalies. It also has benefited from the GRACE based satellite solutions. The EGM2008 based gravity anomaly and geoid can be seen on figure 6.2 and figure 6.3, respectively.

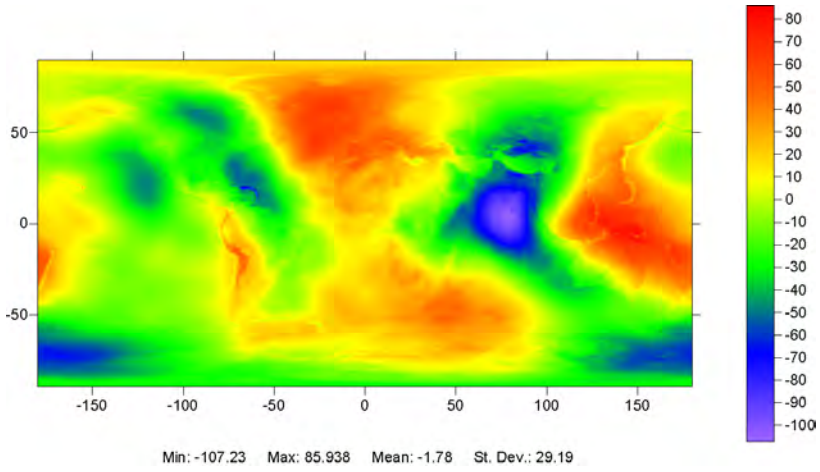

Figure 6.3: Global geoid height based on the EGM2008 up to degree 2190 [m]

6.4 GOCE GRAVITY GRADIENTS

As mentioned in chapter 3, GOCE gravity gradient data are based on 18 months of data from 31. of November 2009 to 30. of April 2011. The data obtained is available on the ESA webpage http://eo-virtual-archive1.esa.int/Index.html#EGG_TRF_2.

The available GOCE level 2 TRF data products, which are offered to the GOCE user community, are in Earth Explorers File Format Standards (EEF) format, *cf.* Floberghagen et al. 2010 [13]. This format is based on XML. However, many existing types of software are unable to use EEF formatted product, and for those cases a Extensible Markup Language (XML) parser is needed. A parser is a program that takes input in the form of sequential instructions, tags or any other defined sequence of tokens, and breaks them up into more easily manageable parts, ESA 2011 [12].

After extracting the GOCE TRF gravity gradients, 31.042.201 records were obtained. Since not all of the available data are of the same quality, some records need to be corrected, calibrated or substituted by interpolated values. Each extracted record has its a flag, and each of those have the following meaning:

- 0. Original Gravity Gradient
- 1. As 0. with temporal corrections added
- 2. As 1, externally calibrated Gravity Gradient
- 3. Outlier suspected, fill-in provided
- 4. Outlier suspected, no fill-in, value is calibrated original value
- 5. Data gap, fill-in provided
- 6. Data gap, no fill-in

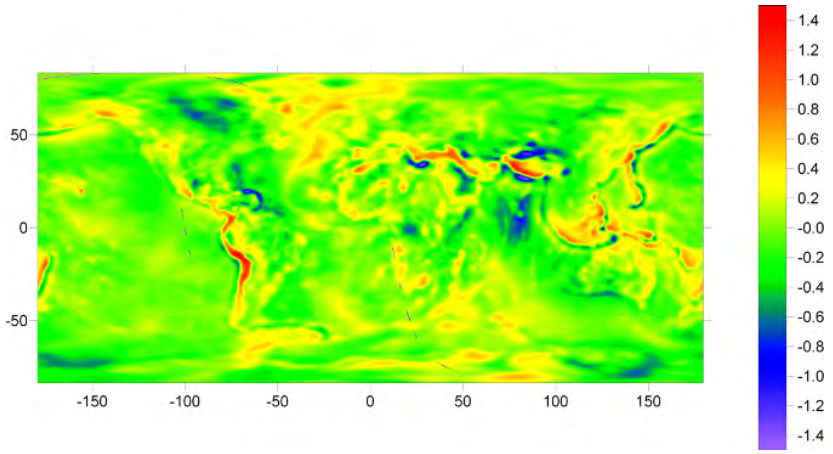

Figure 6.4: GOCE T_{zz} gradient component [E]

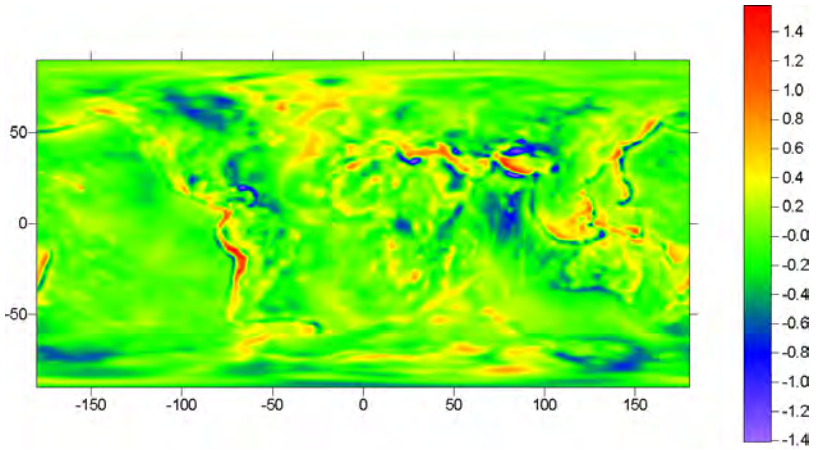

Figure 6.5: Global vertical gradient at mean GOCE altitude (260km), based on the EGM2008 up to degree 2190 [E]

Extracted gravity gradients were then filtered, and only original and externally calibrated gravity gradients were used. After filtering, 30.986.909 records of GOCE gravity gradients were obtained, and they were distributed all over the Earth except for in the polar regions. Figure 6.4 shows the T_{zz} GOCE gradient components, while for comparison EGM2008 based T_{zz} gradient components can be seen on figure 6.5.

Even though the GOCE gradient dataset shown on figure 6.4 contains just data records with flags 2 and 3, and it is then edited with the threshold of 0.03 Eötvös for the errors (figure 6.6), it still contains some gross errors, which can be easily detected on figure 6.4.

From filtered GOCE gravity gradients, observations in the GOCINA region was extracted. The GOCE gravity gradient dataset over the GOCINA region contains 237.897 observations for the T_{xx}, T_{yy} and T_{zz} components.

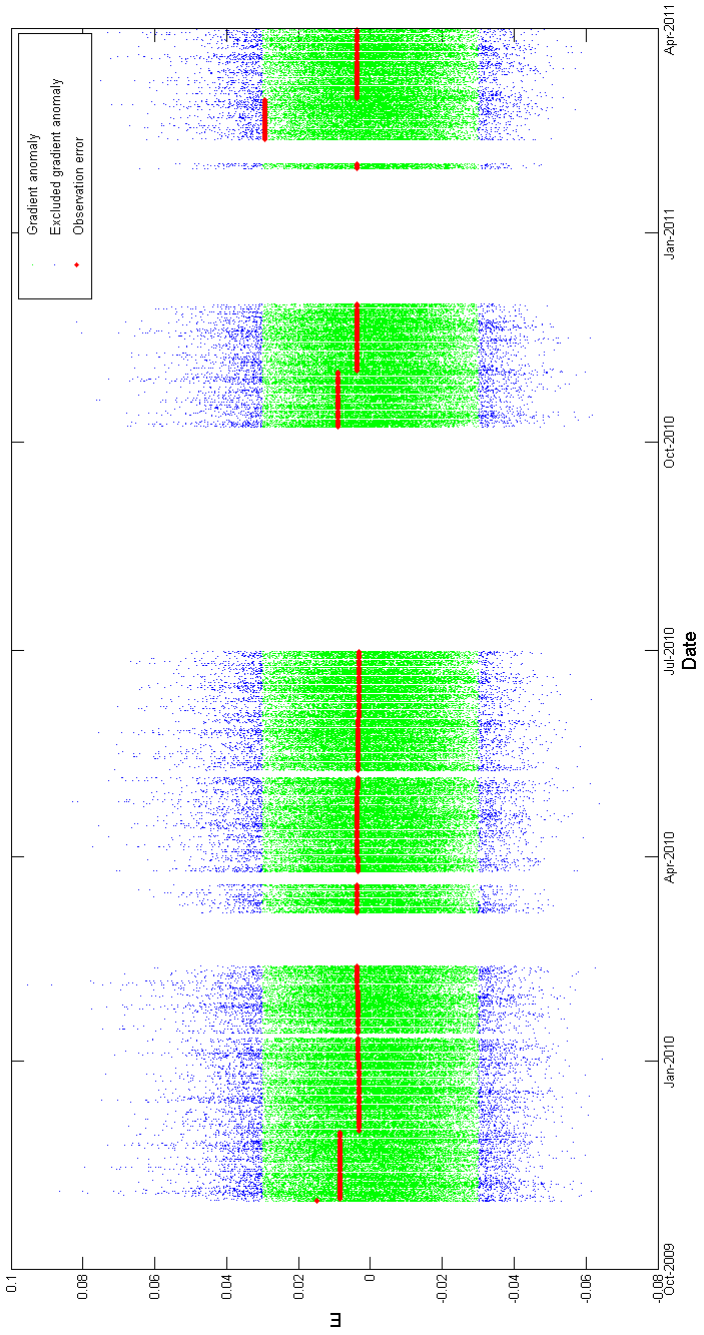

Figure 6.6: GOCE T_{zz} dataset with associated errors throughout the mission span

6.5 MEAN SEE SURFACE DATA

In this study, the DTU10 mean sea surface is used. It is an update of the DNSC08 mean sea surface model (Andersen and Knudsen 2009 [2]).

The DTU10MSS is the time averaged ellipsoidal height of the ocean's surface computed from a combination of satellite altimetry using a total of 8 different satellite missions now covering a period extending to 17 years (1993-2009). The MSS has been derived using a 2-step procedure where a coarse long-wavelength MSS is initially determined from 17 years of temporally averaged mean profiles from TOPEX and JASON-1 merged with the adjusted 8-year mean profiles from ERS-2 and Environmental Satellite (ENVISAT). The MSS is global in coverage; the MSS of the Arctic Ocean to 86.N has been mapped by including laser altimetry from National Aeronautics and Space Administration (NASA)'s Ice, Cloud, and land Elevation Satellite (ICESat) mission. Remaining polar gaps and grid points corresponding to land are filled by interpolation based on a geoid model (Andersen 2011 [1]). Figure 6.8 shows the DTU10 mean sea surface.

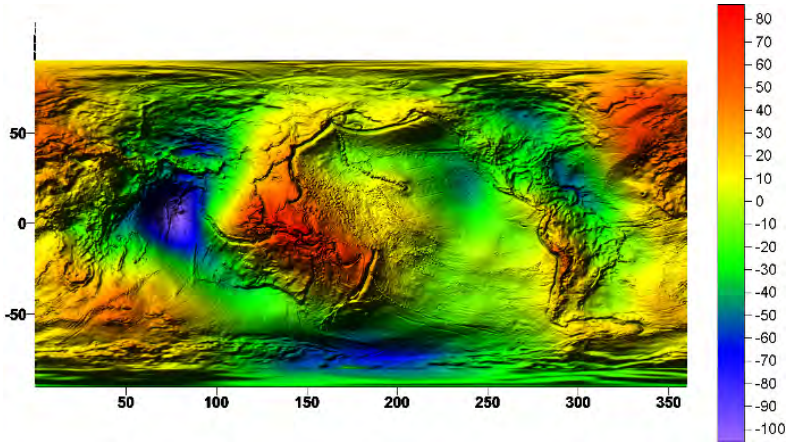

Figure 6.7: DTU10 Mean Sea Surface [m]

6.6 MEAN DYNAMIC TOPOGRAPHY DATA

The mean dynamic topography data is normally defined as the difference between the MSS data and the geoid by using equation 4.2.

In this study three MDT were used as a reference. One of them is the DTU10 MDT. DTU10 MDT was derived by differencing the DTU10 MSS (figure 6.7) and the EGM2008 based geoid (figure 6.7). Using a mean and 3 times standard deviation of the local difference, MSS and geoid outlier inspection was made for all data within each 1 degree region. Finally, the DTU10 MDT was created by reinterpolating the edited data onto the same 1 min grid using a correlation length of 75 km in order

to smooth the grid (Andersen 2011 [1]). The DTU10 MDT is shown on figure 6.8.

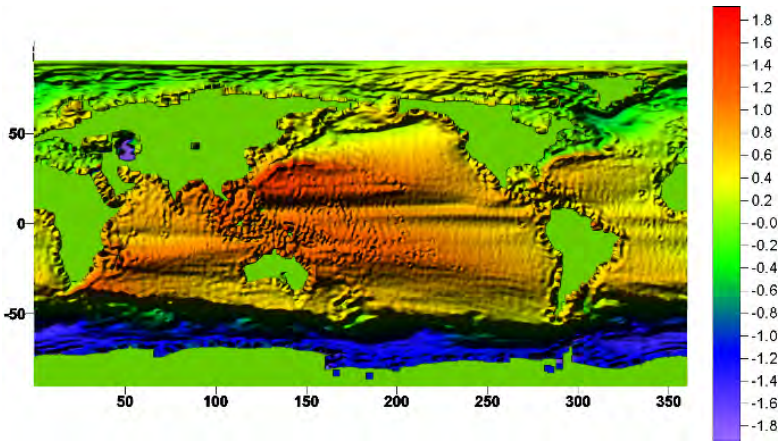

Figure 6.8: DTU10 Mean Dynamic Topography [m]

The second MDT, which is also used as a reference, is the GOCINA Interative Combination Method (ICM) MDT, see figure 6.9. The method of ICM MDT solution involves a starting model for MDT and integrates shipborne, airborne and satellite altimetry derived gravity anomalies, with ocean models. Then it predicts a *better* version of MDT. This is now used for the first MDT and the procedure iterated until the inserted MDT is consistent with the predicted MDT, *cf.* Knudsen 2005 [23].

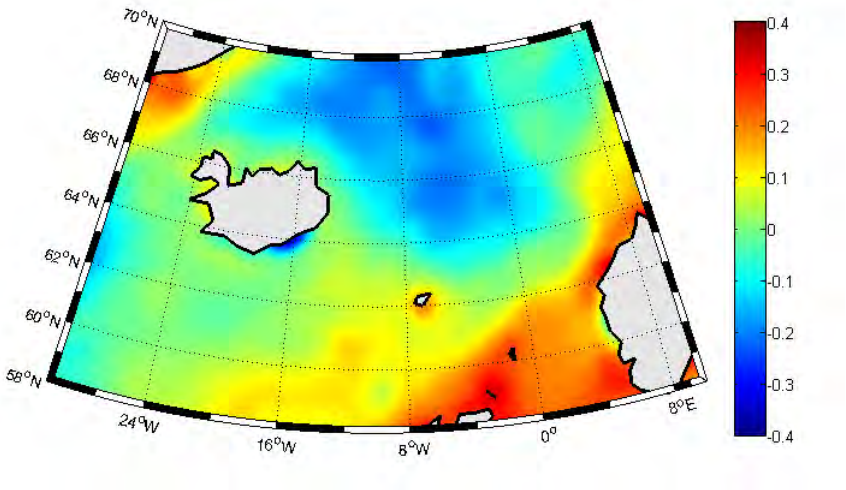

Figure 6.9: GOCINA Mean Dynamic Topography (meters)

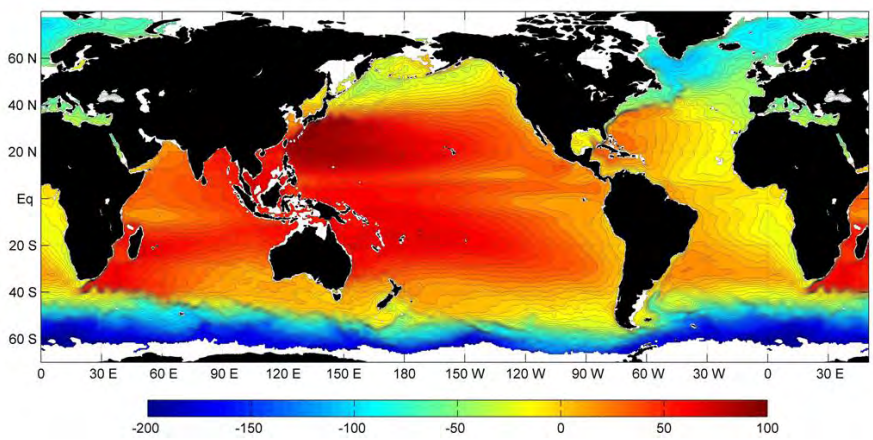

Figure 6.10: Maximenko Mean Dynamic Topography (meters)

The third MDT used here is Maximenko MDT, *i.e.* The 1992-2002 MDT. This MDT is derived by the GRACE satellite data and drifting buoy data using three different techniques. The first method combines sea level observed by the high-accuracy satellite radar altimetry with the geoid model of the GRACE. The second one synthesizes near-surface velocities from a network of ocean drifters, hydrographic profiles, and ocean winds sorted according to the horizontal scales. In the third method, these global datasets are used in the context of the ocean surface momentum balance. Then the second and third methods are used to improve accuracy of the dynamic topography on fine space scales poorly resolved in the first method. When they are used to compute a multiyear time-mean global ocean surface circulation, both contain very similar, new small-scale midocean current patterns, see Maximenko et al. 2009 [31]. Global Maximenko MDT can be seen on the figure 6.10.

Part III

APPLICATION OF METHODS AND VALIDATION

7

RESULTS AND ANALYSIS

This chapter presents the work that has been done on modelling gravity field using GOCE gravity gradients. Firstly, it is described how the methods have been implemented, *i.e.* how the covariance function and the distribution of the point masses were designed. The tests of the RPM method are shown where the long wavelength part of the gravity field up to harmonic degree and order 100 is subtracted from the gravity gradients. Validation of the RPM method is done by the comparison of its results with the LSC method. Then, the modelling of the residual geoid heights by the RPM method, where the complete GOCE Direct model up to harmonic degree and order 240 is subtracted from the gravity gradients, is presented. From the produced residual geoid heights, the enhanced GOCE based geoid is calculated. The recovered enhanced geoid heights are then used for the estimation of the new MDT and ocean's geostrophic circulation in the GOCINA region.

Gravity anomaly residuals recovery from GOCE gradient data using LSC in different areas of the Earth was recently investigated by Tscherning and Arabelos 2011 [48]. There, GOCE vertical (T_{zz}) and along track (T_{yy}) gravity anomalies were used, where the long wavelength part of the gravity field up to degree 36 was subtracted. The best results were obtained in areas with a smooth gravity field, where the difference between the predicted LSC and surface gravity anomalies was *12 mgal*. The investigation in Tscherning and Arabelos 2011 [48] shows that additional use of T_{yy} gravity gradient anomalies provides marginal improvement of the results obtained when only using T_{zz}.

The main objective of this chapter is to show the significance of the remaining signal in the GOCE gravity gradients when subtracting the long wavelength part of the gravity field. Removal of the long wavelength part of the gravity field is done with different global gravity field models, *i.e.* EGM2008 when subtracting the long wavelength part up to harmonic degree and order 100 and GOCE Direct Release 3 model when subtracting the long wavelength part up to harmonic degree and order 240.

The remaining signal of the produced GOCE gradient anomalies is used to recover the shorter wavelength part of the gravity field and geoid by two methods, namely the LSC and the RPM (previously described in chapter 5).

For these calculations, only records from the GOCINA region were used. This results in a dataset containing 237.897 observations.

Even though the used dataset is the GOCE Release 3 gradient product in TRF, some observations have higher errors than expected, *i.e.* larger than 0.03E (Eötvös). For this reason, gradient anomalies are filtered, and all observations with errors exceeding this limit are excluded. This leaves 209.282 observations in the GOCINA region.

For the collocation solution, the program GEOCOL from the Gravsoft package is used. The primary function of the program is the computation of an approximation to the anomalous potential of the earth, T, using least squares collocation, see Tscherning 2005 [47].

The large amount of data is not feasible in GEOCOL, so the observations closest to the knots of a $0.1° \times 0.2°$ grid are selected and used in the further calculation. The selected dataset for GEOCOL collocation solution contains 24.116 observations.

7.1 TRUNCATION OF THE LONG WAVELENGTH PART OF THE GRAVITY FIELD QUANTITIES

The Stokes integral or similar formulae, used to estimate global models of the gravity field, are based on the solution of the external boundary value problem for the anomalous potential T. This approach assumes the disturbing potential to be harmonic on the geoid, which implies that there are no masses outside the geoid. In the case of local gravity field modelling, masses outside of the designed area must be considered. Truncation of the long wavelength of the gravity field in local gravity field modelling ensures that the contribution of the masses outside the area can be neglected.

In order to produce the gravity anomaly, geoid height anomaly and gradient anomaly grid in GOCINA region, the long wavelength part of the gravity field must be subtracted from these gravity field quantities. Figures 7.1, 7.2 and 7.3 show the residual signal of these quantities produced when the EGM2008 global model up to harmonic degree and order 100 is subtracted. These figures can be compared to those containing the full power of each quantity: figure 6.2 with the full EGM2008 based gravity anomaly, 6.3 with the full EGM2008 based geoid heights and 6.5 with full T_{zz} component of the GOCE gradients.

Two are investigated here: one in which the long wavelength part of the gravity field up to spherical harmonic degree and order 100 is subtracted to show that both methods give similar results, and the other in which spherical harmonic degree up to degree and order 240 is subtracted. The latter case is necessary for investigation if remaining

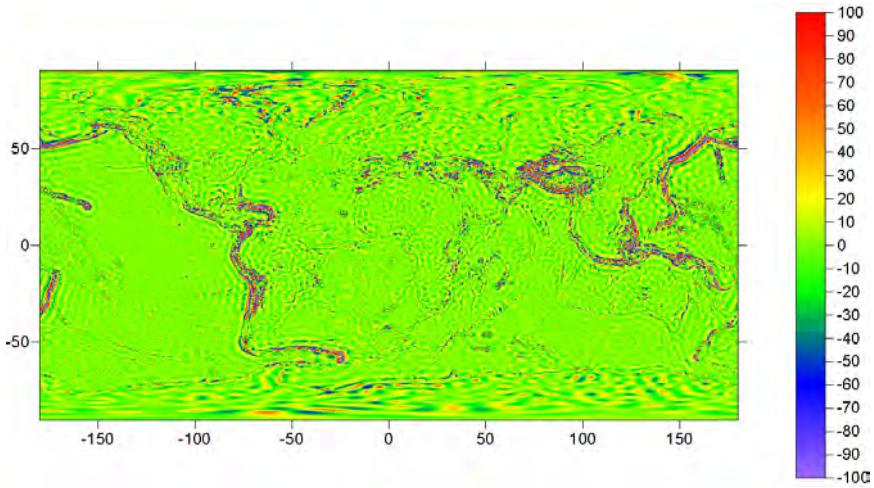

Figure 7.1: EGM2008 based global gravity anomaly residuals, when EGM2008 up to harmonic degree and order 100 is subtracted [mGal]

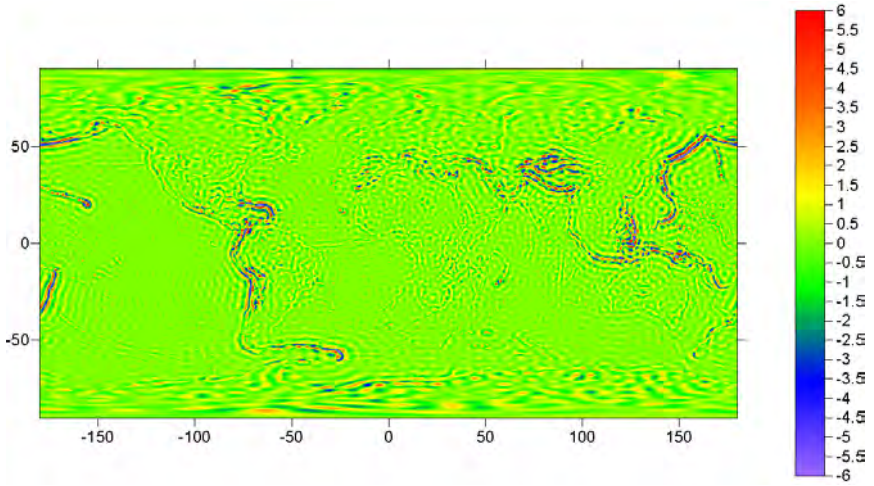

Figure 7.2: EGM2008 based global geoid height anomaly, when EGM2008 up to harmonic degree and order 100 is subtracted [m]

signal in the GOCE gradients can be used for recovery of the gravity field short wavelength part that is not present in the GOCE models.

For prediction of the remaining signal in these gravity field quantities, the long wavelength part of the gravity field needs to be subtracted not only from the input GOCE gradients, T_{yy} and T_{zz}, but also from the predicted functionals, the geoid height and the gravity anomaly. This was done with the Fortran program GEOCOL. Both geoid height and gravity anomaly are calculated by the use of the EGM2008 spherical harmonics set up to degree and order 2190, predicted on a grid with spacing $0.1^\circ \times 0.2^\circ$.

In the next subsections different gravity field quantities, *i.e.* gravity anomaly, geoid heights and gravity gradients, in full power and just short wavelength residuals, will be presented.

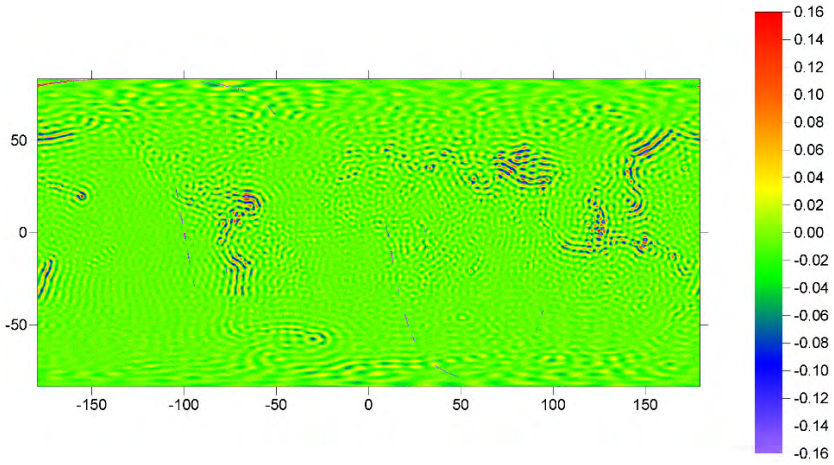

Figure 7.3: Global T_{zz} GOCE gradient anomalies at flight altitude, when EGM2008 up to harmonic degree and order 100 is subtracted[E]

7.1.1 *Gravity anomaly and gravity anomaly residuals derived from different gravitational models*

Gravity grids were created from spherical harmonic coefficients of four different global models; EGM2008, GOCE Direct, GOCE Space wise and GOCE Time wise. Figure 7.4 shows the gravity anomaly based on EGM2008 and GOCE models in the GOCINA region, and statistics are given in table 7.1.

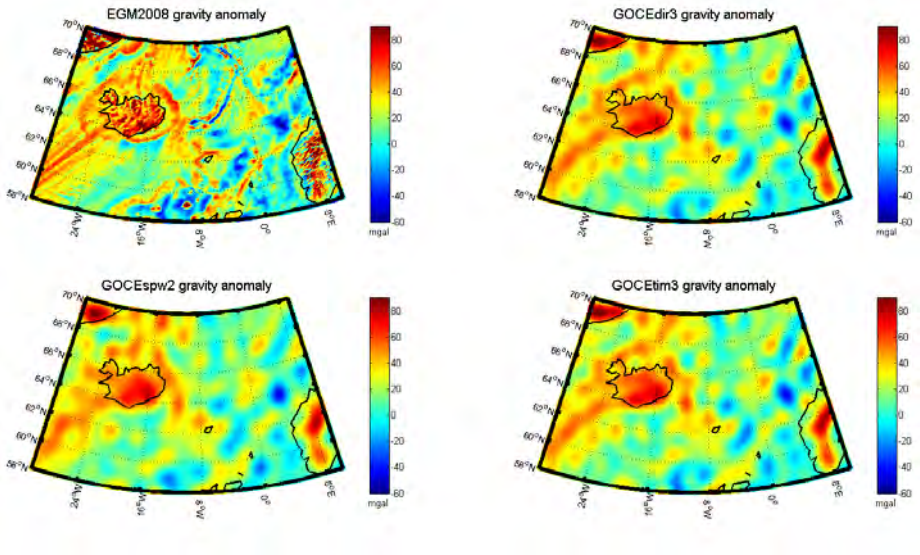

Figure 7.4: Gravity anomaly based on EGM2008 (up to harmonic degree and order 2190), GOCE Direct release 2 (up to harmonic degree and order 240), GOCE Space Wise release 1 (up to harmonic degree and order 210) and GOCE Time Wise release 2 (up to harmonic degree and order 250) global models (up to harmonic degree and order 2190) models

MODEL	MIN	MAX	MEAN	STD. DEV.
Gravity anomaly				
EGM2008	-129.77	284.50	23.21	25.28
GOCE Direct 3	-42.09	97.66	23.12	19.33
GOCE Space wise 2	-43.14	91.99	23.05	18.91
GOCE Time wise 3	-47.12	93.85	23.11	19.73
GOCINA Observations	-106.69	245.74	21.76	26.65
Gravity anomaly residuals				
EGM2008	-161.84	244.72	0.38	20.04
GOCE Direct 3	-38.53	60.02	0.28	11.89
GOCE Space wise 2	-36.70	56.89	0.22	11.23
GOCE Time wise 3	-42.70	55.61	0.27	12.54
GOCINA Observations	-148.70	205.65	-1.03	22.12

Table 7.1: Statistics of the gravity anomaly [mGal] and the gravity anomaly residuals [mGal] in GOCINA region based on observations and different global models (up to maximum harmonic degree of each model: EGM2008 is 2190, GOCE Direct 3 is 240, GOCE Space wise 2 is 210 and GOCE Time wise 250)

It is clear from figure 7.4 that the gravity anomaly based on the EGM2008 global gravitational model contains details not present in the GOCE based solution. This is not a surprise, since the EGM2008 incorporates shipborne, airborne, and satellite altimetry derived gravity anomalies. It also includes satellite based solutions from over a decade of observations from the GRACE mission (*cf.* Pavlis et al. 2008 [36]).

While the GOCE models are based on only 18 months of data, *i.e.* from 1^{th} of November 2009 until 17^{th} of April 2011. Comparison of the gravity anomaly from the GOCE based models shows that the Direct Release 3 and the Time-wise Release 3 reveal the same low frequency features as gravity anomalies from the EGM2008 global model. In the case of gravity anomalies derived by the Space-wise Release 3 approach, features of the field are not so clear as they are in the other two GOCE based gravity anomaly grids. This can also be seen from the statistics, where statistics of EGM2008 based gravity anomaly or gravity anomaly residuals follow the values of the GOCINA observations. In the case of GOCE based gravity anomaly and gravity anomaly residuals, statistic are showing smooth fields with small standard deviations. The Space-wise release 2 shows the biggest deviation from the GOCINA

observables. *i.e.* gravity anomaly and gravity anomaly residuals based on the EGM2008 global model.

7.1.2 *Geoid height and geoid height anomaly derived from different gravitational models*

Here, the geoid heights based on different geopotential models are presented. As a reference, geoid heights based on the EGM2008 are used, which are then compared with those based on the new GOCE geopotential models.

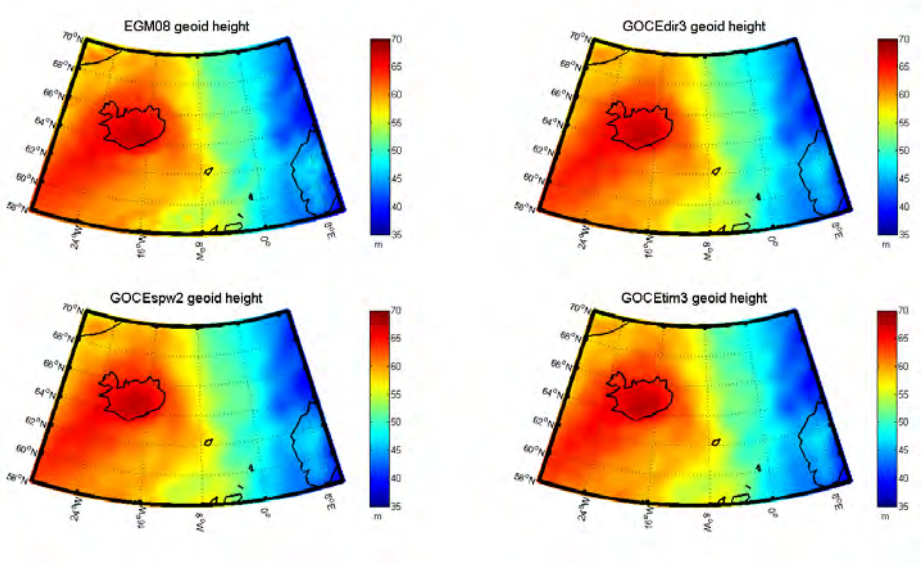

Figure 7.5: Geoid heights based on EGM2008 (up to harmonic degree and order 2190), GOCE Direct release 3 (up to harmonic degree and order 240), GOCE Space Wise release 2 (up to harmonic degree and order 210) and GOCE Time Wise release 3 (up to harmonic degree and order 250) global models (up to harmonic 2190) models

Figure 7.5 shows geoid heights based on different geopotential models. It is hard to see any difference in all the presented geoid heights, but that is not the case if the geoid height anomalies are compared. On figure 7.6, geoid heights anomalies are shown, when the EGM2008 based geoid up to harmonic degree 100 is subtracted. Like in gravity anomaly residuals, here we also see similar differences between different solutions. In particular, the EGM2008 based geoid height anomalies reveal high frequencies, which are not present in the GOCE solutions. Geoid height anomalies based on the GOCE Direct Release 3 and Time-wise Release 3 geopotential models again show signal similarities with the EGM2008, while the solution based on the GOCE Space-wise Release 2 is smoother.

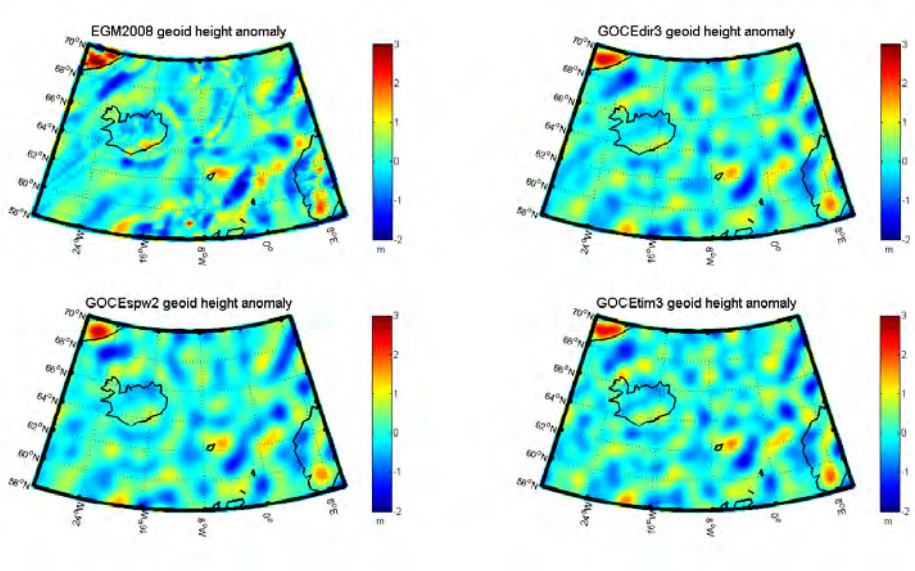

Figure 7.6: Geoid height anomalies when the EGM2008 based geoid up to harmonic degree 100 is subtracted

MODEL	MIN	MAX	MEAN	STD. DEV.
Geoid height				
EGM2008	37.67	68.04	54.97	7.52
GOCE Direct 3	37.34	67.35	54.96	7.51
GOCE Space wise 2	37.52	67.43	54.97	7.51
GOCE Time wise 3	37.58	67.53	54.96	7.51
Geoid height anomaly				
EGM2008	-1.96	3.77	0.02	0.58
GOCE Direct 3	-1.52	2.72	0.01	0.52
GOCE Space wise 2	-1.59	2.74	0.01	0.51
GOCE Time wise 3	-1.59	2.57	0.01	0.53

Table 7.2: Statistics of the geoid height [m] and the geoid height anomaly [m] in GOCINA region based on observations and different global models (up to maximum harmonic degree of each model: EGM2008 is 2190, GOCE Direct 3 is 240, GOCE Space wise 2 is 210 and GOCE Time wise 250)

7.1.3 *GOCE gradients and gradient anomaly*

For prediction of the gravity anomaly residuals and geoid heights, the GOCE gradient observations in the GOCINA region are used. Figure 7.7 shows the dense distribution of T_{yy} and T_{zz} GOCE gradients in the GOCINA region and its power in Eötvös units. Since the power of the T_{yy} component is not as strong as that of the T_{zz}, a different color bar scaling is used. In table 7.3, statistics of these two input datasets are presented, where differences can again be seen by comparing the standard deviation of the two gradient components.

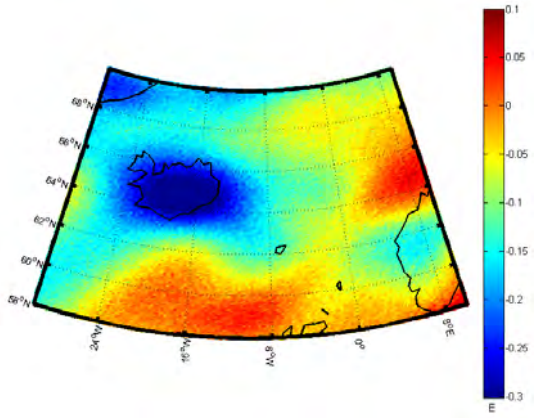

(a) GOCE T_{yy} gradient at satellite altitude

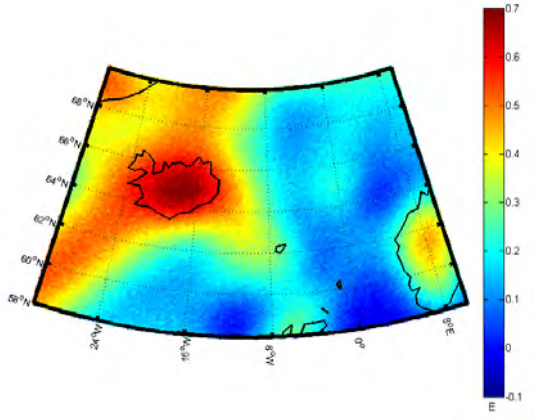

(b) GOCE T_{zz} gradient at satellite altitude

Figure 7.7: GOCE T_{yy} gradient at satellite altitude (a), GOCE T_{zz} gradient at satellite altitude (237.897 observation) (b)

Table 7.3: GOCE Tyy and Tzz gradient statistics in the GOCINA region

Model	Min	Max	Mean	Std. Dev.
Tyy gradient	-0.38	0.09	-0.10	0.08
Tzz gradient	-0.05	0.73	0.28	0.16

MODEL	MIN	MAX	MEAN	STD. DEV.
	T_{yy} **gradient anomaly**			
EGM2008	-0.0536	0.0438	-0.0044	0.0112
GOCE Direct 3	-0.0537	0.0439	-0.0044	0.0112
GOCE Space wise 2	-0.0532	0.0438	-0.0044	0.0113
GOCE Time wise 3	-0.0535	0.0435	-0.0043	0.0112
	T_{zz} **gradient anomaly**			
EGM2008	-0.0625	0.0753	-0.0059	0.0162
GOCE Direct 3	-0.0625	0.0760	-0.0059	0.0161
GOCE Space wise 2	-0.0637	0.0762	-0.0059	0.0162
GOCE Time wise 3	-0.0624	0.0754	-0.0059	0.0162

Table 7.4: GOCE T_{yy} and T_{zz} gradient anomaly statistics when the contribution from different models up to harmonic degree and order 100 are subtracted

Prediction of the gravity anomaly residuals and geoid heights will be carried out using the GOCE gradient dataset. Since the remove-restore method is used in this case, the long wavelength part of the gravity field is subtracted from the input GOCE gradients as well. Removal of the long wavelength part of the gravity field up to harmonic degree and order 100, from the input T_{yy} and T_{zz} gradient data, was carried out with different global models. Statistics of the results, *i.e.* calculated gravity gradient anomalies, are shown in table 7.4.

The mean value of -0.0044E and the standard deviation of 0.0112E in table 7.4 are showing very good agreement of the predicted gravity gradient anomalies when the contribution from different models up to harmonic degree and order 100 is subtracted.

Figure 7.8 shows the resulting T_{yy} and T_{zz} gradient anomaly when the EGM2008 up to harmonic degree and order 100 is subtracted.

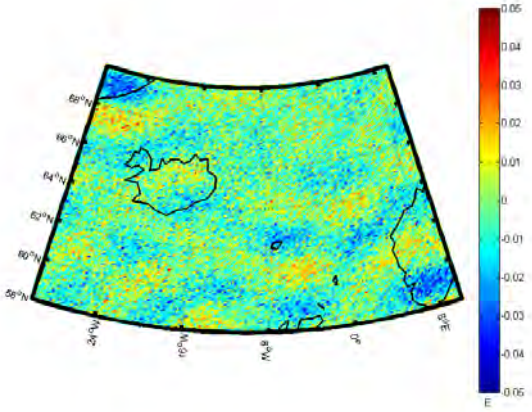

(a) GOCE T_{yy} gradient anomaly reduced EGM08 up to degree and order 100

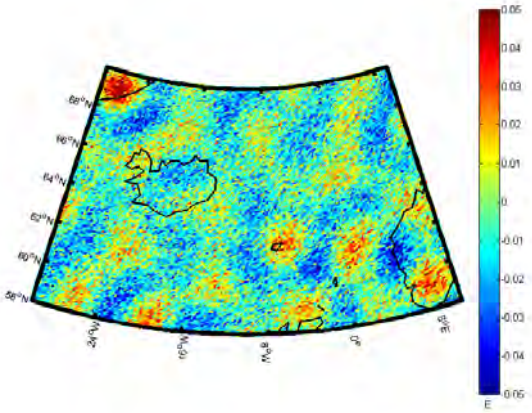

(b) GOCE T_{zz} gradient anomaly reduced EGM08 up to degree and order 100

Figure 7.8: GOCE T_{yy} and T_{zz} gradient anomaly when the EGM2008 up to harmonic degree and order 100 is subtracted

7.2 EMPIRICAL COVARIANCE FUNCTION ESTIMATION

Gravity anomalies are related to the anomalous potential through linear functionals, and the value of the covariance between two quantities is then obtained by applying the linear functionals on the covariance function of the anomalous potential. In local areas, one first removes the long wavelength part of the gravity field, and then the expression representing the local empirical covariance function is applied to the residual data.

Goad et al. 1984. [16] defined a local covariance function as a special case of a global covariance function where the information content of wavelengths longer than the extent of the local area has been removed. The information outside, however nearby, the area is assumed to vary in a manner similar to the information within the area.

Assume that T' is the anomalous potential, where the information content of wavelengths longer than the extent of the local area (φ_1, φ_2, λ_1, λ_2) is subtracted, and that L and L' are two linear functionals associated with the observations $y = L(T')$ and $y' = L'(T')$ located at (φ, λ), (φ', λ'). If the averages over the area are zero, then the local covariance of y or the local crosscovariance between y and y' is given by:

$$C(\psi) = \frac{1}{A} \int_{\varphi_1}^{\varphi_2} \int_{\lambda_1}^{\lambda_2} \frac{1}{2\pi} \int_0^{2\pi} yy' d\alpha \cos(\varphi) d\varphi d\lambda \tag{7.1}$$

where ψ is the spherical distance, A is the size of the area on the unit sphere, and α is the azimuth.

The representation of the covariance function is calculated as an average of the products yy' over the area and an average over the azimuth.

In practice, the observations are given in discrete points in the area and the calculation of the covariance is then done by numerical integration. If the area is subdivided into small cells holding one observation each, and the size of the areas A are assumed to be equal, then the equation is the following:

$$C(k) = \frac{\sum y_i y_j'}{N_k} \tag{7.2}$$

where N_k is the number of products, $y_i y_j'$, in the k^{th} interval.

Suppose T is expanded into spherical harmonics, and a global gravity potential approximation up to degree N is subtracted in order to obtain T'. Then the covariance function, $K(\psi)$, associated with T' is

expressed by a sum of a series of Legendre polynomials of order i, P_i, as a reproducing kernel (*cf.* Tscherning and Rapp 1974 [49]).

$$K(\psi) = \sum_{i=0}^{N} \epsilon_i(T,T) \left(\frac{R_E^2}{rr'}\right)^{i+1} P_i(\cos\psi) + \\ + \sum_{i=N+1}^{\infty} \sigma_i(T,T) \left(\frac{R_E^2}{rr'}\right)^{i+1} P_i(\cos\psi) \tag{7.3}$$

where $\epsilon_i(T,T)$ are the error degree variances related to the potential coefficient set, $\sigma_i(T,T)$ are the potential degree variances, r, r' are the radial distances of y and y', R_E is the mean Earth radius, and R_B is the radius of a Bjerhammar sphere ($R_B < R_E$).

The integer N, relative to the size of the local area, is supposed to fulfill the condition that $\frac{2\pi}{N}$ is smaller than the size of the area where the covariance function is determined.

The degree variances are positive numbers and are related to the spherical power spectrum of the Earth's gravity field. It is well-known that the degree variances tend to zero somewhat faster than i^{-3} and that the *Tscherning - Rapp model 4* is a reasonable choice for degree variances, Tscherning and Rapp 1974 [49].

$$\sigma_i(T,T) = \frac{A}{(i-1)(i-2)(i+4)} \left(\frac{R_B}{R_E}\right)^{2i+2} \tag{7.4}$$

where A is constant in units of $\frac{m}{s^4}$.

When fitting covariance functions, the error degree variances $\epsilon_i(T,T)$ are multiplied by a scaling factor a.

Analytic covariance models are used in LSC. By fitting an analytic model to empirically determined values (e.g. using the program *EMPCOV* on data in a certain region), a covariance function optimal for this region is selected. An analytic model of that kind used in this program is furthermore harmonic in two variable points, P and Q, and positive definite. This assures that the error estimates calculated using LSC are positive. The program *EMPCOV* is a part of *GRAVSOFT* package and it computes an empirical covariance function of vector quantities on a spherical surface by taking the mean of the product sums of samples of scalar values or of the longitudal and transversal components of vector quantities. In order to compute the empirical covariance of anomalous quantities, error degree variances of the reduced part must be included, in this case EGM2008 and GOCE direct model. To compute gravity anomaly degree-variances and error-degree variances from a set of spherical harmonic coefficients from global models, the Fortran program *degv.for* is used. The degree-variances are referred to the mean Earth radius.

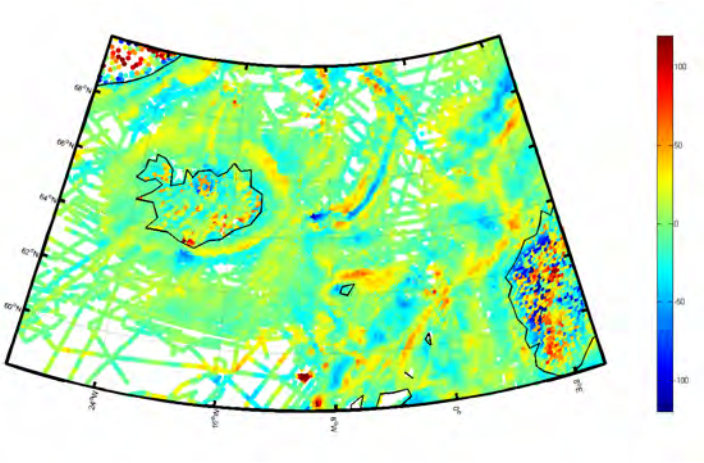

Figure 7.9: GOCINA observed gravity anomaly residuals (subtracted EGM2008 up to harmonic degree and order 100)

Figure 7.9 shows the GOCINA region gravity anomaly residuals where long wavelength part, based on EGM2008, up to harmonic degree and order 100 is subtracted.

Empirical covariance estimations and covariance fitting in GOCINA region was done with three different datasets, *i.e.* all gravity anomalies (figure 7.10), marine gravity anomalies (figure 7.11) and GOCE T_{zz} gradient anomalies (figure 7.12).

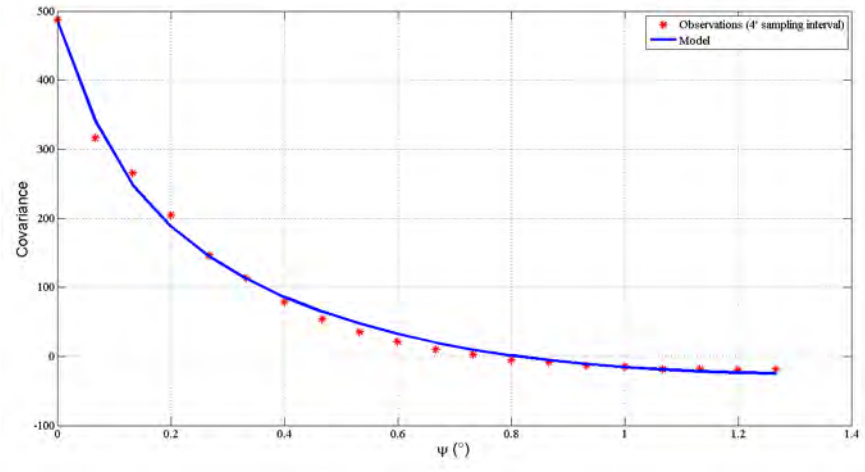

Figure 7.10: Empirical covariance estimations based on all gravity anomaly (ground and marine) in the GOCINA region

To fit empirical covariance functions to isotropic analytic models, the Fortran program *covfit.f* from *GRAVSOFT* package was used, Knudsen 1987 [22]. The variance in each empirical covariance function is reduced for noise, assuming the uncorrelated noise. To be more precise, the gravity anomaly variance is reduced by 25 *mgal* (from 487.88

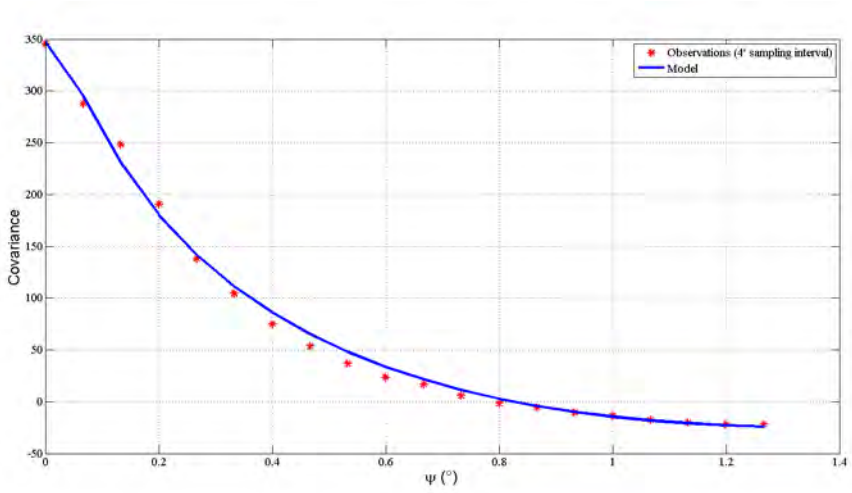

Figure 7.11: Empirical covariance estimations based on just marine gravity anomaly in the GOCINA region

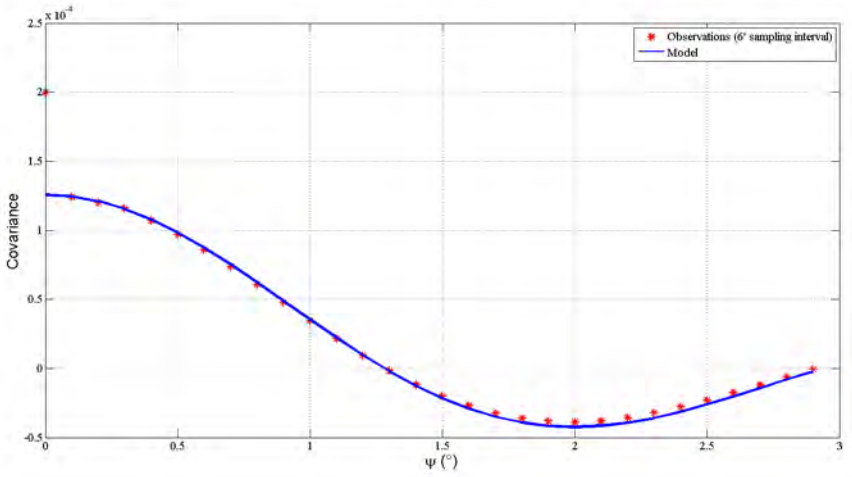

Figure 7.12: Empirical covariance estimations based on GOCE T_{zz} gradient anomalies (EGM2008 up to degree and order 100 is subtracted) available in the GOCINA region

mgal to 462.88 *mgal*), the marine gravity anomaly variance is reduced by 30 *mgal* (from 345.53 *mgal* to 315.53) *mgal* and the gradient variance is reduced by 0.024 *mE* (from 0.1997 *mE* to 0.1757 *mE*).

The parameters obtained by fitting the covariance (table 7.5, where all gravity anomaly values are used) function were used for collocation prediction and reduced point mass solution.

From table 7.5 it can be seen that the empirical covariance function cannot be estimated well by the GOCE gradients alone (if the correlation error or error covariance function of the GOCE gradients is not included). Here, the scaling factor a estimated by the GOCE gradients has a value of 6.3677, which is two orders of magnitude higher than the one estimated by the gravity anomaly observations, *i.e.* 0.0842 . In

a	A	$R_E - R_B$	σ^2	CORRELATION LENGTH
All gravity anomaly				
0.1412	$0.7090 \cdot 10^6$	−1219.83	470.30	0.168
Marine gravity anomaly				
0.0842	$0.7669 \cdot 10^6$	−3503.56	323.13	0.243
GOCE gradients				
6.3677	$0.5918 \cdot 10^6$	−144.96	699.67	0.580
Gravity anomaly and GOCE gradients				
4.9619	$0.6883 \cdot 10^6$	−1118.45	472.18	0.168 (gravity) / 0.580 (gradients)
Marine gravity anomaly and GOCE gradients				
5.0028	$0.7427 \cdot 10^6$	−3300.11	324.20	0.243 (gravity) / 0.580 (gradients)

Table 7.5: Parameters for fitting of the covariance functions in GOCINA region using different datasets. The parameters are: scaling factor a, constant in units of $\frac{m}{s^4}$ A, depth of Bjerhammar sphere ($R_E - R_B$) in meters, variance σ^2, and correlation length in degrees

case of the depth of the Bjerhammar sphere, estimation by the GOCE gradients gives a value of only −145m, while the estimation by the gravity anomaly observations gives −1219m. The reason for this is the altitude of the GOCE measurements and attenuation of the gravity field signal at the 250km altitude, where it fails to capture the fine details of the gravity field.

In the regions where ground data is not known, parameters for fitting of the covariance functions cannot be estimated well by the GOCE gradients alone. However, these can be estimated by altimetry based gravity anomalies.

7.3 COLLOCATION RESULTS

LSC uses an analytical signal covariance function fitted to the empirical covariance function data estimates to determine the geoid and its errors. Here, prediction of the gravity anomaly residuals and the geoid height anomalies by the LSC will be presented.

7.3.1 *Collocation prediction of gravity anomaly in GOCINA region*

To investigate if a higher accuracy or resolution could be obtained by the direct use of GOCE satellite gradients at orbit altitude (*cf.* Forsberg et al. 2011 [15]), prediction of gravity anomaly residuals data using LSC and GOCE *Txx* and *Tzz* gradients were made. The solution was run by GEOCOL.

Gravity anomaly residuals are predicted by the LSC method using GOCE T_{zz}, and using T_{zz} and T_{yy} gravity gradients combined. However prediction was done only with selected GOCE gradient dataset, *i.e.* observations closest to the nods of 0.1 by 0.2 degrees are selected. The data selection was made because too many data points creates a non-feasible calculation in *GEOCOL*. Compared to the LSC method, the RPM method can process all data without selection. This will be elaborated on later in this chapter.

Table 7.6: Statistics for prediction of gravity anomaly residuals and geoid height anomaly by collocation

Gravity anomaly residuals (T_{zz} gradients as input)			
	EGM2008	PREDICTIONS	DIFFERENCE
Mean	0.3761	-0.6802	1.0563
St. dev	20.0414	10.8674	18.7042
Gravity anomaly residuals (T_{zz} and T_{yy} gradients as input)			
	EGM2008	PREDICTIONS	DIFFERENCE
Mean	0.3761	-0.1969	0.5730
St. dev	20.0414	10.4945	18.1730

Geoid height anomaly (T_{zz} gradients as input)			
	EGM2008	PREDICTIONS	DIFFERENCE
Mean	0.0172	-0.0341	0.0514
St. dev	0.5780	0.5037	0.4022
Geoid height anomaly (T_{zz} and T_{yy} gradients as input)			
	EGM2008	PREDICTIONS	DIFFERENCE
Mean	0.0172	-0.0107	0.0280
St. dev	0.5780	0.4972	0.3748

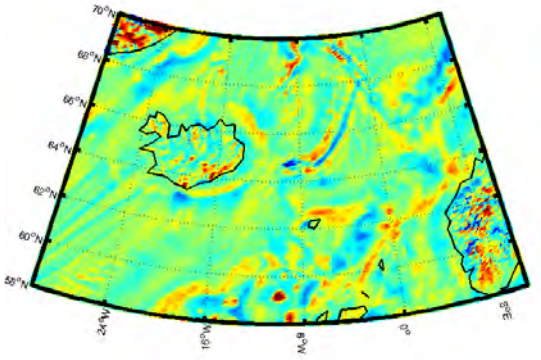

(a) Gravity anomaly residuals based on EGM2008

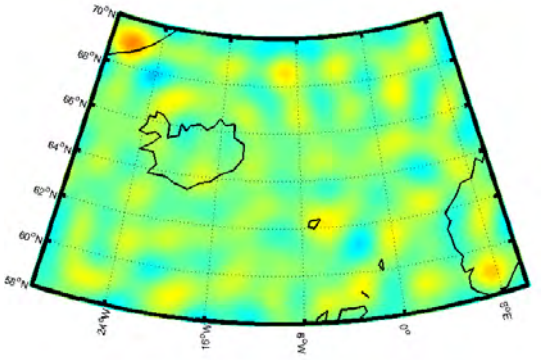

(b) Predicted gravity anomaly residuals by collocation from selected $0.1° \times 0.2°$ GOCE T_{zz} gradient anomaly

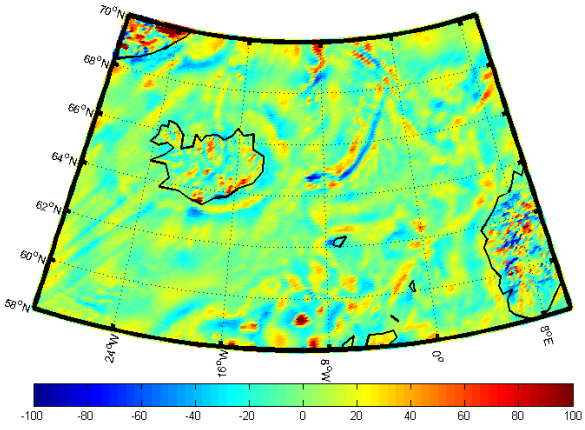

(c) Difference

Figure 7.13: Gravity anomaly residuals based on the EGM2008 [*mGal*](a), predicted gravity anomaly residuals by collocation from selected $0.1° \times 0.2°$ GOCE T_{zz} gradient anomaly [*mGal*] (b) and the difference between the two [*mGal*] (c)

7.3.2 *Collocation prediction of geoid height anomaly in GOCINA region*

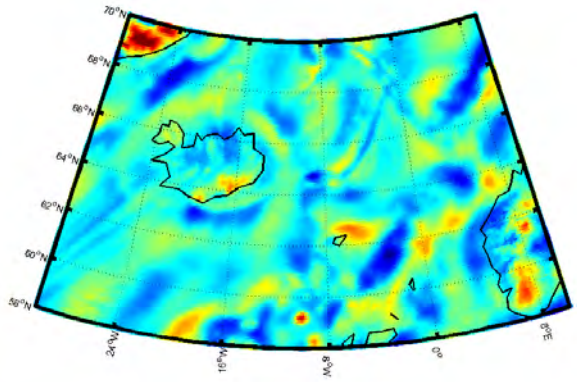

(a) Geoid height anomaly based on EGM2008

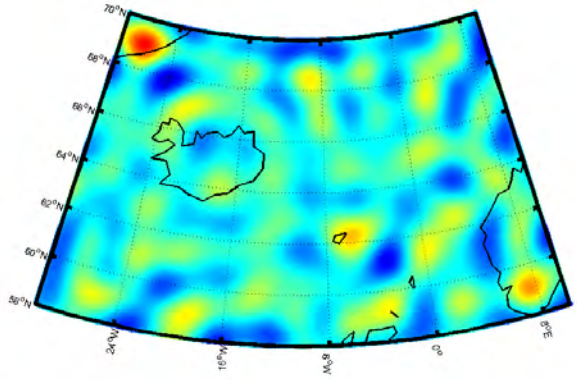

(b) Predicted geoid height anomaly by collocation from selected $0.1° \times 0.2°$ GOCE T_{zz} gradient anomaly

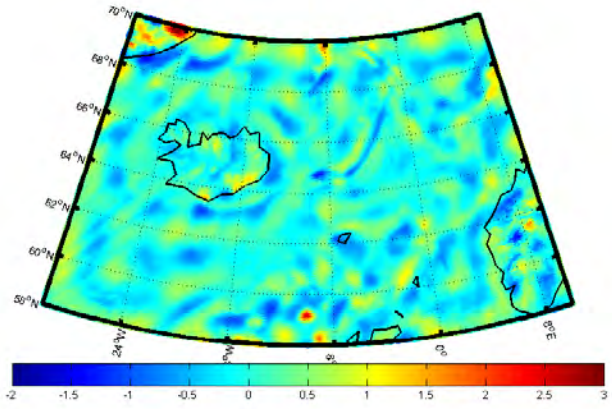

(c) Difference

Figure 7.14: Geoid height anomaly based on EGM2008 [*mGal*] (a), predicted geoid height anomaly by collocation from selected $0.1° \times 0.2°$ GOCE T_{zz} gradient anomaly [*mGal*] (b) and the difference between the two [*mGal*] (c)

It appears that the collocation solution has a lower amplitude than the EGM2008 spherical harmonic model, as expected since a selection/thinning of the gradients were needed, otherwise the agreement

of the reconstructed features is good. The estimated error of predicted gravity at the surface was around 10mGal standard deviation.

Table 7.6 shows two solutions: one where only T_{zz} radial gradients are used, and the other where both T_{zz} and T_{yy} are used for gravity anomaly residuals and geoid heights calculations. Statistics show that adding another component of the gradient measurements marginally improves the solutions for both quantities (gravity anomaly residuals and geoid height anomaly). In the case of differences between the EGM2008 and collocation predicted gravity anomaly residuals improvements of 0.53 *mgal* in the standard deviation (from 18.70 *mgal* to 18.17 *mgal*) and 0.49 *mgal* (from 1.06 *mgal* to 0.57 *mgal*) in the mean value.

The geoid height anomaly difference between EGM2008 and collocation prediction shows improvement in the standard deviation of 0.02 *m* (from 0.40 *m* to 0.38 *m*), while the improvement in the mean value is 0.02 *m* (from 0.05 *m* to 0.03 *m*).

7.4 REDUCED POINT MASS RESULTS

Implementations of the RPM for the regional gravity field determination was described in chapter 5, where it was shown how reduced point mass harmonic functions can be used to represent the (anomalous) gravity potential T locally. The Earth anomalous gravity field, T, at point Q is modeled by a set of base functions, each obtained as the anomalous gravity potential from each point mass m_i located at the position P_i on the surface of an ellipsoid with radius R_M. This radius is smaller than that of the Earth, R_E, and it represents the depth of the point masses. The determination of the appropriate depth of the point masses is done by fitting the function of different gravity field quantities, *i.e.* geoid heights, gravity anomalies and gravity gradients, to the previously described empirical covariance function.

The function of different gravity field quantities, based on the reduced point masses is shown in figure 7.15. The function shows the quantities when using point mass solution for the closed expression, for the contribution up to harmonic degree and order 100, and for the reduced point masses, *i.e.* when the contribution up to harmonic degree and order 100 is subtracted from closed expression.

Fitting of the function for different gravity field quantities to the empirical covariance function was done by comparing empirical covariance estimations based on the GOCE T_{zz} gradient anomalies seen on figure 7.12 to the function of reduced gravity gradients shown on figure 7.15 (right hand side of the plot). Numerous tests with different point mass depths showed that the best results are archived when the R_M is 20 *km* smaller than the mean radius of the GRS80 ellipsoid, *i.e.* when the depth of the point masses is R_M is 20 *km*.

The other issue with the RPM method is the point mass spacing. The grid of point masses should be dense enough to represent fine details of the gravity field as good as possible, and at the same time far enough to prevent large correlation from adjacent point masses. This correlation can cause singularities in the calculations. The spacing of the point masses depends on the content of the residual field which needs to be predicted. Thus, the higher the harmonic degree and order of the reference field that is removed from the observations in the remove-restore method, the closer the point masses can be spaced without causing problems due to the large correlation. In this work, two different global models are used as a reference for reduction, the EGM2008 and the GOCE Direct Release 3. When using the EGM2008, gravity quantities are reduced up to harmonic degree and order 100 and point mass response is determined on a grid with $0.25° \times 0.50°$ spacing. Whereas when using the GOCE Direct Release 3 they are reduced up to harmonic degree and order 240 and point mass grid has $0.125° \times 0.250°$ spacing.

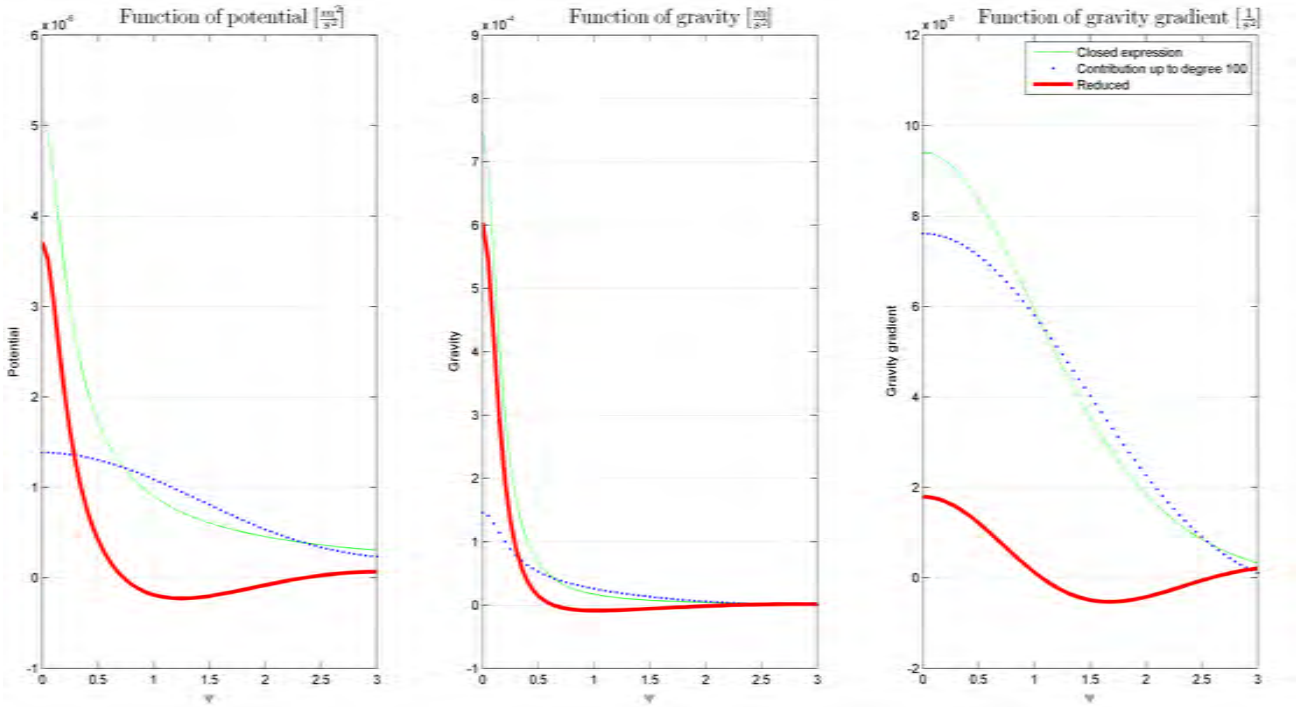

Figure 7.15: Function of the different gravity field quantities in respect to the spherical distance ψ: the gravitational potential $[\frac{m^2}{s^2}]$, the gravity anomaly $[\frac{m}{s^2}]$ and the gravity gradients $[\frac{m^2}{s^2}]$. Function shows the quantities when using point masses solution for the closed expression, for the contribution up to harmonic degree and order 100, and for the reduced point masses.

7.4.1 *Regularization of reduced point mass solution*

The determination of the gravity potential and its quantities from reduced point masses may be a demanding numerical task, and therefore efficient solution strategies are required to solve the corresponding normal equation systems. Correlations between the response from the point masses and downward continuations often causes problems in the inversion. Thus, an algorithm for computing a regularized solution needs to be found.

So far, various algorithms for computing a regularized solution and various methods for choosing the regularization parameter have been proposed in connection with the determination of gravity field functionals on the Earth's surface from satellite gravity gradiometry, e.g. by Xu 1992 [60], Ilk 1993 [20], Bouman 2000 [4], and Lonkhuyzen et al. 2001 [29].

Among the regularization methods for the computation of stable solutions of inverse problems without introducing additional data are Tikhonov regularization (Tikhonov 1963 [43], Tikhonov and Arsenin 1977 [44]), LSC (Moritz 1980 [33]), and truncated singular value decomposition (Lerch et al. 1993 [28]). What really distinguishes them is the choice of the regularization parameter, which involves a trade-off between the norm of the regularized solution and the fit to the given data.

Usually, a diagonal matrix is added to the normal equations matrix, see equation 5.36. The matrix elements are either one, degree-dependent factors, or degree variances of the Earth's gravity field according to Kaula's rule of thumb (Kaula 1966 [21]). This diagonal matrix is scaled by a regularization parameter. In practice, the value of this scaling parameter is determined by a parameter choice rule.

Here, an empirically determined scaling factor for a diagonal matrix is used, based on a trade-off between the strength of the regularization and the fit to the given observations. Even though the regularization parameter was determined empirically, the first starting value was the mean error of the input GOCE gradients, *i.e.* 0.01 E. This parameter squared gives, $10^{-13}\frac{1}{s^2}$, which is the scaling parameter for the identity matrix. This matrix was added to the normal equations matrix. After the preliminary tests, it was concluded that small adjustments for the regularization parameter have to be made.

Figure 7.16 shows the spectrum of predicted residual geoids by the usage of different scaling factor. It can be seen that the result using the scaling parameter $2.5 \cdot 10^{-15}\frac{1}{s^2}$ has the strongest signal above harmonic degree 180, while $10^{-13}\frac{1}{s^2}$ and $2.5 \cdot 10^{-13}\frac{1}{s^2}$ gives the week signal power after harmonic degree 150.

Keeping in mind that the strength of the regularization and the fit to the given observations have to be preserved, different regularization parameters are compared as shown on figure 7.17. It shows the

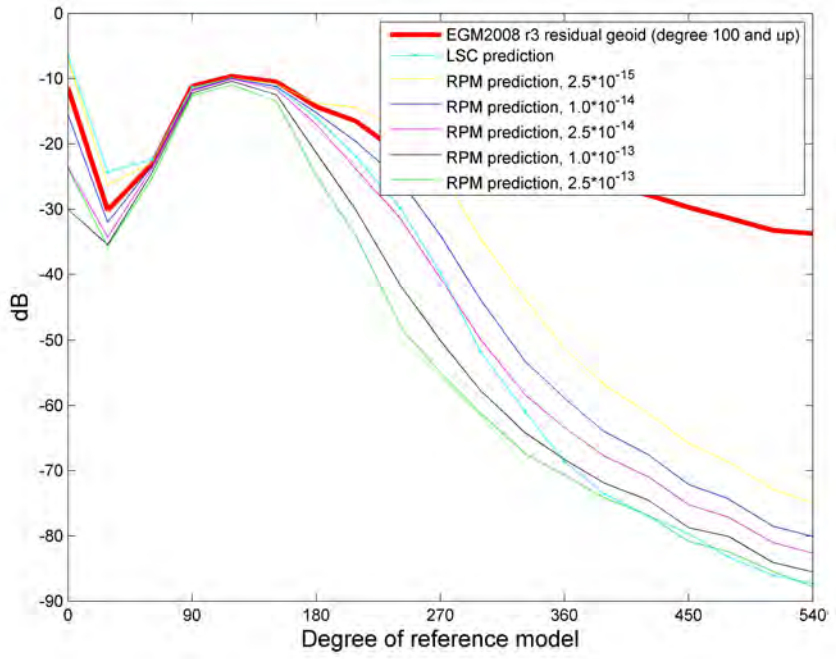

Figure 7.16: Regularization tests - prediction of the residual geoid (degree 100 and up)

spectrum comparison of the difference between the predicted residual geoids and the residual geoid based on EGM2008, when the long wavelength part up to harmonic degree and order 100 is subtracted.

Even though the result using the scaling parameter $2.5 \cdot 10^{-15} \frac{1}{s^2}$ has the strongest signal above harmonic degree 180, after taking the differences between the predicted geoid and the reference EGM2008 residual geoid, it goes off the scale, *i.e.* the power of its difference is higher than the reference.

After further analysis, the regularization parameter of $2.5 \cdot 10^{-14} \frac{1}{s^2}$ was chosen as the right one for this dataset.

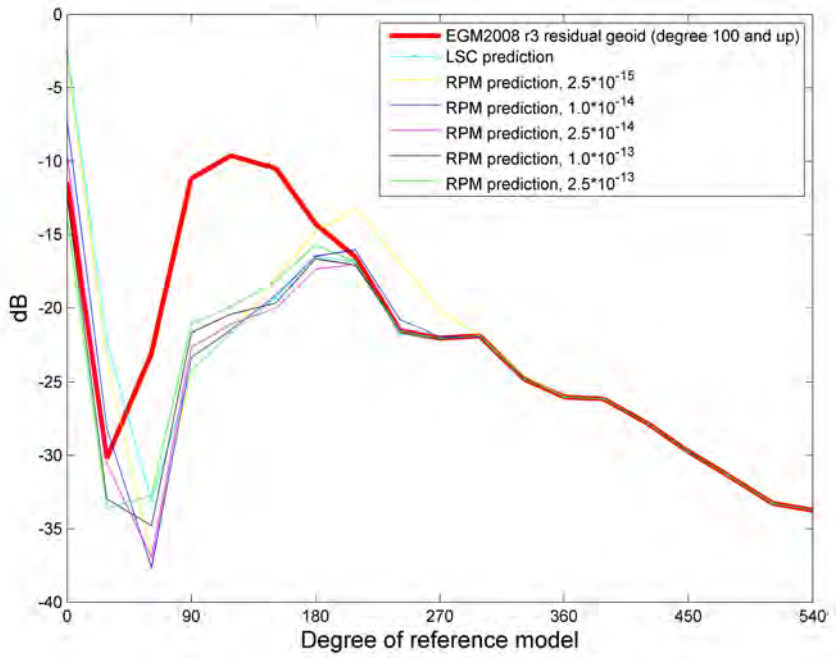

Figure 7.17: Regularization tests - difference between the prediction of the residual geoid (degree 100 and up) and the EGM2008 residual geoid

7.4.2 *Prediction of the gravity gradients using the reduced point mass method*

This subsection shows the results and statistics from the prediction of the gravity gradients using the RPM method.

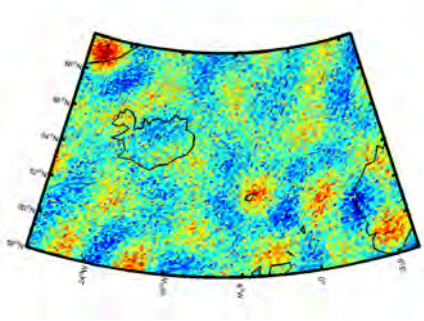

(a) T_{zz} gradient anomaly (contribution from the EGM2008 up to harmonic degree and order 100 is subtracted)

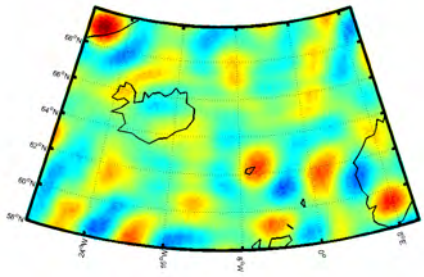

(b) The predicted T_{zz} gradient anomaly by reduced point masses from selected $0.1° \times 0.2°$ GOCE T_{zz} gradient anomaly

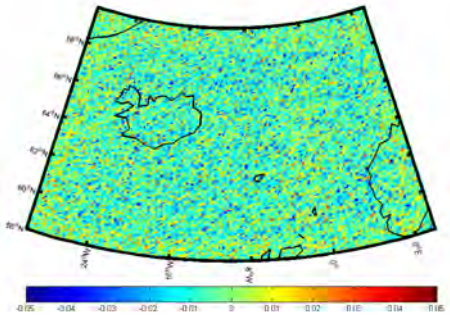

(c) Difference

Figure 7.18: T_{zz} gradient anomaly [E], where the contribution from the EGM2008 up to harmonic degree and order 100 is subtracted (a), predicted T_{zz} gradient anomaly by reduced point masses from selected $0.1° \times 0.2°$ GOCE T_{zz} gradient anomaly (b) and the difference between the two (c)

7.4.3 *Prediction of the gravity anomaly residuals using the reduced point mass method*

Here, the results and statistics from the prediction of the gravity anomaly residuals using the RPM method are presented.

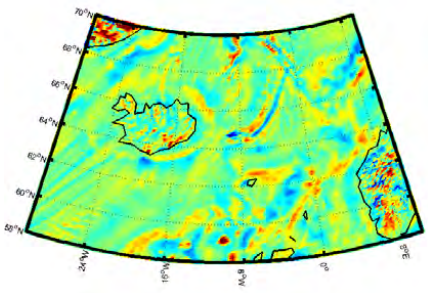

(a) GOCINA gravity anomaly residuals (contribution from the EGM2008 up to harmonic degree and order 100 is subtracted)

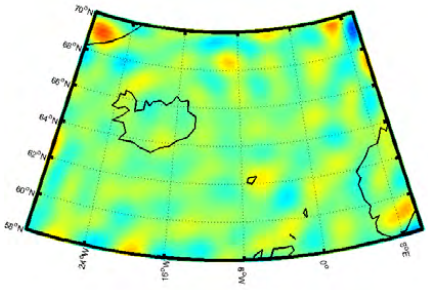

(b) Predicted GOCINA gravity anomaly residuals by reduced point mass method from selected $0.1° \times 0.2°$ GOCE T_{zz} gradient anomaly

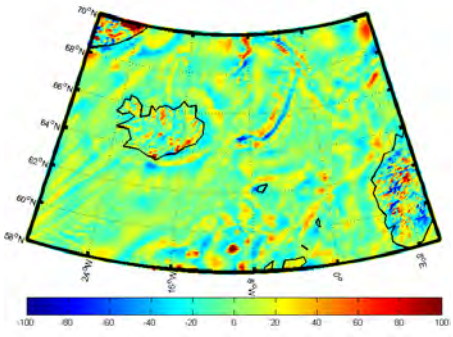

(c) Difference

Figure 7.19: GOCINA gravity anomaly residuals [*mGal*] (contribution from the EGM2008 up to harmonic degree and order 100 is subtracted) (a), predicted GOCINA gravity anomaly residuals by reduced point mass method from selected $0.1° \times 0.2°$ GOCE T_{zz} gradient anomaly (b) and the difference between the two (c)

7.4.4 *Prediction of the geoid height anomaly using the reduced point mass method*

This subsection shows the results and statistics from the prediction of the geoid height anomalies using the RPM method.

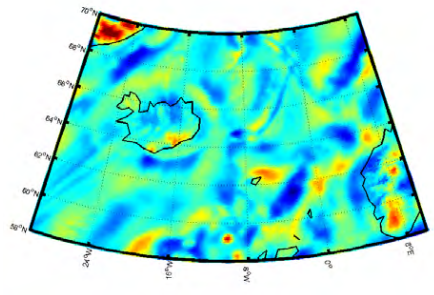

(a) GOCINA geoid height anomaly (contribution from the EGM2008 up to harmonic degree and order 100 is subtracted)

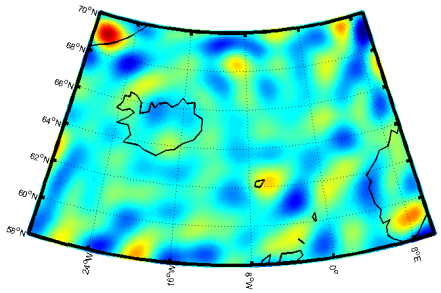

(b) Predicted GOCINA geoid height anomaly by reduced point mass method from selected $0.1° \times 0.2°$ GOCE T_{zz} gradient anomaly

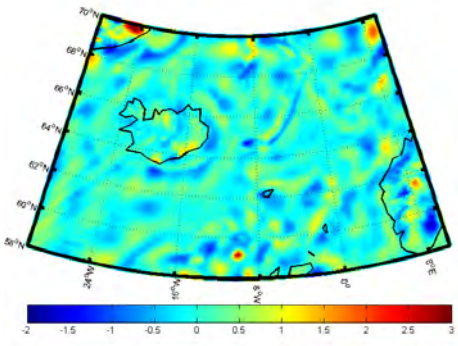

(c) Difference

Figure 7.20: GOCINA geoid height anomaly [m] (contribution from the EGM2008 up to harmonic degree and order 100 is subtracted) (a), predicted GOCINA geoid height anomaly by reduced point mass method from selected $0.1° \times 0.2°$ GOCE T_{zz} gradient anomaly (b) and the difference between the two (c)

Table 7.7: Statistics on the prediction of gradient anomaly [E], gravity anomaly residuals [$mGal$] and geoid height anomaly [m] using the reduced point mass method

Gradient anomaly			
	GOCE T_{zz}	PREDICTIONS	DIFFERENCE
Mean	-0.0135	-0.0041	-0.0094
St. dev	0.0149	0.0131	0.0113
Gravity anomaly residuals			
	EGM2008	PREDICTIONS	DIFFERENCE
Mean	0.3761	-0.1218	0.4980
St. dev	20.0414	11.9745	19.0113
Geoid height anomaly			
	EGM2008	PREDICTIONS	DIFFERENCE
Mean	0.0172	-0.0027	0.0200
St. dev	0.5780	0.5211	0.4049

The RPM method predictions of different gravity field quantities, *i.e.* geoid heights, gravity anomalies and gravity gradients, are shown on figure 7.18, figure 7.19 and figure 7.20, respectivly.

Figure 7.18 shows the prediction of the GOCE T_{zz} gradient anomaly, where the contribution from the EGM2008 up to harmonic degree and order 100 is subtracted. This figure is very important, since it shows how well RPM can predict the GOCE T_{zz} gradient anomaly by inversion method. This example of inverse modelling presents one of the validation of the RPM method.

Based on the figures and the statistics in table 7.7, it can be seen that the RPM prediction clearly shows main features of the local predicted quantities. Values of predictions in the case of gravity anomalies residuals and geoid height anomalies have a good agreement with the observations, *i.e.* EGM2008 based quantities.

7.5 COMPARISON OF THE USED METHODS

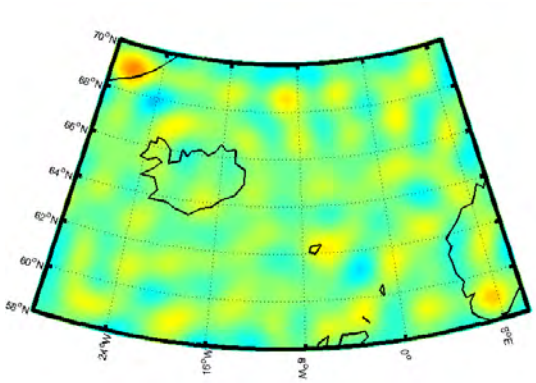

(a) Gravity anomaly residuals predicted by collocation

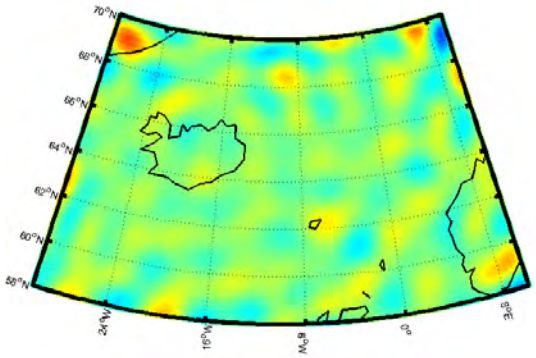

(b) Gravity anomaly residuals predicted by reduced point mass method

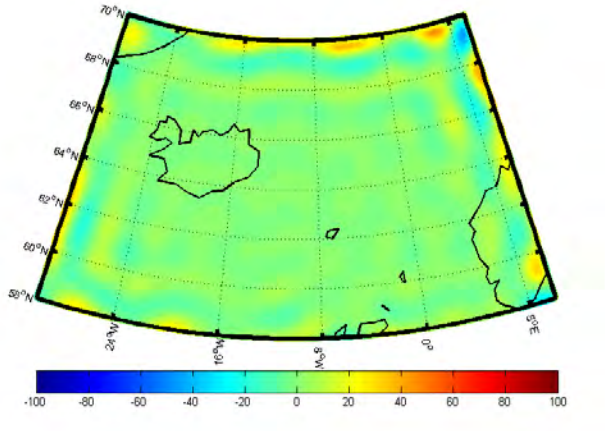

(c) Difference

Figure 7.21: Comparison between the gravity anomaly residuals [*mgal*] predicted using the LSC and the RPM method

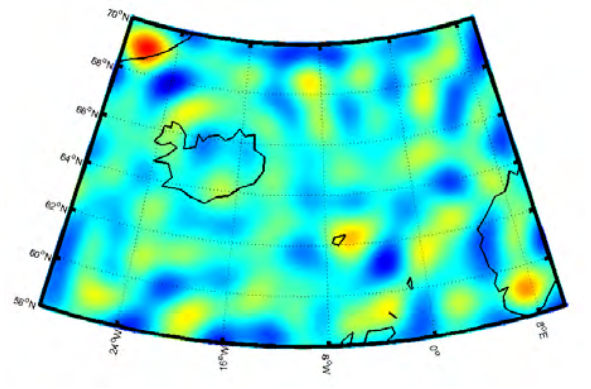

(a) Geoid height anomaly predicted by collocation

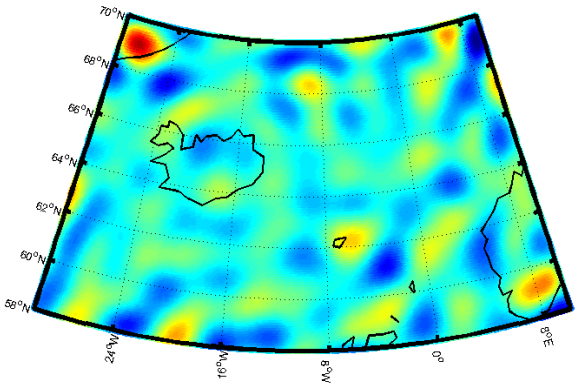

(b) Geoid height anomaly predicted by reduced point mass method

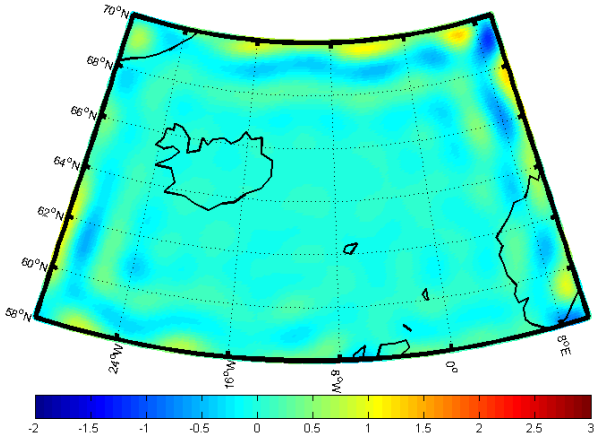

(c) Difference

Figure 7.22: Comparison between geoid height anomaly [m] predicted using the LSC and the RPM method

Table 7.8: Statistics of gravity anomaly residuals [*mGal*] and geoid height anomaly [*m*] prediction by RPM and LSC (when selected $0.1° \times 0.2°$ T_{zz} dataset is used), and by RPM (when all T_{zz} gradient anomalies are used)

Gravity anomaly residuals				
	EGM2008	RPM	RPM (FULL T_{zz})	LSC
Mean	0.3761	-0.1218	0.3643	-0.6802
St. dev	20.0414	11.9745	15.9469	10.8674
Geoid height anomaly				
	EGM2008	RPM	RPM (FULL T_{zz})	LSC
Mean	0.0172	-0.0027	0.0188	-0.0341
St. dev	0.5780	0.5211	0.5922	0.5037

Table 7.9: Gravity anomaly residuals [*mGal*] and geoid height anomaly [*m*] prediction comparison by RPM and LSC (when selected $0.1° \times 0.2°$ GOCE T_{zz} dateset is used), and by RPM (when all T_{zz} gradient anomalies are used)

Gravity anomaly residuals			
	LSC	LSC - RPM	LSC - RPM (FULL T_{zz})
Mean	-0.6802	-0.5584	-1.0445
St. dev	10.8674	7.4811	12.3495
Geoid height anomaly			
	LSC	LSC - RPM	LSC - RPM (FULL T_{zz})
Mean	-0.0341	-0.0314	-0.0529
St. dev	0.5037	0.2393	0.3508

Table 7.10: Gravity anomaly residuals [*mGal*] and geoid height anomaly [*m*] prediction difference by RPM and LSC (when selected $0.1° \times 0.2°$ GOCE T_{zz} dateset is used), and by RPM (when all T_{zz} gradient anomalies are used)

Gravity anomaly residuals			
	EGM08 - LSC	EGM08 - RPM	EGM08 - RPM (FULL T_{zz})
Mean	1.0563	0.4980	0.0119
St. dev	18.7042	19.0113	20.5175
Geoid height anomaly			
	EGM08 - LSC	EGM08 - RPM	EGM08 - RPM (FULL T_{zz})
Mean	0.0514	0.0200	0.0197
St. dev	0.4022	0.4049	0.4072

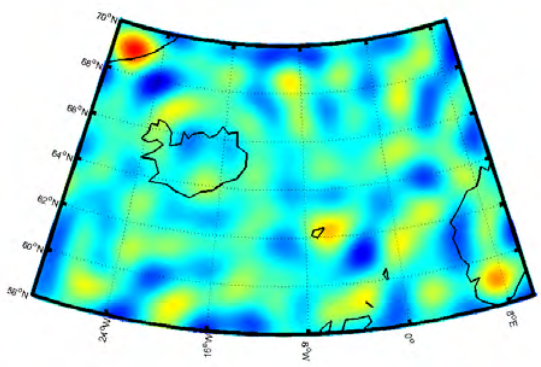

(a) Geoid height anomaly predicted by collocation

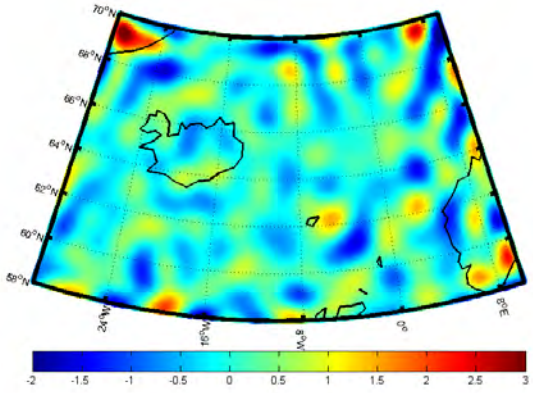

(b) Geoid height anomaly predicted by the reduced point mass method

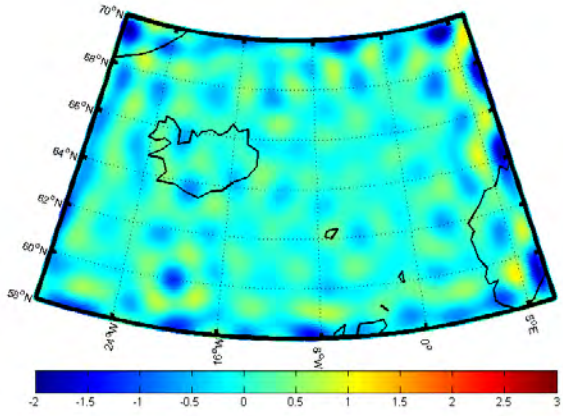

(c) Difference

Figure 7.23: Comparison between geoid height anomaly [*mgal*] predicted by collocation (when using selected $0.1° \times 0.2°$ GOCE T_{zz} gradient anomaly), and by reduced point masses (when using all the T_{zz} gradients anomaly available in the GOCINA region)

Both methods presented here show good agreement in prediction of both the gravity anomalies residuals and the geoid height anomaly. Comparing to the LSC method, the RPM method needs less time for calculation by using a thinned gradient dataset, *i.e.* a selection of values closest to the nods of $0.1° \times 0.2°$ grid.

A comparison of the least squares collocation method solutions when one or two components are used shows that adding the T_{yy} component to the input file marginally changes the result; the standard deviation decreases from 10.87 *mGal* to 10.49 *mGal* in the case of gravity anomaly residuals and from 0.51 *m* to 0.50 *m* when it comes to the geoid height anomaly.

The predicted gravity anomaly residuals had a standard deviation of around 11 *mGal* at the surface for both methods. The same agreement can be noticed in the prediction of the geoid height anomaly, where the standard deviation is around 51 *cm* for both methods.

Since LSC requires the solution of as many linear equations as the number of data, the GOCE gradient data needs to be thinned prior to applying the method. This is not the case for the reduced point masses, where we can decide how many equations we want to solve ourselves. Thus, we decide the number of point mass grid points, with constraints depending on the size of the area, and this number corresponds to the amount of equations needed to be solved.

In the case of reduced point masses, however, there is the possibility of using all gravity gradients available.

In that case, the standard deviation increases from 11.97 *mGal* to 15.95 *mGal* in the case of gravity anomaly residuals and from 0.52 *m* to 0.59 *m* when it comes to the geoid height anomaly, see table 7.8.

One could say that increasing the standard deviation does not mean that the prediction is made any better - in fact, it could imply that it has worsened. However, in these cases, where the standard deviations increase, and it actually goes closer to the standard deviation of the EGM2008 (see the first column in the table 7.8), it can be accepted that there is an improvement in the prediction.

Figure 7.24 shows a power spectra of the geoid height anomaly predicted by the LSC and the RPM methods, when the EGM2008 up to harmonic degree and order 100 is subtracted. A comparison is shown between the prediction using only T_{zz} or both T_{zz} and T_{yy} GOCE gradients by the use of the LSC method. The reason for the selected GOCE gradient dataset (closest to the knots of a $0.1° \times 0.2°$ grid) is that full dataset cannot be processed by the LSC method because the number of the equation that have to be solved is equal to the number of observations. For the RPM method, two different power spectra of geoid height anomaly solutions are shown. The first power spectrum shows the RPM solution in which the selected GOCE gradient dataset is used for the prediction, while the second shows the solution when all available GOCE gravity gradient observations are used.

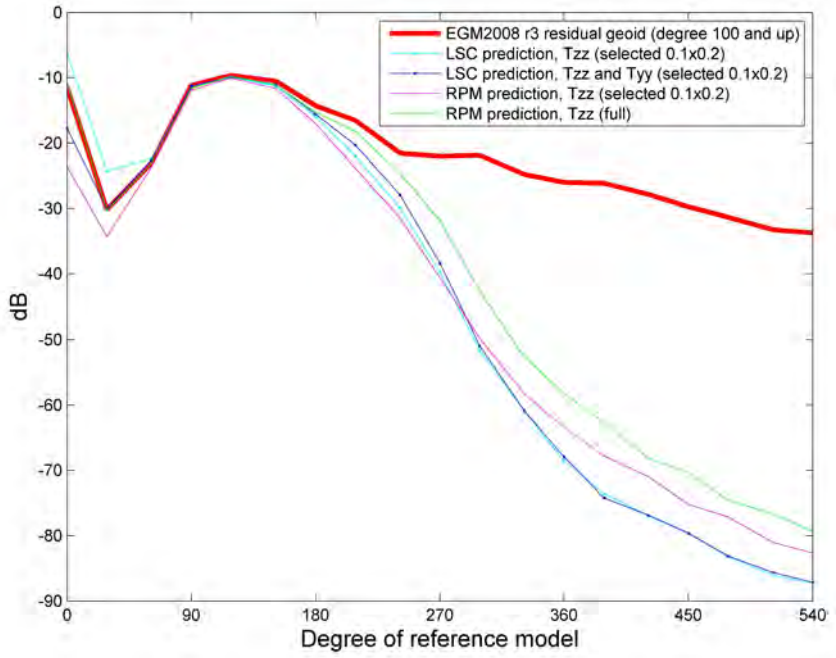

Figure 7.24: Power spectrum of the geoid height anomaly prediction when EGM2008 up to harmonic degree and order 100 is subtracted. The prediction is done by the LSC and the RPM methods with different datasets

From figure 7.24 it can be seen that adding the T_{yy} GOCE gradients component when using the LSC method provides marginal improvements to the results obtained when using only T_{zz}. The same conclusion can be found in the investigation of Tscherning and Arabelos 2011 [48]. However, using more GOCE gradient T_{zz} observations does improve the solution, *i.e.* the power spectrum shows more signal in the RPM solution when all available GOCE gradients are used comparing to the results obtained when using only selected T_{zz} GOCE gradients.

Figure 7.25 shows a power spectrum of the difference between the differently predicted geoid height anomaly (when EGM2008 up to harmonic degree and order 100 is subtracted) and the EGM2008 based geoid height anomaly. When taking the difference form the reference, *i.e.* the EGM2008 based geoid height anomaly, it can be seen that both solutions, by the LSC and the RPM methods, give similar results when the selected GOCE gradient dataset is used. This is not the case for the RPM prediction when all available GOCE gradients are used, where an improvement of the geoid height anomaly prediction in the spectrum band from harmonic degree 120 to 140 can be seen.

Hence, the improvement in the geoid height anomaly prediction by the use of the RPM method and all available GOCE gravity gradients in the GOCINA region can lead to better geoid determination. The

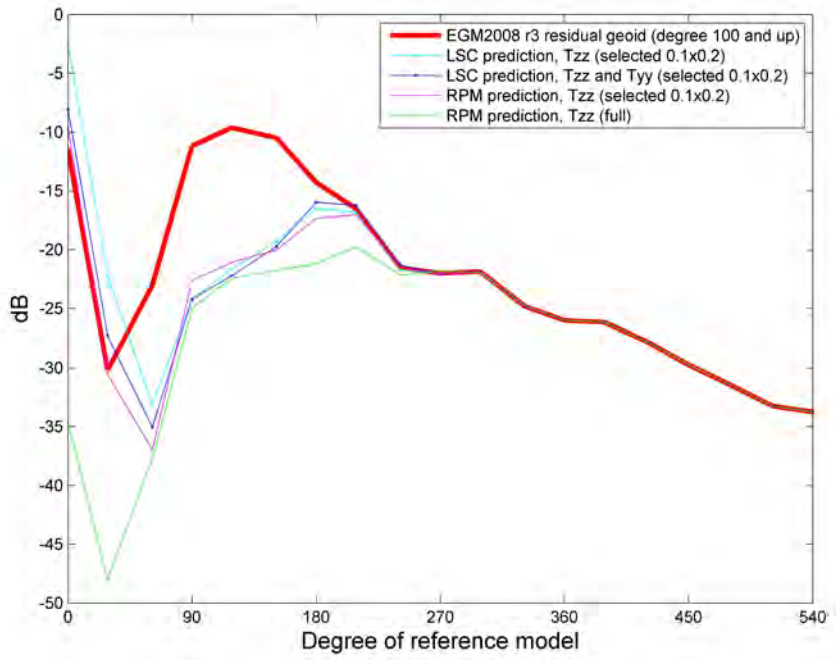

Figure 7.25: Power spectrum of the difference between geoid height anomaly prediction (when EGM2008 up to harmonic degree and order 100 is subtracted) and EGM2008 based geoid height anomaly. Prediction is done by the LSC and the RPM methods with different datasets used.

statistics in the table 7.10, however, do not reflect the improvement. This requires further investigation.

The purpose of this section was to demonstrate the stability of the reduced point mass method by comparing the results to the well stable least squares collocation method. In the next section, both methods will be used when the long wavelength part up to degree and order 240 is subtracted from the GOCE gradients.

7.6 ENHANCING GEOID HEIGHTS WITH GOCE GRADIENTS

Improvements in the geoid height anomaly prediction, when the EGM2008 global model up to harmonic degree and order 100 is subtracted, by the use of the RPM method and all available GOCE gravity gradients was presented in the previous section. Here, the prediction of the gravity anomaly, when the GOCE Direct Release 3 global model up to harmonic degree and order 240 is subtracted, will be presented.

The prediction is made with both methods. When using the LSC method, the selected GOCE T_{zz} and T_{yy} gravity gradients are used. In the case of RPM method, all available GOCE T_{zz} gravity gradients are used. Statistics of the predicted geoid height anomaly in the GOCINA region can be seen in table 7.11.

Table 7.11: Statistics of the geoid height anomaly prediction by the LSC and RPM method when the GOCE Direct release 3 model up to harmonic degree and order 240 is subtracted

Geoid height anomaly by collocation (T_{zz} and T_{yy})			
	EGM2008	COLLOCATION	DIFFERENCE
Mean	0.0075	-0.0007	0.0082
St. dev	0.2793	0.0173	0.2789
Geoid height anomaly by reduced point mass method (T_{zz})			
	EGM2008	RPM	DIFFERENCE
Mean	0.0075	0.0101	-0.0026
St. dev	0.2793	0.0827	0.2895

It can be seen from table 7.11 that prediction of the geoid height anomaly by the RPM method has standard deviation of 0.0827 m, which is higher than the standard deviation of the prediction by the LSC method 0.0173 m. The detailed structures, contained in the harmonic degree and order above 240, are not very well shown in the LSC solution.

If standard deviations of prediction by both methods are compared to the standard deviation of the values of the geoid height anomaly computed by the EGM2008 global model, it can be seen that the standard deviation of prediction by the RPM fits better. However, prediction of the geoid height anomaly over the harmonic degree and order 240 is a very hard task, and results shown here are not of the same magnitude as the EGM2008 based geoid height anomaly (see figure 7.26), where the standard deviation is 0.2793 m.

The reason for this, is the difference in the data used for the calculation, where in the case of the GOCE gravity gradients one may not

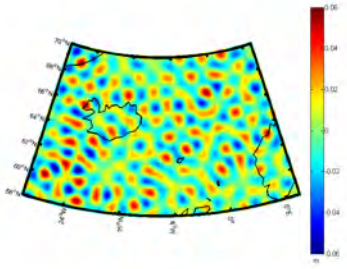

(a) Geoid height anomaly predicted by collocation (T_{zz} and T_{yy} 0.1° × 0.2°)

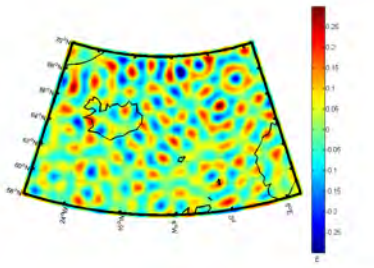

(b) Geoid height anomaly predicted by reduced point masses (all T_{zz})

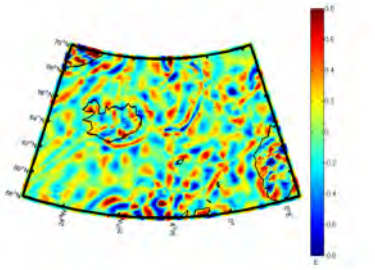

(c) Geoid height anomaly calculated when full GOCE Direct r3 geoid is subtracted from full EGM2008 geoid

Figure 7.26: Comparison between geoid height anomalies from complete EGM2008 model, predicted by collocation and predicted reduced point masses. Long wavelength part up to harmonic degree and order 240 (based on GOCE Direct r3) is subtracted

expect the same resolution as from the EGM2008 based geoid height anomaly solution, where shipborne, airborne, satellite altimetry and GRACE satellite mission data is incorporated (see Pavlis et al. 2008 [36]).

On figure 7.27 the power spectra of the geoid height anomaly predicted by the LSC and the RPM methods are shown. The presented solution are residuals when the contribution from the GOCE Direct Release 3 global model up to harmonic degree and order 240 is subtracted.

It can be seen that the LSC solution gives better results than the RPM solutions when the selected GOCE gravity gradients are used. However, when all available GOCE gravity gradients are included, the RPM methods shows an improvement.

The LSC method includes error degree variances when making predictions, while the RPM method does not include any information about errors. This leads to better representation of the geoid height

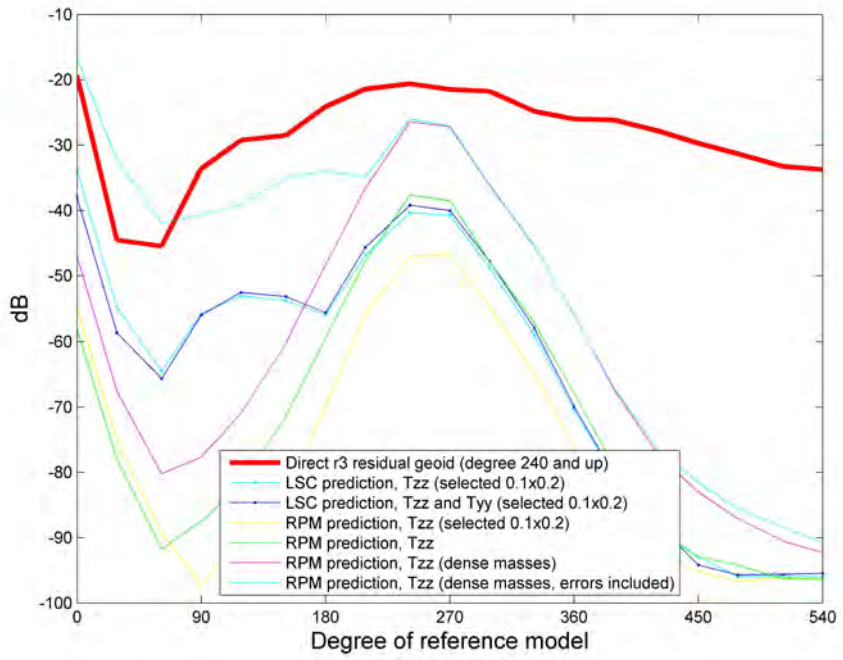

Figure 7.27: Power spectrum of the geoid height anomaly residuals, when Direct release 3 up to harmonic degree and order 240 is subtracted

anomaly by the LSC method in lower degrees, from spherical harmonic degree 60 up to 180, and it can be seen on figure 7.27.

If all GOCE T_{zz} gravity gradients are used in the RPM method (when point masses are distributed in the denser grid, 0.25°x0.125° degree), significant improvement can be seen when comparing to the solutions with only selected GOCE gravity gradients. If a 10 percent error is included for every coefficient which is reduced from the full mass response, a marginal improvement can be seen in the high harmonic degrees (above harmonic degree 200). However, the improvement in the lower band (from harmonic degree 60 to 180) is high.

Figure 7.28 shows a power spectrum of the difference between differently predicted geoid height anomaly (when GOCE Direct Release 3 up to harmonic degree and order 240 is subtracted) and the EGM2008 based geoid height anomaly. It can be seen that all prediction give very similar results when the differences with reference EGM2008 based geoid height anomaly are made. It is clear that recovery of the geoid height anomaly above harmonic degree and order 240 is impossible without use of the all available GOCE gradients. The result from the RPM method when point masses are distributed in the denser grid (0.25°x0.125°) shows a big peak around the spherical harmonic degree 240, which is probably the result of the recovered signal that is present below the harmonic degree 240 and without the error degree variances cannot be represented correctly. However, the solution calculated using 10 percent error shows the same peak.

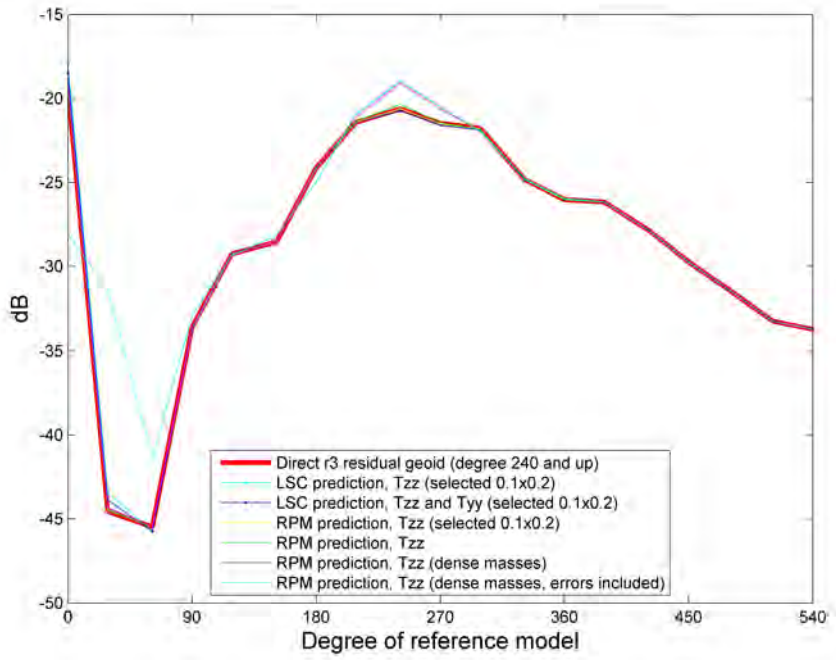

Figure 7.28: Power spectrum of the differences between geoid height anomaly residuals based on the EGM2008 and the geoid height anomaly predicted by different methods (when Direct release 3 up to harmonic degree and order 240 is subtracted)

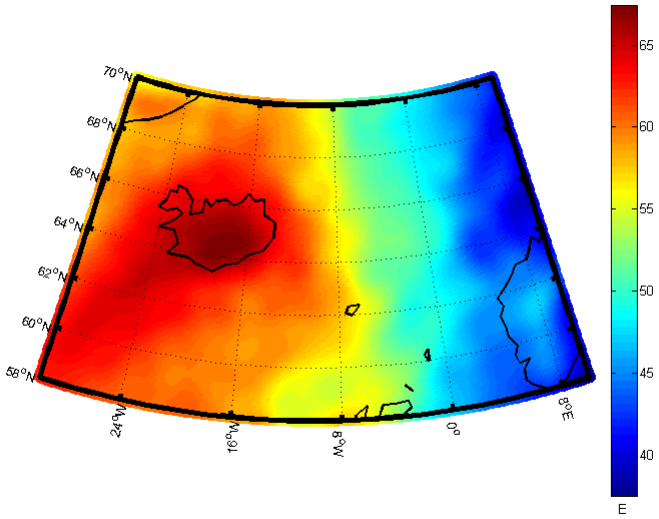

Figure 7.29: The enhanced geoid heights by reduced point mass method when the gradient signal higher than harmonic degree and order 240 is used

The enhanced geoid produced by the RPM method shown on figure 7.26 is then used to enhance the geoid produced by the GOCE Direct

Release 3 spherical harmonic set (up to harmonic degree and order 240). Figure 7.29 shows the enhanced GOCE geoid.

7.7 MERGING ENHANCED GEOID HEIGHTS WITH MEAN SEA SURFACE

The enhanced geoid calculated using the RPM method and GOCE T_{zz} gravity gradients on top of the GOCE Direct Release 3 global model is now used to produce MDT in the GOCINA region.

The MDT is the small residual of two larger fields, the geoid and the MSS. Here, for calculation of the MDT in the GOCINA region the DTU10 MSS is used, see figure 7.30.

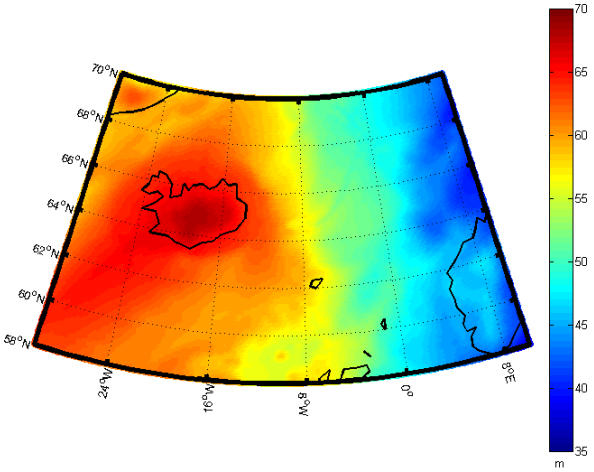

Figure 7.30: DTU10 Mean Sea Surface in GOCINA region

The difference between the DTU10 MSS and the GOCE enhanced geoid, *i.e.* the enhanced GOCE MDT, is shown in figure 7.31. Typical variations in between the MSS and the geoid are up to 100m, whereas for the MDT they are around 1m. In the GOCINA region, variations are around 0.4m.

For the best estimate of the MDT, a proper MDT filtering is required to eliminate the short scale geoid signals to obtain a useful estimate of the MDT. Figure 7.31 shows GOCE Direct enhanced MDT without any filtering and when different filter widths are used.

The best estimate of the MDT is obtained when the filtering minimizes the attenuation of the MDT, while in the same time suppressing the noise due geoid omission and commission errors. Here, a truncated Gaussian filter is used, where the degree of smoothing is proportional to the filter width. The filter width represents the radius at which the Gaussian curve that defines the weighting function has fallen to half of its value at the origin.

Such filtering, in addition to removing noise, also attenuates MDT gradients associated with ocean currents to a degree that is proportional to the filter width. Because of this, it is important to find the minimum filter radius that will adequately remove the noise, and in the same time preserve the MDT's oceanographic content.

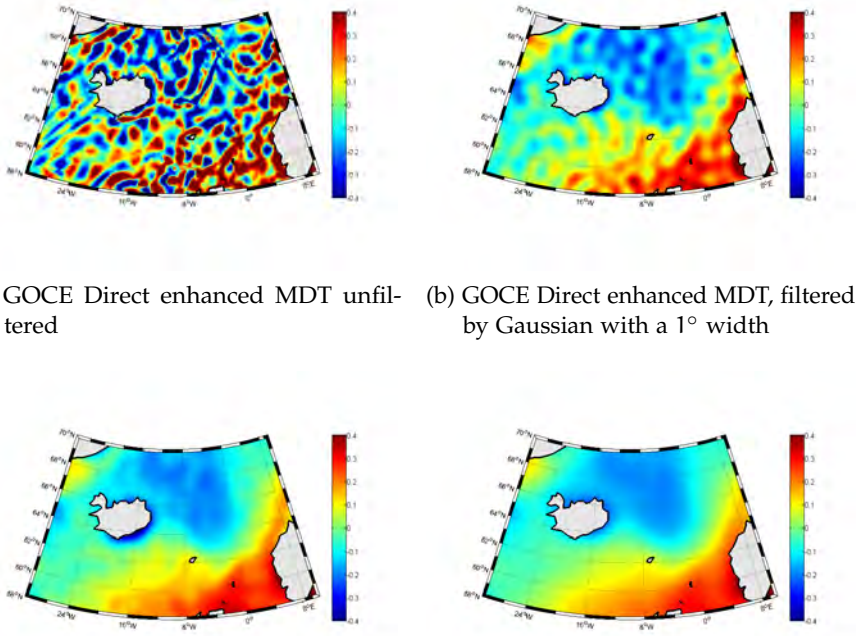

(a) GOCE Direct enhanced MDT unfiltered

(b) GOCE Direct enhanced MDT, filtered by Gaussian with a 1° width

(c) GOCE Direct enhanced MDT, filtered by Gaussian with a 1.5° width

(d) GOCE Direct enhanced MDT, filtered by Gaussian with a 2° width

Figure 7.31: GOCE Direct enhanced MDT, *i.e.* the difference between the DTU10 Mean Sea Surface and GOCE Direct r3 full geoid enhanced with gradients. The mean of 0.50m is subtracted.

In this analysis, a GOCE Direct enhanced MDT, filtered by Gaussian with a 1.5° width, is presented as the final MDT.

Comparison with the different MDT's shows

For the estimation of the quality of the GOCE Direct enhanced MDT, a comparison with the different MDT's is presented. Figure 7.32 shows different MDT's in the GOCINA region: the DTU10 MDT, the DTU10 based MDT calculated in this study, the MDT calculated in the GOCINA project, the Maximenko MDT, the GOCE Direct MDT and the GOCE Direct enhanced MDT.

The DTU10 based MDT calculated in this study shows more informations than the original DTU10 MDT, which is very smooth. The Maximenko MDT incorporates the GRACE satellite and drifting buoy

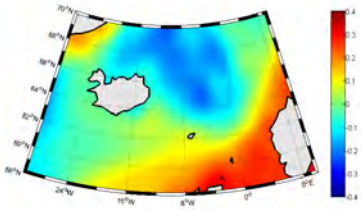

(a) DTU10 MDT

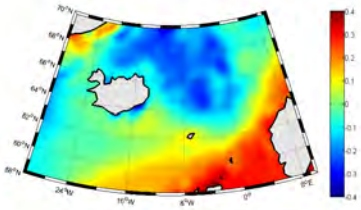

(b) DTU10 MDT 2: difference between DTU10 MSS and EGM2008 geoid geoid up to degree and order 2190

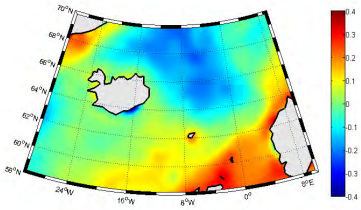

(c) GOCINA project MDT

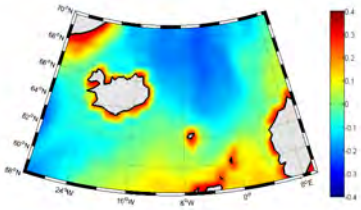

(d) Maximenko MDT

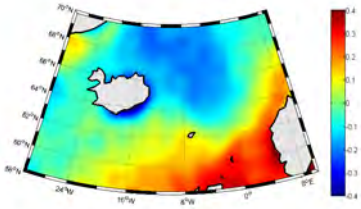

(e) GOCE Direct MDT, filtered by Gaussian with a 1.5 degree width

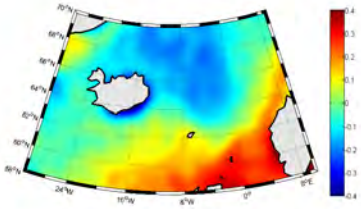

(f) GOCE Direct enhanced MDT, filtered by Gaussian with a 1.5 degree width

Figure 7.32: Different mean dynamic topography in GOCINA region [m])

data, and should show the most detailed oceanographic content. However, because of its low resolution, 0.5° by 0.5°, it doesn't reveal more information than the MDT calculated in GOCINA project. This can be seen especially in the coastal areas, where synergy of low resolution Maximenko MDT grid and land proximity shows an unreliable signal.

Figure 7.33 shows a power spectra of the different MDT estimates. It can be seen that the GOCE Direct MDT has higher signal in the spectrum band from harmonic degree 0 to 140 than the MDT calculated in the GOCINA project. However, the signal contained in the wavelengths shorter than harmonic degrees 140 in the GOCE Direct MDT slowly

attenuates. The DTU10 MDT shows significantly less signal than the GOCE Direct MDT.

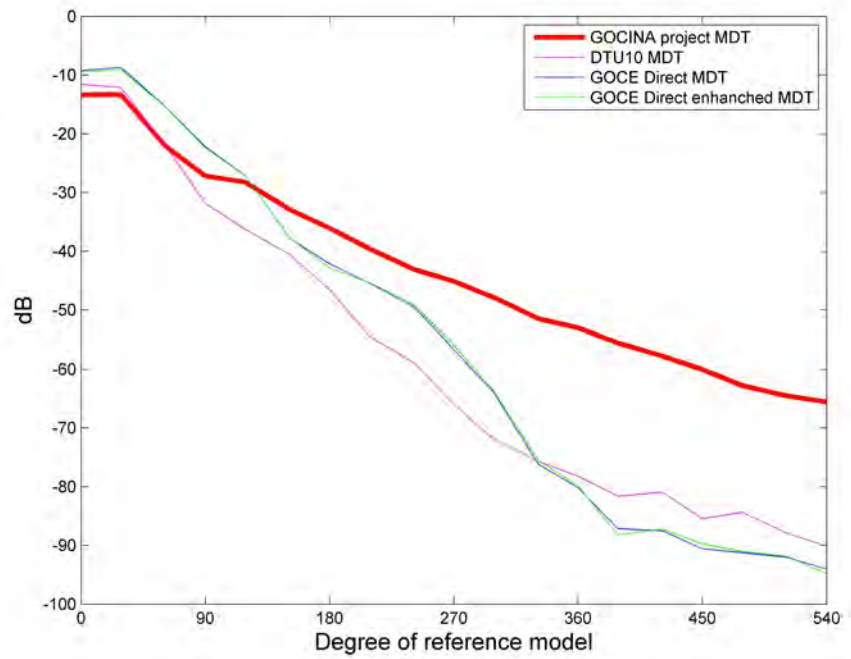

Figure 7.33: Power spectra of different MDT estimates

A comparison of the GOCE Direct MDT and the GOCE Direct enhanced MDT doesn't show significant difference. Thus, even though GOCE data provides a better estimation of the MDT in the GOCINA region than any previously obtained using only satellite observations, it could not be concluded whether the regionally enhanced geoid model estimated using GOCE gradients contribute to a further improvement of the determination of the MDT in the GOCINA area.

Once the MDT has been calculated, it can be used to determine the surface geostrophic currents, which are associated with the slope of the MDT.

Figure 7.34 shows the calculated current speeds from different mean dynamic topography. Here, the current speed reaches a maximum of 0.77 $\frac{m}{s}$, calculated by the GOCINA project MDT. In case of GOCE Direct MDT current speeds, the maximum is 0.46 $\frac{m}{s}$.

The GOCE Direct MDT current speeds reveal all of the gross features of the general circulation in the region are clear. However, the GOCE Direct enhanced MDT does not show improvement over the GOCE Direct MDT. This will require further investigation.

The MDT calculated in GOCINA project, shows even smaller scale details, which makes it the best ocean circulation representation in

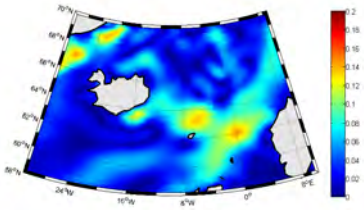

(a) DTU10 MDT current speed

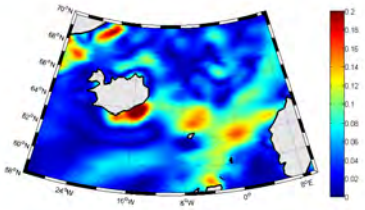

(b) DTU10 MDT 2 current speed

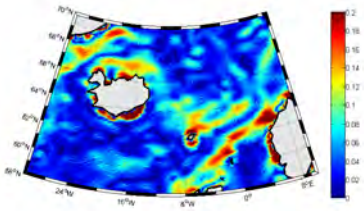

(c) GOCINA project MDT current speed

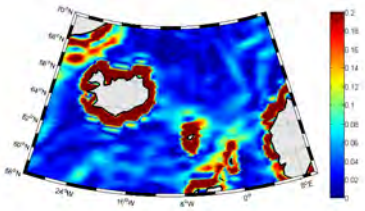

(d) Maximenko MDT current speed

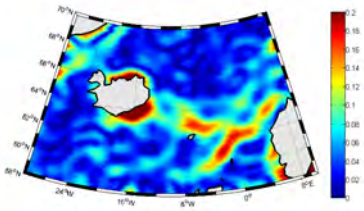

(e) GOCE Direct MDT current speed

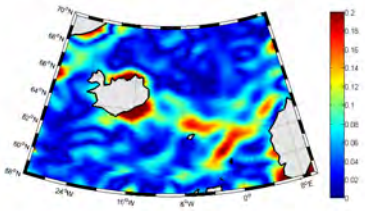

(f) GOCE Direct enhanced MDT current speed

Figure 7.34: Current speed calculated from different mean dynamic topography in the GOCINA region [$\frac{m}{s}$]

this region. However, in case of the DTU10 MDT current speed, the magnitude and the details of the circulation features are far from expected, *i.e.* the maximum current speed of 0.18 $\frac{m}{s}$.

It is worth pointing out that Maximenko MDT current speeds solution with in-situ drifter data gives quite reasonable results, however the low resolution hides general circulation features in this region.

Calculation of the geostrophic surface currents from the GOCE Direct MDT reveals continuation of the North Atlantic current, *i.e.* Norwegian current, as well as the East Greenland Current. Therefore, the model estimates similar current speeds to the ones from the GOCINA project

MDT, showing the ability to better resolve the finer scale features of the ocean circulation than any other satellite mission.

8

CONCLUSIONS AND FUTURE WORK

In this chapter, the thesis conclusions and future work are summarized.

8.1 CONCLUSIONS

The global GOCE mapping of variations in the gravity field with remarkable detail has already made an impact in the ocean science society. Usually, the GOCE spherical harmonic models are combined with high resolution MSS models for deriving global MDT models. In this Ph.D. study, a methodology has been developed for using GOCE gradients on top of the GOCE spherical harmonic models. The study can lead to the additional signal extraction in local areas than the one produced only by GOCE global models. Additionally, predicted signals can then be used for the purpose of local geoid enhancements.

In regional gravity field recovery from GOCE gradients, the Least-Squares Collocation (LSC) method may be used. However, this method requires the solution of as many linear equations as the number of data, thus GOCE gradient data needs to be thinned prior to applying the method. To avoid such thinning, a Reduced Point Mass (RPM) methodology is developed as a part of this study. The RPM is based on the reduced point mass response, and the number of equations we want to solve depends on the number of point masses. Another advantage of the RPM method is that the computation time may be shorter compared to the LSC method. The results presented in this study are based on all available GOCE gradient data in the GOCINA region, *i.e.* 18 months of observations.

A comparison of the solutions from both methods when one (T_{zz}) or two (both T_{yy} and T_{zz}) gradient components are used shows that adding the T_{yy} component to the input file marginally changes the result in gravity filed quantities prediction. However, using more GOCE gradient T_{zz} observations does improve the solution, *i.e.* the power spectrum shows more signal in the RPM solution when all available GOCE gradients are used comparing to the results obtained when using only selected T_{zz} GOCE gradients.

When taking the difference from the reference, *i.e.* the EGM2008 based geoid height anomaly, it can be seen that the solutions from both the LSC and RPM methods give similar results when the selected GOCE

gradient dataset is used. When all available GOCE gradients are used, a significant improvement in the geoid height anomaly prediction can be seen.

The prediction of the gravity field is made using the RPM, when the GOCE Direct Release 3 global model up to harmonic degree and order 240 is subtracted. The enhanced geoid produced with this method is then used to enhance the geoid produced by the GOCE Direct Release 3 spherical harmonic set (up to harmonic degree and order 240).

The difference between the DTU10 MSS and the GOCE enhanced geoid resulted in the GOCE Direct enhanced MDT. A comparison of the GOCE Direct MDT and the GOCE Direct enhanced MDT doesn't show significant differences. Thus, even though GOCE data provides a better estimation of the MDT in the GOCINA region than any previously obtained using only satellite observations, it could not be concluded whether the regionally enhanced geoid model estimated using GOCE gradients contribute to a further improvement of the determination of the MDT in the GOCINA area.

The surface geostrophic currents calculated from the GOCE Direct MDT current speeds reveal that all of the gross features of the general circulation in the region are clear. However, the MDT calculated in the GOCINA project shows the smallest scale details, which makes it the best ocean circulation representation in this region.

8.2 IMPLICATIONS

The resulting technique can supplement the available collection of tools for the MDT determination, and can be applied to other regions of the world oceans where gravity data of high quality and spatial distribution is not available. Recovery of an optimal MDT product from GOCE can lead to improvements in the heat transport estimates and hence lead to benefits from understanding climate and climate changes.

In this thesis, geoid recovery was carried out in the GOCINA region, which is covered mostly by ocean. In the regions with higher gravity anomaly signal oscillations, *i.e.* mountain regions, GOCE gradients can possibly provide even higher geoid enhancements than the ones shown in this thesis, where calculations were carried out in an ocean region.

8.3 IMPROVEMENTS WITH RESPECT TO THE EXISTING METHODS

The methods presented here show good agreement in prediction of both gravity anomalies residuals and geoid height anomaly. The LSC method requires the solution of as many linear equations as the number of data, so GOCE gradient data needs to be thinned prior to applying the method. This is not case for the reduced point mass

method, where the number of equations we want to solve depends on the number of point masses.

Comparing to the LSC method, when using thinned gradient dataset, the RPM method needs less time for calculation. The RPM method also has the possibility to use all gravity gradients available. Using more of the GOCE gradient T_{zz} observations does improve the solution, *i.e.* the power spectrum shows more signal in the RPM solution when all available GOCE gradients are used comparing to the results obtained when using only the selected T_{zz} GOCE gradients.

The results presented in this study are based on all available GOCE gradient data in the GOCINA region, *i.e.* 18 months of observations, which is not presented in any other previous investigation.

8.4 FUTURE WORK AND RECOMMENDATIONS

The GOCE satellite was launched on March 17, 2009. and the firt data was made available to the scientific community on June 29, 2010. It was a completely new type of data and it took some time to understand their content and error sources. The initial testing of the methodology was carried out using those data, and the release 2 data when they became available on March 11, 2011. The GOCE Release 3 data was made available on November, 01 2011., leaving little time during this study to test the RPM method and the computation of the MDT especially. Even though the last available GOCE gradient dataset contains only calibrated gravity gradients, it still contains some errors that needs to be understood. The mean value of the residual gravity gradients in local region is not zero, and it corresponds to the value of the observations error. The tests shown here should be repeated with new data releases.

A further exploration of the new and more precise estimates of the GOCE based MDT can be carried out by removing not just the long wavelength part of the gravity field, but also the short wavelength structure from the GOCE gradients. The short wavelength structure may be reduced by subtracting the terrain effects computed by Residual Terrain Modeling (RTM) method Forsberg 1984 [14].

Additionally, gravity anomalies from satellite altimetry may be used to enhance the recovery of the gravity field and to improve the estimation of the MDT.

It could not be concluded whether the regionally enhanced geoid model estimated using GOCE gradients contribute to a further improvement of the determination of the MDT in the GOCINA area. This will require further investigation.

Part IV

APPENDIX

A

EXPRESSIONS FOR THE FIRST AND SECOND ORDER DERIVATIVES OF THE POTENTIAL IN THE LOCAL-NORTH-EAST UP COORDINATE SYSTEM

Normaly a gravitational potential function is related to position in terms of sperichal coordinates (ϕ, λ, r). The spatial derivatives of interest in connection with the output from a satellite gradiometer are the second partial derivatives with respect to a local Cartesian coordinate system at an arbitrary point in near earth space. The first partial derivatives of a gravitational potential function are the covariant components of the gravitational acceleration vector, a first order tensor. The gravitational gradients, the second partial derivatives of the potential with respect to Cartesian coordinates, are the components of a covariant second order tensor Reed 1973 [37].

A.1 TRANSFORMATION BETWEEN COORDINATE SYSTEMS

As the derivatives of the potential are tensor components, the required transformations are conveniently derived by the methods of tensor calculus.

Geocentric system is presented by $x^p = (x, y, z)$, and in spherical coordinates by $u^p = (\lambda, \phi, r)$. The geocentric system is further described by the unit vector triad $(\hat{i}_1, \hat{i}_2, \hat{i}_3)$ designated as the basis i_p. The local coordinate system is described by the basis e_p, with vectors in triad (e_1, e_2, e_3) that are not unit vectors. Here local rectangular coordinate system (η, ξ, ζ) is defined by the e_p basis.

Position vector of an arbitrary point P in space given in terms of the geocentric Cartesian coordinates by:

$$r = x^P i_P = x\hat{i}_1 + y\hat{i}_2 + z\hat{i}_3 \tag{A.1}$$

Geocentric coordinates are functionally related to the spherical coordinates by:

$$x^P = x^P(u^P) \tag{A.2}$$

which is given by:

$$\begin{aligned} x &= r\cos\varphi\cos\lambda \\ y &= r\cos\varphi\sin\lambda \\ z &= r\sin\varphi \end{aligned} \tag{A.3}$$

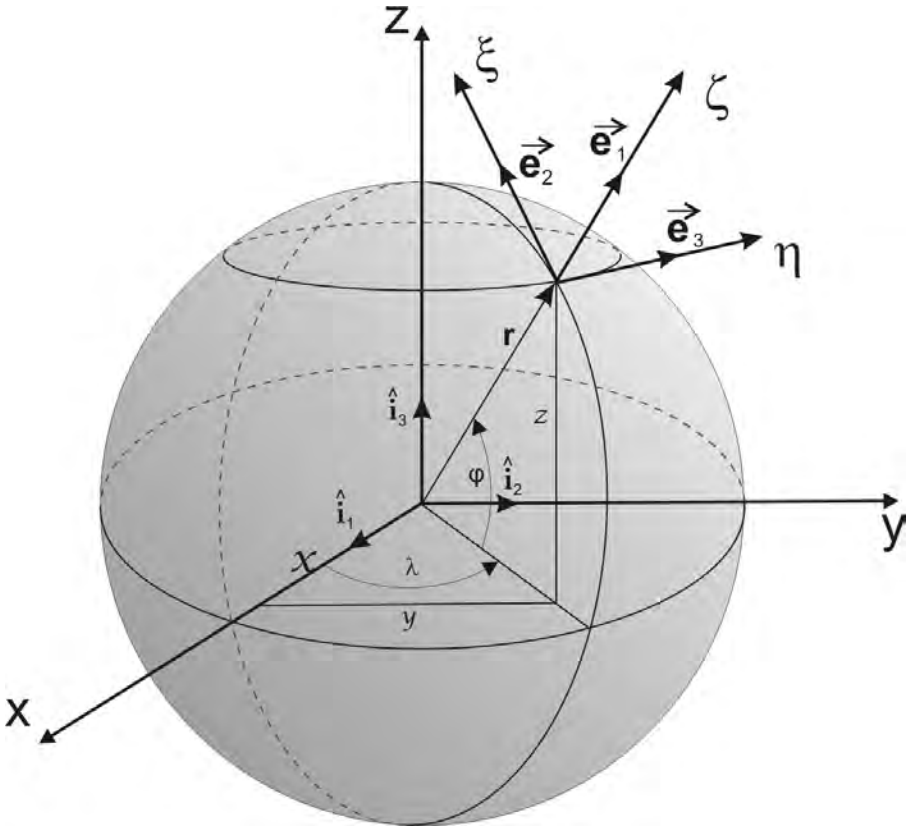

Figure A.1: Coordinate systems and basis vectors

The covariant basis e_P of the local coordinate system at the point P is given by:

$$e_q = i_P \frac{\partial x^P}{\partial u^q} \tag{A.4}$$

Partial derivatives $\frac{\partial x^P}{\partial u^q}$ can be obtained using equation A.3:

$$\frac{\partial(x,z,y)}{\partial(\lambda,\varphi,r)} = \begin{bmatrix} -r\cos\varphi\sin\lambda & -r\sin\varphi\sin\lambda & \cos\varphi\cos\lambda \\ r\cos\varphi\cos\lambda & -r\sin\varphi\sin\lambda & \cos\varphi\sin\lambda \\ 0 & r\cos\varphi & \sin\varphi \end{bmatrix} \tag{A.5}$$

Geocentric basis i_P in terms of the local basis e_P is obtained by:

$$i_P = e_S \frac{\partial u^S}{\partial x_P} \tag{A.6}$$

And substituting (A.4) into A.6, gives:

$$i_P = i_P \frac{\partial x^P}{\partial u^q} \frac{\partial u^S}{\partial x^P} \tag{A.7}$$

which is true only if:

$$\frac{\partial x^P}{\partial u^q} \frac{\partial u^S}{\partial x^P} = \sigma_q^S = \begin{cases} 1 & s = q \\ 0 & s \neq q \end{cases} \tag{A.8}$$

The matrix of partial derivatives $\frac{\partial u^S}{\partial x^P}$ is the inverse of A.5 (Reed 1973 [37]). Where determinant is:

$$\begin{aligned} \det\left[\frac{\partial(x,z,y)}{\partial(\lambda,\varphi,r)}\right] =& r^2\cos\varphi\sin^2\varphi\sin^2\lambda + \\ &+ r^2\cos^3\varphi\cos^2\lambda + \\ &+ r^2\cos^3\varphi\sin^2\lambda + \\ &+ r^2\sin^2\varphi\cos\varphi\cos^2\lambda = \\ &= r^2\sin^2\varphi\cos\varphi + r^2\cos^3\varphi = \\ &= r^2\cos\varphi \end{aligned} \tag{A.9}$$

And elements of the $\frac{\partial u^S}{\partial x^P}$ are:

$$\begin{aligned} \frac{\partial(\lambda,\varphi,r)'}{\partial(x,z,y)}_{(1,1)} &= -r\sin\varphi\sin\lambda\sin\lambda - r\cos^2\varphi\sin\lambda = -r\sin\lambda \\ \frac{\partial(\lambda,\varphi,r)'}{\partial(x,z,y)}_{(1,2)} &= r\cos\varphi\sin\varphi\cos\lambda \\ \frac{\partial(\lambda,\varphi,r)'}{\partial(x,z,y)}_{(1,3)} &= r^2\cos^2\varphi\cos\lambda \\ \frac{\partial(\lambda,\varphi,r)'}{\partial(x,z,y)}_{(2,1)} &= -r\sin^2\varphi\cos\lambda - r\cos^2\varphi\cos\lambda = r\cos\lambda \\ \frac{\partial(\lambda,\varphi,r)'}{\partial(x,z,y)}_{(2,2)} &= -r\cos\varphi\sin\varphi\sin\lambda \\ \frac{\partial(\lambda,\varphi,r)'}{\partial(x,z,y)}_{(2,3)} &= r^2\cos^2\varphi\sin\lambda \\ \frac{\partial(\lambda,\varphi,r)'}{\partial(x,z,y)}_{(3,1)} &= -r\sin\varphi\cos\varphi\sin\lambda\cos\lambda + r\sin\varphi\cos\varphi\sin\lambda\cos\lambda = 0 \\ \frac{\partial(x,z,y)'}{\partial(\lambda,\varphi,r)}_{(3,2)} &= -r\cos^2\varphi\sin^2\lambda - r\cos^2\varphi\cos^2\lambda = -r\cos^2\varphi \\ \frac{\partial(\lambda,\varphi,r)'}{\partial(x,z,y)}_{(3,3)} &= r\cos\varphi\sin\varphi\sin^2\lambda + r\cos\varphi\sin\varphi\cos^2\lambda = -r^2\cos\varphi\sin\varphi \end{aligned} \tag{A.10}$$

Multiply by determinant, one can get

$$\frac{\partial(\lambda,\varphi,r)}{\partial(x,z,y)} = \begin{bmatrix} \frac{-\sin\lambda}{r\cos\varphi} & \frac{\cos\lambda}{r\cos\varphi} & 0 \\ \frac{-\sin\varphi\cos\lambda}{r} & \frac{-\sin\varphi\sin\lambda}{r} & \frac{-\cos\lambda}{r} \\ \cos\varphi\cos\lambda & \cos\varphi\sin\lambda & \sin\varphi \end{bmatrix} \tag{A.11}$$

By taking the inner products:

$$g_{pq} = e_p \cdot e_q \tag{A.12}$$

covarian matrix tensor of the surface is obtained:

$$g_{pq} = \begin{bmatrix} r^2\cos^2\varphi & 0 & 0 \\ 0 & r^2 & 0 \\ 0 & 0 & 1 \end{bmatrix} \tag{A.13}$$

Inverting A.13 yields the contracovariant metric tensor:

$$g^{pq} = \begin{bmatrix} \frac{1}{r^2}\cos^2\varphi & 0 & 0 \\ 0 & \frac{1}{r^2} & 0 \\ 0 & 0 & 1 \end{bmatrix} \tag{A.14}$$

Here Christoffel symbols of the second kind are introduced:

$$\left\{ \begin{matrix} 1 \\ p \quad q \end{matrix} \right\} = \begin{bmatrix} 0 & -\tan\varphi & \frac{1}{r} \\ -\tan\varphi & 0 & 0 \\ \frac{1}{r} & 0 & 0 \end{bmatrix}$$

$$\left\{ \begin{matrix} 3 \\ p \quad q \end{matrix} \right\} = \begin{bmatrix} \sin\varphi\cos\varphi & 0 & 0 \\ 0 & 0 & \frac{1}{r} \\ 0 & \frac{1}{r} & 0 \end{bmatrix}$$

$$\left\{ \begin{matrix} 3 \\ p \quad q \end{matrix} \right\} = \begin{bmatrix} -r\cos^2\varphi & 0 & 0 \\ 0 & -r & 0 \\ 0 & 0 & 0 \end{bmatrix} \tag{A.15}$$

By making use of the Christoffel symbols and equations A.4 and A.5, derivatives of the e_p basis vectors are:

$$\frac{\partial e^p}{\partial u_q} = \left\{ \begin{matrix} s \\ p \quad q \end{matrix} \right\} e_s \tag{A.16}$$

For the contravariant components $e^P = g^{Pq} e_P$, expression is:

$$\frac{\partial e^P}{\partial u_q} = -\left\{ \begin{matrix} & S & \\ p & & q \end{matrix} \right\} e^S \tag{A.17}$$

If potential is considered, $V = V(u^P) = V(\lambda, \varphi, r)$, gradient of V is defined in the (x, y, z) or (η, ξ, ζ) Cartesian coordinate system.

$$\overline{\nabla} V = \frac{\partial V}{\partial u^P} e^P$$

$$\overline{\nabla} V = \frac{\partial V}{\partial u^P} g^{PP} e_P \tag{A.18}$$

For $\overline{\nabla} V$ in local coordinate system:

$$\overline{\nabla} V = \frac{1}{r^2 \cos^2 \varphi} V_\lambda e_1 + \frac{1}{r^2} V_\varphi e_2 + V_r e_3 \tag{A.19}$$

Vector triad defining e_P basis are not all unit vectors. To obtain the correct physical components in the local coordinate system e_P basis must be normalized.

$$\begin{aligned} \hat{e}_1 &= \frac{1}{r \cos \varphi} e_1 \\ \hat{e}_2 &= \frac{1}{r} e_2 \\ \hat{e}_3 &= e_3 \end{aligned} \tag{A.20}$$

Equation A.18 in the normalized basis is:

$$\nabla V = \frac{1}{r \cos \varphi} V_\lambda \hat{e}_1 + \frac{1}{r} V_\varphi \hat{e}_2 + V_r \hat{e}_3 \tag{A.21}$$

First order derivatives in the local (η, ξ, ζ) system are:

$$\begin{aligned} V_\eta &= \frac{1}{r \cos \varphi} \frac{\partial V}{\partial \lambda} \\ V_\xi &= \frac{1}{r} \frac{\partial V}{\partial \varphi} \\ V_\zeta &= V_r \end{aligned} \tag{A.22}$$

To form second order derivatives, notataion $\overline{\nabla\nabla}$ will be used to distinguish the computation for the Laplacian $\overline{\nabla}^2 V$. The operator $\overline{\nabla}$

can be expressed in terms of the contravariant basis e_P and spherical coordinates by:

$$\overline{\nabla} V = e^P \frac{\partial}{\partial u^P} \tag{A.23}$$

Then:

$$\begin{aligned} \overline{\nabla\nabla} V &= e^P \frac{\partial}{\partial u^P} \left(\frac{\partial V}{\partial u^q} e^q \right) \\ &= e^P \left(\frac{\partial^2 V}{\partial u^P \partial u^q} e^q + \frac{\partial V}{\partial u^q} \frac{\partial e^q}{\partial u^P} \right) \end{aligned} \tag{A.24}$$

Using A.17, equation A.24 takes form:

$$\overline{\nabla\nabla} V = \left(\frac{\partial^2 V}{\partial u^P \partial u^q} e^q - \frac{\partial V}{\partial u^s} \left\{ \begin{matrix} s \\ p \quad q \end{matrix} \right\} \right) e^P e^q \tag{A.25}$$

where the term inside the parenthesis is the covariant derivative of the acceleration vector. The basis vector s must be normalized to give the proper physical components in the local Cartesian system (Reed, 1973, [37]). Using the normalized basis $\hat{e}_P$ from A.21 and the

Christoffel symbols from A.15 in equation A.24 dyadic equation (in the dyad basis $\hat{e}_p\ \hat{e}_q$) can be obtained:

$$\overline{\nabla\nabla}V_{(P=1,q=1)} = \left(\frac{\partial^2 V}{\partial\lambda^2} - \frac{\partial V}{\partial\varphi}\sin\varphi\cos\varphi + \frac{\partial V}{\partial r}r\cos^2\varphi\right)e^1e^1$$

where

$$e^1 = g^{1q}e_1 = \frac{1}{r^2\cos^2\varphi}e_1 = \frac{1}{r^2\cos^2\varphi}r\cos\varphi\hat{e}_1 = \frac{1}{r\cos\varphi}\hat{e}_1$$

then

$$\begin{aligned}
\overline{\nabla\nabla}V_{(P=1,q=1)} &= \left(\frac{\partial^2 V}{\partial\lambda^2} - \frac{\partial V}{\partial\varphi}\sin\varphi\cos\varphi + \frac{\partial V}{\partial r}r\cos^2\varphi\right)\frac{1}{r^2\cos^2\varphi}\hat{e}_1\hat{e}_1\\
\overline{\nabla\nabla}V_{(P=1,q=2)} &= \left(\frac{\partial^2 V}{\partial\lambda\partial\varphi} + \frac{\partial V}{\partial\lambda}\tan\varphi\right)e^1e^2 =\\
&= \left(\frac{\partial^2 V}{\partial\lambda\partial\varphi} + \frac{\partial V}{\partial\lambda}\tan\varphi\right)\frac{1}{r\cos\varphi}\hat{e}_1\frac{1}{r^2}r\hat{e}_2 =\\
&= \left(\frac{\partial^2 V}{\partial\lambda\partial\varphi} + \frac{\partial V}{\partial\lambda}\tan\varphi\right)\frac{1}{r^2\cos\varphi}\hat{e}_1\hat{e}_2\\
\overline{\nabla\nabla}V_{(P=1,q=3)} &= \left(\frac{\partial^2 V}{\partial\lambda\partial r} - \frac{\partial V}{\partial\lambda}\frac{1}{r}\right)e^1e^3 =\\
&= \left(\frac{\partial^2 V}{\partial\lambda\partial r} - \frac{\partial V}{\partial\lambda}\frac{1}{r}\right)\frac{1}{r\cos\varphi}\hat{e}_1g^{3q}e_3 =\\
&= \left(\frac{\partial^2 V}{\partial\lambda\partial r} - \frac{\partial V}{\partial\lambda}\frac{1}{r}\right)\frac{1}{r\cos\varphi}\hat{e}_1\hat{e}_3\\
\overline{\nabla\nabla}V_{(P=2,q=1)} &= \left(\frac{\partial^2 V}{\partial\varphi\partial\lambda} + \frac{\partial V}{\partial\lambda}\tan\varphi\right)e^2e^1 =\\
&= \left(\frac{\partial^2 V}{\partial\varphi\partial\lambda} + \frac{\partial V}{\partial\lambda}\tan\varphi\right)\frac{1}{r^2\cos\varphi}\hat{e}_2\hat{e}_1\\
\overline{\nabla\nabla}V_{(P=2,q=2)} &= \left(\frac{\partial^2 V}{\partial\varphi^2} + \frac{\partial V}{\partial r}r\right)e^2e^2 = \left(\frac{\partial^2 V}{\partial\varphi^2} + \frac{\partial V}{\partial r}r\right)\frac{1}{r^2}\hat{e}_2\hat{e}_2\\
\overline{\nabla\nabla}V_{(P=2,q=3)} &= \left(\frac{\partial^2 V}{\partial\varphi\partial r} - \frac{\partial V}{\partial\varphi}\frac{1}{r}\right)e^2e^3 = \left(\frac{\partial^2 V}{\partial\varphi\partial r} - \frac{\partial V}{\partial\varphi}\frac{1}{r}\right)\frac{1}{r}\hat{e}_2\hat{e}_3\\
\overline{\nabla\nabla}V_{(P=3,q=1)} &= \left(\frac{\partial^2 V}{\partial r\partial\lambda} - \frac{\partial V}{\partial\lambda}\frac{1}{r}\right)e^3e^1 = \left(\frac{\partial^2 V}{\partial r\partial\lambda} - \frac{\partial V}{\partial\lambda}\frac{1}{r}\right)\frac{1}{r\cos\varphi}\hat{e}_3\hat{e}_1\\
\overline{\nabla\nabla}V_{(P=3,q=2)} &= \left(\frac{\partial^2 V}{\partial r\partial\varphi} - \frac{\partial V}{\partial\varphi}\frac{1}{r}\right)e^3e^2 = \left(\frac{\partial^2 V}{\partial r\partial\varphi} - \frac{\partial V}{\partial\varphi}\frac{1}{r}\right)\frac{1}{r}\hat{e}_3\hat{e}_2\\
\overline{\nabla\nabla}V_{(P=3,q=3)} &= \left(\frac{\partial^2 V}{\partial r^2} - 0\right)e^3e^3 = \frac{\partial^2 V}{\partial r^2}\hat{e}_3\hat{e}_3
\end{aligned} \tag{A.26}$$

$$
\begin{aligned}
\overline{\nabla\nabla}V = &\left(\frac{\partial^2 V}{\partial\lambda^2} - \frac{\partial V}{\partial\varphi}\sin\varphi\cos\varphi + \frac{\partial V}{\partial r}r\cos^2\varphi\right)\frac{1}{r^2\cos^2\varphi}\hat{e}_1\hat{e}_1 + \\
&+ \left(\frac{\partial^2 V}{\partial\lambda\partial\varphi} + \frac{\partial V}{\partial\lambda}\tan\varphi\right)\frac{1}{r^2\cos\varphi}\hat{e}_1\hat{e}_2 + \\
&+ \left(\frac{\partial^2 V}{\partial\lambda\partial r} - \frac{\partial V}{\partial\lambda}\frac{1}{r}\right)\frac{1}{r\cos\varphi}\hat{e}_1\hat{e}_3 \\
&+ \left(\frac{\partial^2 V}{\partial\varphi\partial\lambda} + \frac{\partial V}{\partial\lambda}\tan\varphi\right)\frac{1}{r^2\cos\varphi}\hat{e}_2\hat{e}_1 \\
&+ \left(\frac{\partial^2 V}{\partial\varphi^2} + \frac{\partial V}{\partial r}r\right)\frac{1}{r^2}\hat{e}_2\hat{e}_2 \\
&+ \left(\frac{\partial^2 V}{\partial\varphi\partial r} - \frac{\partial V}{\partial\varphi}\frac{1}{r}\right)\frac{1}{r}\hat{e}_2\hat{e}_3 \\
&+ \left(\frac{\partial^2 V}{\partial r\partial\lambda} - \frac{\partial V}{\partial\lambda}\frac{1}{r}\right)\frac{1}{r\cos\varphi}\hat{e}_3\hat{e}_1 \\
&+ \left(\frac{\partial^2 V}{\partial r\partial\varphi} - \frac{\partial V}{\partial\varphi}\frac{1}{r}\right)\frac{1}{r}\hat{e}_3\hat{e}_2 \\
&+ \frac{\partial^2 V}{\partial r^2}\hat{e}_3\hat{e}_3
\end{aligned}
\tag{A.27}
$$

Thus, the second order derivatives of the potential, or the gravitational gradients, in the (η, ξ, ζ) system from A.27 are:

$$
\begin{aligned}
V_{\eta\eta} &= \frac{1}{r^2\cos^2\varphi}\frac{\partial^2 V}{\partial\lambda^2} - \frac{\tan\varphi}{r^2}\frac{\partial V}{\partial\varphi} + \frac{1}{r}\frac{\partial V}{\partial r} \\
V_{\xi\xi} &= \frac{1}{r^2}\frac{\partial^2 V}{\partial\varphi^2} + \frac{1}{r}\frac{\partial V}{\partial r} \\
V_{\zeta\zeta} &= \frac{\partial^2 V}{\partial r^2}
\end{aligned}
\tag{A.28}
$$

First order derivatives of potential in respect to latitude φ_P and longitude λ_P can be expressed by differentiation of cosine of spherical distance t ($t = \cos\psi$):

$$
\begin{aligned}
\frac{\partial V}{\partial\varphi_P} &= \frac{\partial V}{\partial t}\frac{\partial t}{\partial\varphi_P} \\
\frac{\partial V}{\partial\lambda_P} &= \frac{\partial V}{\partial t}\frac{\partial t}{\partial\lambda_P}
\end{aligned}
\tag{A.29}
$$

Then the second order derivatives are:

$$\begin{aligned}\frac{\partial V^2}{\partial \varphi_P^2} &= \frac{\partial}{\partial \varphi_P}\left(\frac{\partial V}{\partial t}\frac{\partial t}{\partial \varphi_P}\right) = \frac{\partial^2 V}{\partial \varphi_P \partial t}\frac{\partial t}{\partial \varphi_P} + \frac{\partial V}{\partial t}\frac{\partial^2 t}{\partial \varphi_P^2} = \\ &= \frac{\partial^2 V}{\partial t^2}\frac{\partial t}{\partial \varphi_P}\frac{\partial t}{\partial \varphi_P} + \frac{\partial V}{\partial t}\frac{\partial^2 t}{\partial \varphi_P^2} = \\ &= \frac{\partial^2 V}{\partial t^2}\left(\frac{\partial t}{\partial \varphi_P}\right)^2 + \frac{\partial V}{\partial t}\frac{\partial^2 t}{\partial \varphi_P^2}\end{aligned} \tag{A.30}$$

$$\begin{aligned}\frac{\partial V^2}{\partial \lambda_P^2} &= \frac{\partial}{\partial \lambda_P}\left(\frac{\partial V}{\partial t}\frac{\partial t}{\partial \lambda_P}\right) = \frac{\partial^2 V}{\partial \lambda_P \partial t}\frac{\partial t}{\partial \lambda_P} + \frac{\partial V}{\partial t}\frac{\partial^2 t}{\partial \lambda_P^2} = \\ &= \frac{\partial^2 V}{\partial t^2}\frac{\partial t}{\partial \lambda_P}\frac{\partial t}{\partial \lambda_P} + \frac{\partial V}{\partial t}\frac{\partial^2 t}{\partial \lambda_P^2} = \\ &= \frac{\partial^2 V}{\partial t^2}\left(\frac{\partial t}{\partial \lambda_P}\right)^2 + \frac{\partial V}{\partial t}\frac{\partial^2 t}{\partial \lambda_P^2}\end{aligned}$$

If inverse distance $\frac{1}{l}$ is expressed by:

$$\frac{1}{l} = \frac{1}{\sqrt{r_P^2 + r_q^2 - 2r_P r_q \cos\psi}} \tag{A.31}$$

where

$$t = \cos\psi = \sin\varphi_P \sin\varphi_q + \cos\varphi_P \cos\varphi_q \cos(\Delta\lambda) \tag{A.32}$$

Then derivatives of potential (equation 2.6)in respect to spherical distance t are expressed by:

$$\frac{\partial V}{\partial t} = \frac{r_P r_q}{(r_P^2 + r_q^2 - 2r_P r_q t)^{\frac{3}{2}}} = \frac{r_P r_q}{l^3} \tag{A.33}$$

and

$$\frac{\partial^2 V}{\partial t^2} = \frac{3(r_P r_q)^2}{(r_P^2 + r_q^2 - 2r_P r_q t)^{\frac{5}{2}}} = \frac{3r_P^2 r_q^2}{l^5} \tag{A.34}$$

Derivatives of potential in radial direction r, are expressed by:

$$\begin{aligned}\frac{\partial V}{\partial r_P} &= \frac{-\frac{1}{2}l^{-1}(2r_P - 2r_q t)}{l^2} \\ &= -\frac{r_P - r_q t}{l^3}\end{aligned} \tag{A.35}$$

$$\begin{aligned}\frac{\partial^2 V}{\partial r_P^2} &= -\frac{l^3 - (r_P - r_q t)\, 3l^2 \frac{1}{2} l^{-1} \left(2r_P - 2r_q t\right)}{l^6} \\ &= -\frac{1}{l^3} + 3\frac{(r_P - r_q t)^2}{l^5}\end{aligned} \tag{A.36}$$

To expand equation A.28 completely, derivation of cosine of spherical distance in respect longitude and latitude needs to be defined. First order derivatives are:

$$\begin{aligned}\frac{\partial t}{\partial \varphi_P} &= \cos\varphi_P \sin\varphi_q - \sin\varphi_P \cos\varphi_q \cos(\Delta\lambda) \\ \frac{\partial t}{\partial \lambda_P} &= -\cos\varphi_P \cos\varphi_q \sin(\Delta\lambda)\end{aligned} \tag{A.37}$$

and the second order derivatives are:

$$\begin{aligned}\frac{\partial^2 t}{\partial \varphi_P^2} &= -\sin\varphi_P \sin\varphi_q - \cos\varphi_P \cos\varphi_q \cos(\Delta\lambda) = -t \\ \frac{\partial^2 t}{\partial \lambda_P^2} &= -\cos\varphi_P \cos\varphi_q \cos(\Delta\lambda)\end{aligned} \tag{A.38}$$

Finally, expansions of equations A.28, for second order derivatives of the potential in the (η, ξ, ζ) system, are:

$$
\begin{aligned}
V_{\eta\eta} &= \frac{1}{r_P^2 \cos^2\varphi_P}\frac{\partial^2 V}{\partial \lambda_P^2} - \frac{\tan\varphi_P}{r_P^2}\frac{\partial V}{\partial \varphi_P} + \frac{1}{r_P}\frac{\partial V}{\partial r_P} = \\
&= \frac{1}{r_P^2 \cos^2\varphi_P}\left[\frac{\partial V}{\partial t}\frac{\partial^2 t}{\partial \lambda_P^2} + \frac{\partial^2 V}{\partial t^2}\left(\frac{\partial t}{\partial \lambda_P}\right)^2\right] - \\
&- \frac{\tan\varphi_P}{r_P^2}\frac{\partial t}{\partial \varphi_P}\frac{\partial V}{\partial t} + \frac{1}{r_P}\left(-\frac{r_P - r_q t}{l^3}\right) = \\
&= \frac{1}{r_P^2 \cos^2\varphi_P}\left[\left(-\cos\varphi_P \cos\varphi_q \cos(\Delta\lambda)\right)\frac{r_P r_q}{l^3} + \right. \\
&\left. + \left(\cos^2\varphi_P \cos^2\varphi_q \sin^2(\Delta\lambda)\right) 3\frac{r_P^2 r_q^2}{l^5}\right] - \\
&- \frac{\tan\varphi_P}{r_P^2}\left(\cos\varphi_P \sin\varphi_q - \sin\varphi_P \cos\varphi_q \cos(\Delta\lambda)\right)\frac{r_P r_q}{l^3} - \\
&- \frac{r_P - r_q t}{r_P l^3} = \\
&= \frac{r_q}{r_P l^3}\left[-\frac{\cos\varphi_q}{\cos\varphi_P}\cos(\Delta\lambda) + \cos^2\varphi_q \sin^2(\Delta\lambda) 3\frac{r_P r_q}{l^2}\right] - \\
&- \left(\frac{\sin\varphi_P}{\cos\varphi_P}\cos\varphi_P \sin\varphi_q - \frac{\sin\varphi_P}{\cos\varphi_P}\sin\varphi_P \cos\varphi_q \cos(\Delta\lambda)\right)\frac{r_q}{r_P l^3} - \\
&- \frac{r_P}{r_P l^3} + \frac{r_q t}{r_P l^3} = \\
&= \frac{r_q}{r_P l^3}\left[-\frac{\cos\varphi_q}{\cos\varphi_P}\cos(\Delta\lambda) + \cos^2\varphi_q \sin^2(\Delta\lambda) 3\frac{r_P r_q}{l^2}\right] - \\
&- \left(\sin\varphi_P \sin\varphi_q - \frac{\cos^2\varphi_P - 1}{\cos\varphi_P}\cos\varphi_q \cos(\Delta\lambda)\right)\frac{r_q}{r_P l^3} - \\
&- \frac{r_P}{r_P l^3} + \frac{r_q t}{r_P l^3} = \\
&= \frac{r_q}{r_P l^3}\left[-\frac{\cos\varphi_q}{\cos\varphi_P}\cos(\Delta\lambda) + \cos^2\varphi_q \sin^2(\Delta\lambda) 3\frac{r_P r_q}{l^2}\right] - \\
&- \left(t - \frac{\cos\varphi_q}{\cos\varphi_P}\cos(\Delta\lambda)\right)\frac{r_q}{r_P l^3} - \frac{r_P}{r_P l^3} + \frac{r_q t}{r_P l^3} = \\
&= \frac{r_q}{r_P l^3}\left[-\frac{\cos\varphi_q}{\cos\varphi_P}\cos(\Delta\lambda) + \cos^2\varphi_q \sin^2(\Delta\lambda) 3\frac{r_P r_q}{l^2}\right. \\
&\left. -t + \frac{\cos\varphi_q}{\cos\varphi_P}\cos(\Delta\lambda) + t\right] - \frac{1}{l^3} \\
&= \frac{r_q}{r_P l^3}\left[\cos^2\varphi_q \sin^2(\Delta\lambda) 3\frac{r_P r_q}{l^2}\right] - \frac{1}{l^3} = \\
V_{\eta\eta} &= 3\frac{r_q^2}{l^5}\cos^2\varphi_q \sin^2(\Delta\lambda) - \frac{1}{l^3}
\end{aligned}
\tag{A.39}
$$

$$
\begin{aligned}
V_{\xi\xi} &= \frac{1}{r_P^2}\frac{\partial^2 V}{\partial \varphi_P^2} + \frac{1}{r_P}\frac{\partial V}{\partial r_P} = \\
&= \frac{1}{r_P^2}\left[\frac{\partial V}{\partial t}\frac{\partial^2 t}{\partial \varphi_P^2} + \frac{\partial^2 V}{\partial t^2}\left(\frac{\partial t}{\partial \varphi_P}\right)^2\right] + \frac{1}{r_P}\left(-\frac{r_P - r_q t}{l^3}\right) = \\
&= \frac{1}{r_P^2}\left[(-\sin\varphi_P \sin\varphi_q - \cos\varphi_P \cos\varphi_q \cos(\Delta\lambda))\,\frac{r_P r_q}{l^3} + \right. \\
&+ \left.(\cos\varphi_P \sin\varphi_q - \sin\varphi_P \cos\varphi_q \cos(\Delta\lambda))^2\,\frac{3r_P^2 r_q^2}{l^5}\right] - \\
&- \frac{r_P - r_q t}{r_P l^3} = \\
&= \frac{1}{r_P^2}\left[\frac{-t r_P r_q}{l^3} + (\cos\varphi_P \sin\varphi_q - \sin\varphi_P \cos\varphi_q \cos(\Delta\lambda))^2\,\frac{3r_P^2 r_q^2}{l^5}\right] - \\
&- \frac{r_P}{r_P l^3} + \frac{r_q t}{r_P l^3} = \\
&= \frac{r_q}{r_P l^3}\left[-t + (\cos\varphi_P \sin\varphi_q - \sin\varphi_P \cos\varphi_q \cos(\Delta\lambda))^2\,\frac{3r_P r_q}{l^2}\right] - \\
&- \frac{1}{l^3} + \frac{r_q t}{r_P l^3} = \\
&= \frac{r_q}{r_P l^3}\left[-t + (\cos\varphi_P \sin\varphi_q - \sin\varphi_P \cos\varphi_q \cos(\Delta\lambda))^2\,\frac{3r_P r_q}{l^2} + t\right] - \\
&- \frac{1}{l^3} \\
V_{\xi\xi} &= 3\frac{r_q^2}{l^5}(\cos\varphi_P \sin\varphi_q - \sin\varphi_P \cos\varphi_q \cos(\Delta\lambda))^2 - \frac{1}{l^3}
\end{aligned}
\tag{A.40}
$$

$$
V_{\zeta\zeta} = \frac{\partial^2 V}{\partial r_P^2} = -\frac{1}{l^3} + 3\frac{(r_P - r_q t)^2}{l^5} \tag{A.41}
$$

Applying the Laplacian operator Δ to V, we can obtain *Laplacian differential equation* ΔV:

$$
\Delta V = V_{\eta\eta} + V_{\xi\xi} + V_{\zeta\zeta} \tag{A.42}
$$

$$
\begin{aligned}
\Delta V &= 3\frac{r_q^2}{l^5}\cos^2\varphi_q \sin^2(\Delta\lambda) - \frac{1}{l^3} + \\
&+ 3\frac{r_q^2}{l^5}\left(\cos\varphi_P \sin\varphi_q - \sin\varphi_P \cos\varphi_q \cos(\Delta\lambda)\right)^2 - \frac{1}{l^3} - \\
&- \frac{1}{l^3} + 3\frac{(r_P - r_q t)^2}{l^5} = \\
&= 3\frac{(r_P - r_q t)^2}{l^5} - \frac{3}{l^3} + 3\frac{r_q^2}{l^5}\left[\cos^2\varphi_q(1 - \cos^2(\Delta\lambda) + \cos^2\varphi_P \sin^2\varphi_q - \right. \\
&\left. -2\cos\varphi_P \sin\varphi_q \sin\varphi_P \cos\varphi_q \cos(\Delta\lambda) + \sin^2\varphi_P \cos^2\varphi_q^2 \cos^2(\Delta\lambda)\right] = \\
&= 3\frac{(r_P - r_q t)^2}{l^5} - \frac{3}{l^3} + 3\frac{r_q^2}{l^5}\left[\cos^2\varphi_q - \cos^2\varphi_q \cos^2(\Delta\lambda)(1 - \sin^2\varphi_P) + \right. \\
&\left. + \cos^2\varphi_P \sin^2\varphi_q - 2\cos\varphi_P \sin\varphi_q \sin\varphi_P \cos\varphi_q \cos(\Delta\lambda)\right] = \\
&= 3\frac{(r_P - r_q t)^2}{l^5} - \frac{3}{l^3} + 3\frac{r_q^2}{l^5}\left[\cos^2\varphi_q - \cos^2\varphi_P \cos^2\varphi_q \cos^2(\Delta\lambda) + \right. \\
&\left. + \cos^2\varphi_P \sin^2\varphi_q - \cos\varphi_P \sin\varphi_q \sin\varphi_P \cos\varphi_q \cos(\Delta\lambda) - \right. \\
&\left. - \cos\varphi_P \sin\varphi_q \sin\varphi_P \cos\varphi_q \cos(\Delta\lambda)\right] = \\
&= 3\frac{(r_P - r_q t)^2}{l^5} - \frac{3}{l^3} + 3\frac{r_q^2}{l^5}\left[\cos^2\varphi_q + \cos^2\varphi_P \sin^2\varphi_q - \right. \\
&\left. - \cos\varphi_P \cos\varphi_q \cos(\Delta\lambda)(\cos\varphi_P \cos\varphi_q \cos(\Delta\lambda) + \sin\varphi_q \sin\varphi_P) - \right. \\
&\left. - \cos\varphi_P \sin\varphi_q \sin\varphi_P \cos\varphi_q \cos(\Delta\lambda)\right] = \\
&= 3\frac{(r_P - r_q t)^2}{l^5} - \frac{3}{l^3} + 3\frac{r_q^2}{l^5}\left[\cos^2\varphi_q + (1 - \sin^2\varphi_P)\sin^2\varphi_q - \right. \\
&\left. - \cos\varphi_P \cos\varphi_q \cos(\Delta\lambda)t - \cos\varphi_P \sin\varphi_q \sin\varphi_P \cos\varphi_q \cos(\Delta\lambda)\right] = \\
&= 3\frac{(r_P - r_q t)^2}{l^5} - \frac{3}{l^3} + 3\frac{r_q^2}{l^5}\left[\cos^2\varphi_q + \sin^2\varphi_q - \right. \\
&\left. - \sin\varphi_q \sin\varphi_P(\sin\varphi_q \sin\varphi_P + \cos\varphi_P \cos\varphi_q \cos(\Delta\lambda)) - \right. \\
&\left. - \cos\varphi_P \cos\varphi_q \cos(\Delta\lambda)t\right] = \\
&= 3\frac{(r_P - r_q t)^2}{l^5} - \frac{3}{l^3} + 3\frac{r_q^2}{l^5}\left[1 - \sin\varphi_q \sin\varphi_P t - \right. \\
&\left. - \cos\varphi_P \cos\varphi_q \cos(\Delta\lambda)t\right] = \\
&= 3\frac{(r_P - r_q t)^2}{l^5} - \frac{3}{l^3} + 3\frac{r_q^2}{l^5}\left[1 - t(\sin\varphi_q \sin\varphi_P + \cos\varphi_P \cos\varphi_q \cos(\Delta\lambda))\right] = \\
&= -\frac{3}{l^3} + 3\frac{(r_P - r_q t)^2}{l^5} + 3\frac{r_q^2}{l^5}\left[1 - t^2\right] = \\
&= -\frac{3}{l^3} + 3\frac{r_P^2 - 2r_P r_q t + r_q^2 t^2}{l^5} + 3\frac{r_q^2 - r_q^2 t^2}{l^5} = \\
&= -\frac{3}{l^3} + 3\frac{r_P^2 - 2r_P r_q t + r_q^2}{l^5} = -\frac{3}{l^3} + 3\frac{l^2}{l^5} \\
\Delta V &= 0
\end{aligned}
\tag{A.43}
$$

B

PUBLICATIONS

The papers that were part of this Ph.D. project are included on the pages hereafter.

C.C. Tscherning, M. Veicherts, and M. Herceg: *Reduced point mass or multipole base functions*. In the Honor of Proffessor emeritus Demetrius N. Arbelos, 2010.

Point-mass functions or multipole base-functions are harmonic functions, which may be used to represent the (anomalous) gravity potential T globally or locally. The functions may be expressed by closed expressions or as sums of Legendre series. In both cases at least the two first terms must be removed since they are not present in T. For local applications the effect of a global gravity model is generally removed (and later restored). Then more terms need to be removed or substituted by terms similar to error-degree variances. We have done some calculations to illustrate the effect of reducing the point mass or multipole functions, i.e. showing how the first zero-crossing as a function of spherical distance comes closer to zero when more terms are removed.

Matija Herceg and Per Knudsen: *Full resolution geoid from GOCE gradients for ocean modeling*. ESA Living Symposium proceedings, Bergen, 2010.

The main objective of the study is to improve the methodology for combining GOCE gravity field models with satellite altimetry to derive optimal dynamic ocean topography models for oceanography. Since dynamic ocean topography determination is the difference between the sea surface and the geoid, the definition of both surfaces is of great significance. Here a method for geoid determination, using simulated GOCE gradients and the point mass method, is used for the regional determination of the gravity field that is not recovered by the global GOCE gravity model of spherical harmonic coefficients up to degree and order 200. Comparisons with the GOCINA mean dynamic topography show that the GOCE gradients enhance the determination of the mean dynamic topography at wavelength not recovered by the planned global GOCE gravity field model.

Reduced point mass or multipole base functions.

C.C.Tscherning, M.Veicherts,[1] M.Herceg[2],

[1]*Niels Bohr Institute, University of Copenhagen, Denmark.*

[2]*DTU Space, Denmark.*

Juliane Maries Vej 30, DK 2100 Copenhagen Oe, Denmark.

Abstract: Point-mass functions or multipole base-functions are harmonic functions, which may be used to represent the (anomalous) gravity potential (*T*) globally or locally. The functions may be expressed by closed expressions or as sums of Legendre series. In both cases at least the two first terms must be removed since they are not present in *T*. For local applications the effect of a global gravity model is generally removed (and later restored). Then more terms need to be removed or substituted by terms similar to error-degree variances. We have done some calculations to illustrate the effect of reducing the point mass or multipole functions, i.e. showing how the first zero-crossing as a function of spherical distance comes closer to zero when more terms are removed.

1. Introduction.

Linear combinations of point mass functions or mass multipoles have been used for the representation of the global (***W***) or regional anomalous gravity potential, ***T***, see e.g. Balmino (1974), Hauck and Lelgemann (1985), Vermeer (1982, 1989, 1990,1992,1993), Marchenko et al., (2001), Ballani et al. (1993), Wu (1984).

The anomalous potential *T*, is equal to the difference between *W* and a global gravity field model like EGM96 (Lemoine et al., 1998), ie. it is a harmonic function.

For a point mass base function we have for an approximation to *T*:

$$T = \sum_{i=1}^{I} \frac{GM_i}{l_i} \qquad (1)$$

where G is the gravitational constant, M_i is the mass, I the number of point masses and l_i is the distance from the mass located at the point Q_i to the point of evaluation, P, see Fig. 1. The distance from the origin to P and Q_i is denoted r_P , r_{Qi}, respectively and the first will always be larger than the other. The angle (spherical distance) between the vectors to P and Q_i is denoted ψ.

Fig. 1.

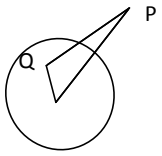

We now drop the subscript on Q. The distance l, from P to Q is then $l = \sqrt{r_P^2 + r_Q^2 - 2r_P r_Q \cos(\psi)}$. For the inverse distance we have

$$\frac{1}{l} = \frac{1}{r_P}\sum_{i=0}^{\infty}\left(\frac{r_Q}{r_P}\right)^i P_i(\cos\psi) \qquad (2)$$

where P_i are the Legendre polynomials. Multipole-functions are derive from the inverse distance function by integration or differentiation (compare Tscherning and Rapp (1974)), and will be denoted f.

$$T(P) = \sum_{i=1}^{M} a_i f_i(P) \qquad (3)$$

The estimate $\tilde{T}$ is determined so that $\sum_{i=1}^{M}\left(\{L_i T\} - obs_i\right)^2$ = min, where M is the number of observations and L_i are the linear functionals associated with the observations. In the computations described below we only consider height anomalies (geoid heights), gravity disturbances and second-order radial derivatives.

We intend to show that in order to make the functions suitable for regional gravity field modeling low-degree terms may be removed or substituted by appropriate weights.

2. Higher order derivatives,

For derivatives with respect to r_P we have series expansions similar to eq. (2), where the terms for the first derivative are multiplied with $-(i+1)/r_P$ and for the second derivative with $(i+1)*(i+2)/r_P^2$. Closed expressions for the derivatives are easily found.

$$\frac{\partial \frac{1}{l}}{\partial r_P} = \frac{(r_Q t - r_P)}{l^3} \qquad (4)$$

$$\frac{\partial^2 \frac{1}{l}}{\partial r_P^2} = \left(\frac{3(r_P - r_Q t)^2}{l^2} - \frac{1}{l^3} \right) \qquad (5)$$

Point masses are not the only harmonic functions which may be used as base functions when approximating *T*, see e.g. Tscherning (1972), Hauck and Lelgemann (1985) but we will only deal with point mass and excentric multipoles base functions, since they fully represents the message of this paper.

3. Reduced point masses.

From eq. (2) we see that if we use the representation eq. (1), it will contain terms of degree zero and one, which are not present in *T*. So they have to be removed, simply by subtracting from the closed expressions the first two terms in eq. (2) or its derivative. (This is not done for the examples of closed expressions in section 5). But what if we subtract from the data (and later add back) the contribution from a global model like EGM96, complete to degree N ?

$$T_N = \frac{GM}{r_P} \sum_{n=0}^{N} \left(\frac{a}{r_P} \right)^n \sum_{m=-n}^{n} C_{nm} P_{nm}(\sin\varphi) \begin{Bmatrix} \cos(m\lambda), m \geq 0 \\ \sin(|m|\lambda), m < 0 \end{Bmatrix} \qquad (6)$$

Here φ is the geocentric latitude , λ the longitude, P_{nm} the normalized Legendre functions and a a scale factor close to the semi-major axis. C_{nm} are the normalized

Stokes coefficients with error-estimates σ^2_{nm} . Degree-variances and error-degree-variances are sums of the C_{nm} squared, σ^2_{nm} respectively, for a fixed degree, n, multiplied with $(GM/a)^2$.

As pointed out by Arabelos (1980) we can not simply put to zero the first N terms. Here a solution was found, i.e. that the first terms were not put to zero, but put equal to the so-called error-degree variances, $\sigma^2_{E,l}$ contingently scaled by a factor α so as to reflect if the model was better (α≤1) or worse (α≥1) in an area.

To get a little more insight into this, let us interpret the point mass potential as a reproducing kernel in a Hilbert space, where the functions are harmonic down to a Bjerhammar-sphere with radius R_B inside the Earth and $r_Q < R_B$. Using a Kelvin transformation we obtain a point D outside the sphere

$$\frac{R_B^2}{r_P r_D} = \frac{r_Q}{r_P} \qquad (7)$$

So that $L=\sqrt{1 - 2\frac{R_B^2}{r_P r_D}\cos(\psi) + \left(\frac{R_B^2}{r_P r_D}\right)^2}$. Then $K(P,D)= \frac{\frac{R_B^2}{r_P r_D}}{L}$ is the so-called Krarup kernel, Krarup (1969). When interpreted as a covariance function, it has unitless degree-variances equal to 1, i.e. it is not well suited to represent the anomalous potential, since the degree-variances of T tends to zero like $n^{-3} * q$, $q < 1$, see Tscherning and Rapp (1974). So instead of point mass base functions one should consider using potentials of other types of masses, like a bar, see Hauck and Lelgemann (1985, Fig. 2) or excentric multipoles (Marchenko et al., 2001).

There are other inherent problems using mass-type base functions. Which depth should be used for the masses. Should they form a grid ? (Vermeer (1990)). This has been studied extensively by e.g. Barthelmes and Kautzleben (1983) and Barthelmes (1985). We will not discuss this here, but show tables of reduced point mass functions.

4. Excentric multipoles – covariance functions.

The covariance functions generally used in least-squares collocation may be interpreted as excentric multipoles using the Kelvin transformation. For two points outside the Earth, P and D, we have typically (Tscherning and Rapp, (1974)) for the covariance of the anomalous potential,

$$cov(r_P, r_Q, \psi) = \sum_{i=2}^{\infty} \frac{A}{(i-1)(i-2)(i+4)} \left(\frac{R_B^2}{r_Q r_P}\right)^{i+1} P_i(\cos\psi) \qquad (8)$$

which is the linear combination of 3 excentric multipoles:

$$F_k(r_P, r_Q, \psi) = \sum_{i=2}^{\infty} \frac{A_k}{(i-k)} \left(\frac{r_Q}{r_P}\right)^{i+1} P_i(\cos\psi) \qquad (9)$$

Each of these may be represented by a closed expression. The first terms corresponding to the maximal degree of the global model used, should be substituted by the (scaled potential) error-degree-variances.

$$cov_N(r_P, r_Q, \psi) = \sum_{i=2}^{N} a\sigma_i^e \left(\frac{R_B^2}{r_Q r_P}\right)^{i+1} P_i(\cos\psi) \qquad (10)$$

5. Reduced point mass and excentric multipole base functions - examples.

The interesting functions are those which represent the geoid (height anomaly) and the first and second derivative with respect to r_P. All quantities are *anomalous* quantities with respect to EGM96 complete to degree N=24. We consider geoid and gravity disturbance at height zero and the second order radial derivative at 250 km altitude. For the latter we will put the mass-point at depth 242.5 km, corresponding to data (r_P) at 250 km. The Bjerhammar sphere will be put at 1.46 km depth.

In the first example (Table 1) we use as observation **one** (anomalous) radial gravity gradient observation equal to 0.15 Eötvöes, at height 250 km (M=1 in eq. (3)). The latitude and the longitude are set to zero for the mass-point, but the latitude for the point P increases in steps from zero. Table 2 shows the same function, now with the quantities evaluated at zero altitude.

In Table 3 we have corresponding values obtained using the covariance function eq. (8), (10) and again with the same gravity gradient observation as used in Table 1 and 2.

We have here calculated values with spherical distance 1.0 degree and so that the value for the second order radial derivative is 0.15 Eötvös.

Table 1. Closed and Reduced Point mass functions at altitude 250 km. Note the location of the first zero-crossing. For the reduced function all terms up to degree 24 have been set equal to zero.

ψ	Closed expression	Reduced to deg. 24.	Closed	Reduced	Closed	Reduced
	Geoid (m)		Gravity disturbance (mgal)		2. order radial deriv. (Eötvös)	
0.0	0.85	0.29	-2.41	-1.79	0.150	0.150
1.0	0.80	0.24	-2.03	-1.37	0.106	0.100
2.0	0.70	0.14	-1.34	-0.62	0.043	0.028
3.0	0.59	0.05	-0.81	-0.09	0.012	-0.005
4.0	0.49	-0.02	-0.49	0.16	0.002	-0.014
5.0	0.42	-0.05	-0.31	0.24	-0.001	0.013
6.0	0.37	-0.05	-0.21	0.23	-0.002	-0.010
7.0	0.32	-0.05	-0.14	0.17	-0.002	-0.007
8.0	0.29	-0.03	-0.11	0.10	-0.001	-0.003
9.0	0.26	-0.01	-0.10	0.01	-0.001	0.000
10.0	0.23	0.00	-0.06	-0.02	0.000	0.002

Table 2. Closed and Reduced Point mass functions at zero altitude. Note the location of the first zero-crossing and the values for zero spherical distance. The location is for the geoid at 3^0. This corresponds (approximately) to the location of the first zero-point for the first Legendre polynomium in the series eq. (8). (Legendre polynomials have as many zero points as the degree in the interval from -90^0 to 90^0 distributed approximately equidistantly, see Heiskanen and Moritz, 1967, Fig. 1-8).

ψ	Closed expression	Reduced to deg. 24.	Closed	Reduced	Closed	Reduced
	Geoid (m)		Gravity disturbance (mgal)		2. order radial deriv. (Eötvös)	
0.0	3.56	3.13	-49.2	-55.3	13.9	16.1
1.0	1.93	1.24	-7.87	-7.26	-0.11	-0.18
2.0	1.09	0.31	-1.48	0.04	-0.14	-0.21
3.0	0.75	0.02	-0.51	0.98	-0.053	-0.10

Table 3. Values computed using a degree-variance model (eq.(8)) with depth to the Bjerhammar-sphere equal to 1.56 km. Error.degree-variances from EGM96 used to degree 24, scaled with $\alpha = 1.03$. Computed using Least-Squares-Collocation with only one observation (completely equivalent to using eq. (3)).

ψ	Second order radial derivative. Altitude= 250 km. Eöetvöes units.	Geoid. Zero altitude. Units m.	Gravity anomaly. Zero altitude. Units mgal.
0.0	0.15	2.11	13.11
1.0	0.13	1.80	10.36
2.0	0.08	1.23	5.33
3.0	0.03	0.46	1.40
4.0	-0.03	-0.04	-0.87
5.0	-0.03	-0.32	-1.86
6.0	-0.03	-0.43	-2.01
7.0	-0.02	-0.41	-1.66
8.0	-0.02	-0.30	-1.08

Again we see the location of the first zero-crossing, which makes the function well suited for representing data where the contribution from EGM96 to degree 24 has been subtracted.

A FORTRAN program redpmass.f for doing these or similar calculations is available as http://cct.gfy.ku.dk/redpmass.f , 2010.05.20.

4. **Conclusion**.

Closed or reduced point mass or multipole functions may be used to represent the anomalous potential. When used regionally referring to a global gravity field model, the first terms must be removed or substituted by error-degree-variances.

For point-mass or multipole functions the terms up to the lowest degree of the reference potential (the global model) have here been put equal to zero. However,

it might be possible to find (unitless) terms representing the power in the frequencies which the global model have not removed, corresponding to error-degree variances.

If covariance functions (corresponding to multipole base functions) are used, error degree-variances (scaled) may be used. This assures that the model in an appropriate manner weights the regional frequencies with respect to the global model used.

References:

Arabelos, D.: Untersuchungen zur gravimetrischen Geoidbestimmung, dargestellt am Testgebiet Griechenland. Wiss. Arb. d. Fachrichtung Vermessungswesen d. Universitaet Hannover, Hannover 1980.

Ballani, L., J.Engel and E.Grafarend: Global base functions for the mass density in the interior of a massive body (Earth), Manuscripta Geodaetica, Vol. 18, no. 2, pp. 99-114, 1993.

Balmino, G.: La Representation du Potentielle par Masses Ponctuelles. Bulletin Geodesique, No. 3, 1974.

Barthelmes,F.: Untersuchungen zur Approximation des aeusseren Gravitationsfeldes der Erde durch Punktmassen mit optimierten Positionen. Veroeff. Zentralinstituts fuer Physik der Erde, Nr. 92,Potsdam, DDR, 1986.

Barthelmes,F. and H. Kautzleben: A New Method of Modelling the Gravity Field of the Earth by Point Masses. Proc. of the IAG Symposia, Vol.1, pp 442-448, Dep. of Geodetic Science and Surveying, The Ohio State University, 1983.

Hauck, H. and D.Lelgemann: Regional gravity field approximation with buried masses using least-norm collocation. Manuscripta Geodaetica, Vol. 10, no. 1, pp. 50-58, 1985.

Heiskanen, W.A. and H. Moritz: Physical Geodesy. W.H. Freeman & Co, San Francisco, 1967.

Krarup, T.: A Contribution to the Mathematical Foundation of Physical Geodesy. Meddelelse no. 44, Geodætisk Institut, København 1969.

Lemoine, F.G., S.C. Kenyon, J.K. Factor, R.G. Trimmer, N.K. Pavlis, D.S. Chinn, C.M. Cox, S.M. Klosko, S.B. Luthcke, M.H. Torrence, Y.M. Wang, R.G. Williamson, E.C. Pavlis, R.H. Rapp, and T.R. Olson, The Development of the Joint NASA GSFC and the National Imagery and Mapping Agency (NIMA) Geopotential Model EGM96, NASA/TP-1998-206861, Goddard Space Flight Center, Greenbelt, MD, July, 1998.

Marchenko, A.N., F.Barthelmes, U.Meyer and P.Schwintzer: Regional geoid determination: An application to airborne gravity data in the Skagerrak. STR01/07, GFZ Potsdam, 2001.

Tscherning, C.C. and R.H.Rapp: Closed Covariance Expressions for Gravity Anomalies, Geoid Undulations, and Deflections of the VerticalImplied by Anomaly Degree-Variance Models. Reports of the Department of Geodetic Science No. 208, The Ohio State University, Columbus, Ohio, 1974.

Tscherning, C.C.: Representation of Covariance Functions Related to the Anomalous Potential of the Earth using Reproducing Kernels. The Danish Geodetic Institute Internal Report No. 3, 1972.

Vermeer, M.: The use of mass point models for describing the Finnish gravity field. Proceedings, 9th Meeting Nordic Geodetic Commission, Sept. 1982, Gaevle, Sweden 1982.

Vermeer, M.: Modelling of gravity gradient tensor observations using buried shells of mass quadrupoles. In: Lecture Notes for Nordiska Forskarkurser 18/1988 "Modern Techniques in Geodesy and Surveying", Ebeltoft, Denmark, Sept. 1988, pp. 461-478. National Survey and Cadastre of Denmark, Publications 4. Series Vol. 1, Copenhagen 1989.

Vermeer, M.: Work on satellite gravity gradiometry using a burried masses grid representation. Study on Precise Gravity Field Determination Methods and mission requirements (Phase 2), FinalReport, Part 510B, pp. 1-18, ESA contract 8153/88/F/FL, 1990

Vermeer,M.: FGI Studies on Satellite Gravity Gradiometry. 1.Experiments with a 5-degree buried masses representation. Report 89:3, Finnish Geodetic Institute, Helsinki, 1989.

Vermeer, M.: Geoid determination with mass point frequency domain inversion in the Mediterranean. Mare Nostrum 2, GEOMED report, Madrid, pp. 109-119, 1992.

Vermeer, M.: Optimal combination of satellite gravity gradiometry and satellite tracking by GPS: Simulations using frequency domain mass points inversion software. 19 pp. In: Study of the gravity field determination using gradiometry and GPS, Phase 1, Final report ESA Contract 9877/92/F/FL, April 1993.

Wu, X.: Point-mass model of local gravity field. Acta Geod. et Cartog. Vol.13, 1984.

FULL RESOLUTION GEOID FROM GOCE GRADIENTS FOR OCEAN MODELING

Matija Herceg and Per Knudsen

Technical University of Denmark, National Space Institute, Juliane Maries vej 30, 2100 Copenhagen, Denmark,
Email: mher@space.dtu.dk; pk@space.dtu.dk

ABSTRACT

The main objective of the study is to improve the methodology for combining GOCE gravity field models with satellite altimetry to derive optimal dynamic ocean topography models for oceanography. Since dynamic ocean topography determination is the difference between the sea surface and the geoid, the definition of both surfaces is of great significance. Here a method for geoid determination, using simulated GOCE gradients and point mass method, is used for the regional determination of the gravity field that is not recovered by the planned global GOCE gravity model of spherical harmonic coefficients up to degree and order 200. Comparisons with the GOCINA mean dynamic topography show that the GOCE gradients enhance the determination of the mean dynamic topography at wavelength not recovered by the planned global GOCE gravity field model.

Key words: Point mass; Geoid; GOCE gravity gradients; Satellite altimetry; Ocean modelling.

1. INTRODUCTION

Combining GOCE geoid models with satellite altimetric observations of the sea surface height, might lead to substantial improvements in the modelling of the ocean transport and circulation. The primary requirement for oceanographers is to have access to an accurate geoid and its error covariance at the highest spatial resolution and accuracy possible.

In this paper a test area in GOCINA region (see Fig. 1) is chosen for the calculation of the geoid. GOCINA (Knudsen et al. [6]) is a multi-disciplinary project for developing generic tools for simultaneous analysis of sea surface height and geoid related observations to enhance ocean analysis using Earth observation data from the European Space Agency missions ENVISAT and GOCE. This project will examine the mass and heat exchange across the Greenland-Scotland Ridge as well as the current running along the continental shelf from the Bay of Biscay to the northern Norwegian Sea. The project supported the GOCE mission with a set of specific recommendations for integrating GOCE in ocean circulation studies and an accurate geoids model for validation purposes.

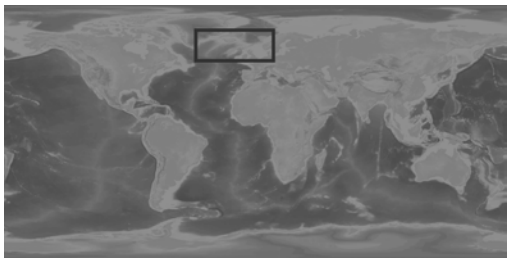

Figure 1. The GOCINA region

Geoid determination by means of the point mass can be used as an alternative method to the conventional methods for geoid determination, and the space-wise approach to GOCE data analysis can rely on at least two different independent solutions - numerical integration and least-square collocation, and they can be used to cross check the results (Migliaccio et al. [10]). Since no real GOCE data are available at this time, simulated gradient data are used taken from deliverables of GOCINA project.

Mission scenarios of GOCE have been simulated to provide a unique easily accessible data set for various comparisons. The second phase of work package 5 of GOCINA project involves the interaction of GOCINA with GOCE; producing gradients covering the GOCINA area at satellite height for validation purposes. Real shipborne and airborne gravimetry was compared with synthetic but theoretically rigorous gravity anomalies derived from satellite altimetry and oceanography. This combination of different disciplines has resulted in gravity coverage over the GOCINA region of the Atlantic that is complete and has an accuracy of locally representative free air anomalies that has hitherto not been matched on adjacent land. In this process a set of gravity gradient tensor values for comparison with future GOCE measurements has been also computed. They are evaluated at satellite altitude over the northern Atlantic Ocean between Europe and Greenland from about 53N to 72N.

2. POINT MASS METHOD

There are different implementations of the point mass methodology for geoid determination, and they are already described in many publications (Vermeer [14]). The method used in this study calculates dipole masses distributed over two Cartesian grids, one at the 10 km and the another at the 70 km bellow the reference ellipsoid. Then, from such dipole masses, the geoid is calculated.

In point mass method, the Earth anomalous gravity field, T, at point Q is modeled by the set of base functions, each obtained as the anomalous gravity potential from each point mass m_i located at the position P_i on the surface of the ellipsoid with radius R_M which is smaller than the Earth mean radius R_E. Radius R_M is 10km smaller than the mean radius of the GRS80 ellipsoid for one grid, and 60km smaller for the second grid of the dipole point masses.

$$T(Q) = \sum_i T_i(Q) \tag{1}$$

where

$$T_i(Q) = Gm_i \frac{1}{|P_i - Q|} = Gm_i \frac{1}{\sqrt{s_i^2 + z_i^2}} \tag{2}$$

where s is the horizontal distance and z is the height difference between the points. In this case Cartesian coordinates are used for simplicity.

Now, any quantity associated with the gravity field may be obtained by applying a linear functional on T, i.e.

$$y(Q) = L(T(Q)). \tag{3}$$

For geoid heights the relation is simply obtained using Bruns formula:

$$N(Q) = \frac{T(Q)}{\gamma} \tag{4}$$

where γ is the normal gravity.

The vertical component of the gradients are then computed as the second order derivative of the gravity potential along z direction, i.e.

$$\frac{\partial^2}{\partial z^2} T_i(Q) = -Gm_i \frac{1}{(s_i^2 + z_i^2)^{\frac{3}{2}}} + 3Gm_i \frac{z_i^2}{(s_i^2 + z_i^2)^{\frac{5}{2}}} \tag{5}$$

Using the least squares method and formula for second order derivatives of gravitational potential, where masses

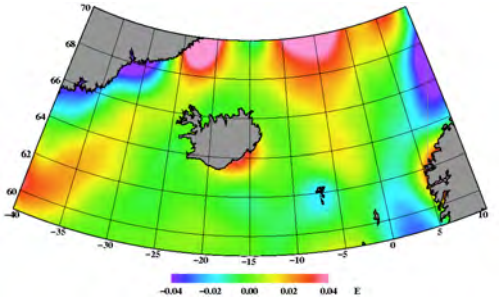

Figure 2. Vertical gradients relative to the EGM96 model to harmonic degree 200

are unknowns, grids of point masses on the two different level below the ellipsoid were created. The solution for the same two point mass grids were then used for geoid determination.

From the GOCINA gradients the EGM96 model up to degree of 200 (Lemoine et al. [9]) was subtracted to form gradients residuals. Because of the difference between the reference (EGM96 up to degree of 200) and actual gravity, centrifugal potential is not considered (Heiskanen & Moritz [3]). The produced gradients residuals may then be used for calculation of geoid residual, which can be used to enhance the gravity field as well as the mean dynamic topography. Subsequently, in this analysis the solutions are compared with the geoid and the mean dynamic topography from GOCINA project.

3. RESULTS

Formulas shown in the previous section are implemented in Matlab. As a first step, the vertical components of the GOCINA gradients were interpolated on the Cartesian grid at the mean satellite altitude using bilinear interpolation (Forsberg & Tscherning [2]). To produce residual gradient grid, the reference EGM96 gradients up to degree 200 were subtracted. A maximum harmonic degree of 200 was chosen to simulate use of a GOCE gravity harmonic expansion model. All calculations were made only on the GOCINA region.

Gridded residual vertical gradients at satellite altitude (258 km) can be seen on Fig. 2. The statistics are shown in Tab. 1. At GOCE flight altitude the magnitude of the vertical gradients relative to a spherical harmonic expansion to degree 200 is reduced substantially to about 0.025 E$\ddot{o}$tv$\ddot{o}$s (E). The dominant positive values are found in the northern part of the region as well as south of Greenland. Negative values are seen outside the coasts of Norway and Greenland respectively.

From those second order derivatives the buried point masses at the depth of R_1 = 10 km and R_1 = 70 km below

Table 1. Statistics of the vertical gradients relative to the EGM96 model to harmonic degree 200 (E)

Min	Max	Mean	Std
-0.05	0.04	0.000	0.025

Table 2. Statistics of the differences between input gradients and gradients calculated from the point masses using back solution (E)

Min	Max	Mean	Std
-0.01	0.01	0.000	0.001

the ellipsoid respectively, were calculated using a least squares inversion method. At both depths point masses are located at regular grids having spacing of 0.25 degrees and 0.5 degrees in latitude and longitude respectively. Those grid spacings were chosen to model the gravity field associated with harmonic degrees between 200 and 400 where the main improvements are expected to occur. Then gradients were calculated back using the estimated point masses and compared to the initial (input) gradients. The statistics of the residuals can be seen in the Tab. 2. Both the mean and the standard deviation are very close to zero. Hence, the observations are well modeled using the point masses as they are implemented in this test.

From the buried point mass grids the geoid heights were computed, but changing the formulas using equations 4. The calculated geoid is shown in Fig. 3. The statistics are shown in Tab. 3. Compared with the Fig. 2 the geoid heights show the same general pattern as the gradients. However, the geoid heights show more short wavelengths features than the gradients. The standard deviation of the geoid heights is 21 cm.

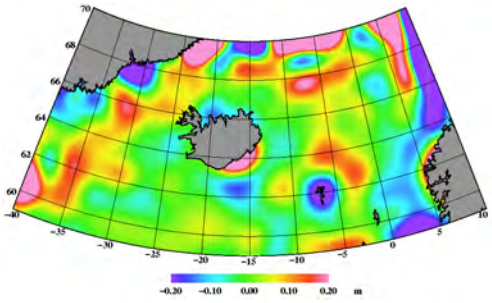

Figure 3. Residual geoid calculated using point mass method

The geoid solution was compared to the GOCINA geoid. EGM96 reference geoid up to degree 200 was subtracted from this geoid to form another residual geoid for evaluation of the geoid modeled using point mass method. GOCINA residual geoid was filtered using Gaussian filtering with a width of 1 degree to filter out short wavelength features of the geoid that may not be recovered from gradients at 258 km altitude. Filtered geoid can be seen on Fig. 4. The standard deviation of the filtered GOCINA geoid relative to the EGM96 model is 38 cm (Tab. 4). Compared to the result of the point mass solution, both geoid models show similar features with relatively high values southeast of Greenland as well as in the northern part of the region. However, the magnitude of the geoid based on the point mass solution is smaller and it appears to be smoother.

Table 3. Statistics of the residual geoid calculated using point mass method (m)

Min	Max	Mean	Std
-1.52	1.26	0.00	0.21

Table 4. Statistics of the filtered GOCINA geoid relative to EGM96 to harmonic degree 200 (m)

Min	Max	Mean	Std
-2.46	2.13	0.00	0.38

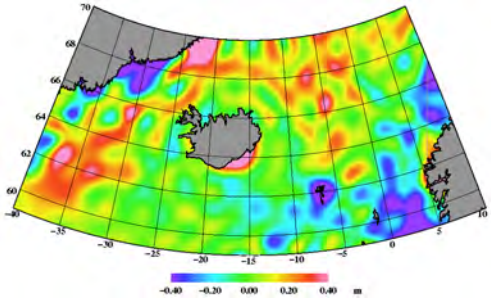

Figure 4. Filtered GOCINA geoid relative to the EGM96 up to harmonic degree 200

Fig. 5 shows the difference between the geoid based on the point masses and the GOCINA geoid described above. The statistics of the differences are shown in Tab. 4. The standard deviation of the differences is 19 cm. Hence, the magnitude of the unknown part of the simulated geoid is reduced from 38 cm to 19 cm. The short wavelength features are still present in the differences, but the main positive values southeast of Greenland and in the norther part of the region have been reduced. Also the negative values in the southeastern part of the region have been reduced. Hence, this preliminary test of the point mass method demonstrates its ability to recover parts of the gravity field that are not recovered by a spherical harmonic expansion truncated at harmonic degree and order 200.

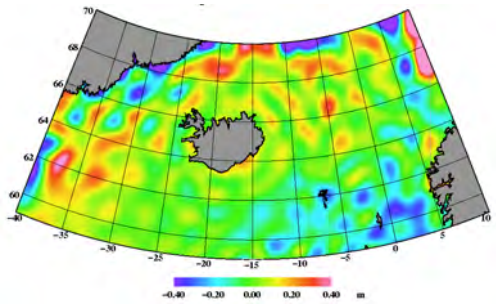

Figure 5. Difference between the two residual geoid solutions

Table 5. Statistics of the difference between two geoid residual solutions and two full geoid solutions (m)

	Min	Max	Mean	Std
Geoid residual difference	-0.84	0.89	0.00	0.19
Full geoid difference	-2.13	1.95	0.00	0.32

4. MEAN DYNAMIC TOPOGRAPHY

The other objective of this analysis is to study how well the geoid enhancement improves the estimation of the mean dynamic topography (MDT). The important thing is that point mass method, using just simulated GOCE gradient data (with subtracted reference field), may provide an enhanced solution for geoid determination (see Tab. 2 and 4). Also for this analysis the results of the GOCINA project is used. With the presence of the high quality gravity data in GOCINA region together with the high resolution geoid, it is clear that a very good representation of the mean dynamic topography can be achieved. The GOCINA mean dynamic topography was derived using a mean sea surface derived from satellite altimetry in combination with shipborne and airborne gravity data. It is shown in Fig. 6. The pattern of the geostrophic ocean surface circulation is reflected on the mean dynamic topography.

Comparisons are made using the GOCINA MDT and an MDT derived by differencing the mean sea surface and the two geoid models. In the first comparison an MDT is obtained using the mean sea surface minus the EGM96 geoid model up to harmonic degree 200. This MDT was filtered in a similar manner as the GOCINA geoid residuals as described above. The differences between the two MDTs are shown in Fig. 7 and the statistics are shows in Tab. 6. As expected, the differences are similar to the differences between the GOCINA geoid relative to EGM96 shown in Fig. 4. High values are found southeast of Greenland and in the northern part of the region.

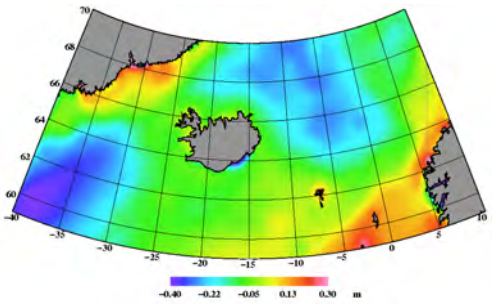

Figure 6. GOCINA mean dynamic topography

Table 6. Statistics of the differences between GOCINA MDT and MDT based on the EGM96 up to degree 200 (m)

Min	Max	Mean	Std
-1.84	0.83	0.02	0.21

Negative values are found in the southeastern part of the region. The standard deviation of the differences is 21 cm.

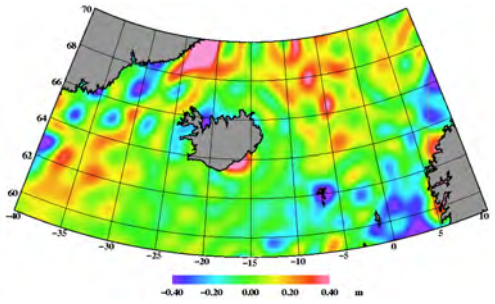

Figure 7. Differences between GOCINA MDT and MDT based on the EGM96 up to degree 200

Then the MDT obtained from the mean sea surface and the EGM96 geoid model was corrected using the point mass geoid solution. Subsequently, the comparison with the GOCINA MDT was repeated. The differences between the GOCINA MDT and the corrected MDT are shown in Fig. 8 and the statistics are shows in Tab. 7. Again the differences are similar to the differences between the GOCINA geoid relative to enhanced geoid shown in Fig. 5. In this case, the standard deviation of the differences is 18 cm. Hence, the magnitude of the unknown part of the simulated MDT reduces from 21 cm to 18 cm. The short wavelength features are present in the differences, but the main positive values southeast of

Table 7. Statistics of the differences between GOCINA MDT and MDT based on the geoid enhanced using point mass solution (m)

Min	Max	Mean	Std
-1.48	0.97	0.01	0.18

Greenland and in the norther part of the region have been reduced. Also the negative values in the southeastern part of the region have been reduced.

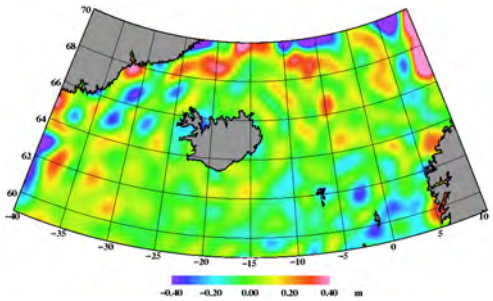

Figure 8. Differences between GOCINA MDT and MDT based on the geoid enhanced using point mass solution

5. DISCUSSION

In this study simulated GOCE gradients and the point mass method are used for the regional determination of the parts of the gravity field that are not recovered by the planned global GOCE gravity model of spherical harmonic coefficients up to degree and order 200. The study is carried out utilizing the geoid and MDT models derived in the GOCINA project. The point mass method is rather basic, but well suited for carrying out regional modelling tasks. The preliminary results show that parts of the gravity field associated with harmonic degrees larger than degree 200 may be recovered using this method. Hence, the gravity gradients contain more valuable signal than will be recovered in the planned harmonic expansion up to degree 200, so this method led to improvements in the estimation of the geoid. The enhanced geoid serve as a reference surface for satellite altimetry and provide improvements in the mean dynamic topography which in turn may be used to improve the modelling of the ocean circulation. Further studies on how to structure the point masses as dipoles within the earth to optimize the estimation are needed. Also, the error propagation should be studied rigorously, so that the contribution from the other components of the GOCE gradients can be studied properly.

REFERENCES

[1] Antunes, C., Pail, R.,Catalo, J., Point mass method applied to the regional gravimetric determination of the geoid, Stud. geophys. geod, 47, 495-509 (2003)

[2] Forsberg, R., Tscherning C.C., GRAVSOFT Geodetic Gravity Field Modelling Programs (overview manual), Danish National space center, 2008

[3] Heiskanen, W.A., Moritz, H., Physical geodesy, W. H. Freeman, San Francisco, 1967

[4] Knudsen, P., and the GOCINA Team: Integration of Altimetry and GOCE Geoid For Ocean Modelling: Results From The GOCINA Project. Proc. 3rd International GOCE User Workshop, Frascati, Italy, ESA Publications SP-627, ISBN 92-9092-938-3, 2007.

[5] Knudsen, P., Forsberg, R., Andersen, O., Solheim D., Hipkin R., Haines K., Johannessen J., Hernandez F., The GOCINA project - An overview and status, European Space Agency, Issue.569, 2004

[6] Knudsen, P., O. B. Andersen, R. Forsberg, H.P. Fh, A.V. Olesen, A.L. Vest, D. Solheim, O.D. Omang, R. Hipkin, A. Hunegnaw, K. Haines, R. Bingham, J.-P. Drecourt, J.A. Johannessen, H. Drange, F. Siegismund, F. Hernandez, G. Larnicol, M.-H. Rio, and P. Schaeffer: GOCINA Geoid and Ocean Circulation in the North Atlantic Final Report. Danish National Space Center, Technical Report, No. 5, 2006.

[7] Knudsen, P., O. B. Andersen, R. Forsberg, H.P. Fh, A.V. Olesen, A.L. Vest, D. Solheim, O.D. Omang, R. Hipkin, A. Hunegnaw, K. Haines, R. Bingham, J.-P. Drecourt, J.A. Johannessen, H. Drange, F. Siegismund, F. Hernandez, G. Larnicol, M.-H. Rio, and P. Schaeffer: Combining altimetric/gravimetric and ocean model mean dynamic topography models in the GOCINA region. IAG symposia, Vol. 130, Springer Verlag, ISBN-10 3-540-49349-5, 3-10, 2007.

[8] Knudsen, P., Tscherning, C.C., Error Characteristics of Dynamic Topography Models Derived from Altimetry and GOCE Gravimetry, Proceeding of the Dynamic Planet 2005, IAG Symposia Series, Springer Verlag

[9] Lemoine, F. G., S. C. Kenyon, J. K. Factor, R.G. Trimmer, N. K. Pavlis, D. S. Chinn, C. M. Cox, S. M. Klosko, S. B. Luthcke, M. H. Torrence, Y. M. Wang, R. G. Williamson, E. C. Pavlis, R. H. Rapp and T. R. Olson, The Development of the Joint NASA GSFC and NIMA Geopotential Model EGM96, NASA Goddard Space Flight Center, Greenbelt, Maryland, 20771 USA, July 1998.

[10] Migliaccio, F., M. Reguzzoni, F. Sanso and C.C.Tscherning: Collocation versus numerical integration in GOCE data analysis. Poster presented IUGG/IAG General Assembly, Symposium G03, Sapporo, July 2003, and paper prepared for JoG.

[11] Lehmann, R., The method of free-positioned point masses - on the Gulf of Bothnia, Ceo-Forschungs-Zentrum Potsdam, Telegrafenberg A 17, O-1561 Potsdam, FRG, 1993.

[12] Sanso, F. and Tscherning, C.C,: Fast Spherical Collocation - Theory and Examples. J. of Geodesy, Vol. 77, pp. 101-112, DOI 10.1007/s00190-002-0310-5, 2003.

[13] Telford, W.M., Geldart L.P., Sheriff R.E., Keys D.A., Applied geophisics, Cambridge University Press, 1985

[14] Vermeer, M., Mass point geopotential modelling using fast spectral techniques, Manuscr. Geod., Vol. 20, No. 5, p. 362 - 378, 1995

[15] Vermeer, M., Regularization Constraints in Mass Point Grids and their Relation to Gravity Field Stochastics, Finnish Geodetic Institute, Geodeetinrinne 2, FIN-02430 Masala, Finland, 1998

[16] http://gocinascience.spacecenter.dk/

BIBLIOGRAPHY

[1] O. B. Andersen. The DTU10 Global Gravity field and Mean Sea Surface - improvements in the Arctic. 2011.

[2] O. B. Andersen and P. Knudsen. DNSC08 mean sea surface and mean dynamic topography models. *Jounal of Geophysical research, VOL. 114*, 2009.

[3] Samuels Beckett. Worstward ho, 1983.

[4] J. Bouman. Quality assessment of satellite-based global gravity field models. *Netherlands Geodetic Commission, Delft*, 2000.

[5] J. Bouman, R. Koop, C. C. Tscherning, and P. Visser. Calibration of GOCE SGG data using high-low SST, terrestrial gravity data and global gravity field models. *Journal of Geodesy*, 2004.

[6] R. Bringhurst. *The Elements of Typographic Style*. Version 2.5. Hartley & Marks, Publishers, Point Roberts, WA, USA, 2002.

[7] S.L. Bruinsma, J.C. Marty, G. Balmino, R. Biancale, C. Boerste, O. Abrikosov, and Neumayer H. GOCE Gravity Field Recovery by Means of the Direct Numerical Method. *Presented at the ESA Living Planet Symposium, 27th June - 2nd July, 2010, Bergen, Norway*, 2010.

[8] S. Chanfang, L. Fei, and H. Weifeng. Geoid, Quasigeoid Fitting Based on Equivalent Point Masses. *Geomatics and Information Science of Wuhan University*, 2011.

[9] O. Colombo. Numerical Methods for Harmonic Analysis on the Sphere. 1981.

[10] M. R. Drinkwater, R. Haagmans, D. Muzi, A. Popescu, R. Floberghagen, M. Kern, and M. Fehringer. The GOCE gravity mission: ESA's first core Earth explorer. *Proceedings of 3rd International GOCE User Workshop, 6-8 November, 2006, Frascati, Italy, ESA SP-627, 2007*, 2007.

[11] ESA. GOCE newsletter, issue 2.1. Technical report, ESA, 2011.

[12] ESA. *XML Parser*, 2011.

[13] R. Floberghagen, D. Muzi, F. De la Feld, Weymiens B., R. Rummel, T. Gruber, and R. Van Hees. GOCE High Level Processing Facility: GOCE Level 2 Product Data Handbook. 2010.

[14] R. Forsberg. A Study of Terrain Reductions, Density Anomalies and Geophysical Inversion Methods in Gravity Field Modelling. 1984.

[15] R. Forsberg, A. V. Olesen, H. Yildiz, and C. C. Tscherning. Polar Gravity Fields from GOCE and airborne gravity. *Proceedings of the GOCE User Workshop, Munich*, 2011.

[16] C. C. Goad, C. C. Tscherning, and M. M. Chin. Gravity empirical covariance values for the Continental United States. *Journal of Geophysics Research*, Vol. 89, No. B9:7962–7968, 1984.

[17] H. Hauck and D. Lelgemann. Regional gravity field approximation with buried masses using least-norm collocation. *Manuscripta Geodaetica*, Vol. 10, no. 1:pp. 50–58, 1985.

[18] W.A. Heiskanen and H. Moritz. *Physical Geodesy*. W.H. Freeman, San Francisco, 1967.

[19] M. Herceg, M. Reguzzoni, and F. Sansó. Approximate global modeling of the gravity potential from observations with non uniform noise. Presented at: IUGG 2011 General Assembly, Earth on the Edge: Science for a Sustainable Planet, 28 June - 7 July 2011. Melbourne, Australia, 2011.

[20] K.H. Ilk. Regularization for high resolution gravity field recovery by future satellite techniques. *Akademie Verlag, Berlin*, pages 189–214, 1993.

[21] W.M. Kaula. *Theory of Satellite Geodesy: Applications of Satellites to Geodesy*. Dover Publications, Mineola, New York, USA, 1966.

[22] P. Knudsen. Estimation and modelling of the local empirical covariance function using gravity and satellite altimeter data. *Bulletin Geodesique*, vol. 61:pp. 145–160, 1987.

[23] P. Knudsen. GOCINA: Geoid and Ocean Circulation in the North Atlantic. Technical report, 2005.

[24] P. Knudsen, O. B. Andersen, R. Forsberg, A. V. Olesen, A. L. Vest, H. P. FÃ¶h, D. Solheim, O. D. Omang, R. Hipkin, A. Hunegnaw, K. Haines, R. Bingham, J.-P. Drecourt, J. A. Johannessen, H. Drange, F. Siegismund, F. Hernandez, G. Larnicol, M.-H. Rio, and P. Schaeffer. Geoid and Ocean Circulation in the North Atlantic. Technical report no. 5, Danish National Space Center, 2006.

[25] P. Knudsen, R. Bingham, O. B. Andersen, and M.-H. Rio. A global mean dynamic topography and ocean circulation estimation using a preliminary GOCE gravity model. *Springer-Verlag 2011*, 2011.

[26] R. Koop. *Global gravity modelling using satellite gravity gradiometry*. Publications on Geodesy 38, Delft, 1993.

[27] T. Krarup. *Mathematical foundation of geodesy*. 1969.

[28] F. Lerch, H. Iz, and J. Chan. Gravity model solution based upon SLR data using eigenvalue analysis: Alternative methodology. *D. Smith and D. Turcotte (Eds.), Contributions of Space Geodesy and Geodynamics - Earth Dynamics. Geodynamics Series, American Geophysical Union*, 24:213–219, 1993.

[29] M. Lonkhuyzen, R. Klees, and J. Bouman. Regularization for the gravity field recovery from GOCE observations. *Proc IAG Int Symp Gravity, Geoid Geodynamics, Banff*, 2001.

[30] A.N. Marchenko, F Barthelmes, U. Meyer, and P. Schwintzer. Regional geoid determination: An application to airborne gravity data in the Skagerrak. *GFZ Potsdam*, 2001.

[31] N. Maximenko, P. Niiler, M. H. Rio, O. Melnichenko, L. Centurioni, D. Chambers, V. Zlotnicki, and B. Galperin. Mean dynamic topography of the ocean derived from satellite and drifting buoy data using three different techniques. *J. Atmos. Oceanic Tech.*, 26(9):1910–1919, 2009.

[32] F. Migliaccio, M. Reguzzoni, F. Sansó, C.C. Tscherning, and M. Veicherts. GOCE data analysis: the space-wise approach and the first space-wise gravity field model. *Proceedings of the ESA Living Planet Symposium, 28 Jun 2 Jul 2010, Bergen, Norway, ESA Publications Division, Nordwijk, The Netherlands, SP-686.*, 2010.

[33] H. Moritz. *Advanced physical geodesy*. Karlsruhe, Wichmann, 1980.

[34] R. Pail, H. Goiginger, R. Mayrhofer, W.-D. Schuh, J. M. Brockmann, I. Krasbutter, E. Höck, and T. Fecher. GOCE gravity field model derived from orbit and gradiometry data applying the time-wise method. *Proceedings - ESA Living Planet Symposium, Bergen, Norway, 28 June - 2 July (ESA SP-686)*, 2010.

[35] R. Pail, S. Bruinsma, F. Migliaccio, C. Foerste, H. Goiginger, W.-D Schuh, E. Höck, M. Reguzzoni, J. M. Brockmann, O. Abrikosov, M. Veicherts, T. Fecher, R. Mayrhofer, I. Krasbutter, F. Sanso, and C. C. Tscherning. First GOCE gravity field models derived by three different approaches. *Jounal of Geodesy, in review*, 2011.

[36] N.K. Pavlis, S.A. Holmes, S.C. Kenyon, and J.K. Factor. An Earth Gravitational Model to Degree 2160: EGM2008. *Presented at the 2008 General Assembly of the European Geosciences Union, Vienna, Austria, April 13-18, 2008.*, 2008.

[37] G. B. Reed. Application of kinematical geodesy for determining the short wave length components of the gravity field by satellite gradiometry. 1973.

[38] M. H. Rio. *GUT tutorial: GOCE User Toolbox (GUT) Implementation and Supporting Scientific Studies*. ESA, 2009.

[39] R. Rummel. Satellite gradiometry, Lecture notes in Earth Sciences, Vol 7, 1986.

[40] R. Rummel and O. L. Colombo. Gravity field determination from Satellite gradiometry. *JOURNAL OF GEODESY*, Volume 59, Number 3:233–246, 1985.

[41] R. Rummel, K. Schwarz, and M. Gerstl. Least squares collocation and regularization. *Journal of Geodesy*, 53:343–361, 1979. ISSN 0949-7714. URL http://dx.doi.org/10.1007/BF02522276. 10.1007/BF02522276.

[42] F. Sansó and C. C. Tscherning. Fast spherical collocation: theory and examples. *Journal of Geodesy*, 77, 2003.

[43] A.N. Tikhonov. Regularization of incorrectly posed problems. *Sov Math Dokl 4*, pages 1035–1038, 1963.

[44] A.N. Tikhonov and V.Y. Arsenin. *Solutions of Ill-posed problems*. Wiley, New York, 1977.

[45] W. Torge. *Geodesy*. Walter de Gruyter, 2001.

[46] C. C. Tscherning. Covariance Expressions for Second and Lower Order Derivatives of the Anomalous Potential. *Reports of the Department of Geodetic Science No. 225, The Ohio State University, Columbus, Ohio*, 1976.

[47] C. C. Tscherning. Program GEOCOL. *University of Copenhagen, Denmark*, 2005.

[48] C. C. Tscherning and D. Arabelos. Gravity anomaly and gradient recovery from GOCE gradient data using LSC and comparisons with known ground data. *Proceedings 4th International GOCE user workshop, ESA Publications Division, Nordwijk, The Netherlands*, 2011.

[49] C. C. Tscherning and R. H. Rapp. Closed Covariance Expressions for Gravity Anomalies, Geoid Undulations, and Deflections of the Vertical Implied by Anomaly Degree-Variance Models. *Reports of the Department of Geodetic Science No. 208, The Ohio State University, Columbus, Ohio*, 1974.

[50] C. C. Tscherning and M. Veicherts. GOCE External Calibration: Calibration of GOCE gradiometer data in the MBW using ground data. *Journal of Geodesy 78, i; Springer, Berlin*, 2006.

[51] C. C. Tscherning and M. Veicherts. Optimization of Gradient Prediction. 2007.

[52] M. Vermeer. The use of mass point models for describing the Finnish gravity field. *Proceedings, 9th Meeting Nordic Geodetic Commission, Gaevle, Sweden*, 1982.

[53] M. Vermeer. FGI Studies on Satellite Gravity Gradiometry. 1.Experiments with a 5-degree buried masses representation. *Report 89:3, Finnish Geodetic Institute, Helsinki*, 1989.

[54] M. Vermeer. Work on satellite gravity gradiometry using a burried masses grid representation. Study on Precise Gravity Field Determination Methods and mission requirements (Phase 2). *Final Report, Part 510B*, pages pp. 1–18, 1990.

[55] M. Vermeer. Geoid determination with mass point frequency domain inversion in the Mediterranean. *Mare Nostrum 2, GEOMED report, Madrid*, pages pp. 109–119, 1992.

[56] M. Vermeer. Optimal combination of satellite gravity gradiometry and satellite tracking by GPS: Simulations using frequency domain mass points inversion software. *Study of the gravity field determination using gradiometry and GPS, Phase 1, Final report*, 1993.

[57] M. Vermeer. Mass point geopotential modelling using fast spectral techniques. *Manuscr. Geod.*, Vol. 20, No. 5:p. 362 – 378, 1995.

[58] P. N. A. M. Visser. GOCE gradiometer: estimation of biases and scale factors of all six individual accelerometers by precise orbit determination. *Jounal of Geodesy*, 2008.

[59] X. Wu. Point-mass model of local gravity field. *Acta Geod. et Cartog.*, Vol.13, 1984.

[60] P.L. Xu. Determination of Surface Gravity Anomalies using Gradiometric Observables. *Geophys. J. Int.*, 110:321–332, 1992.

[61] H. Yildiz. A study of regional gravity field recovery from GOCE vertical gravity gradient data in the Auvergne test area using collocation. *Studia Geophysica et Geodetica*, 2011.

[62] R.C.A. Zandbergen. *Satellite Altimeter Data Processing, From Theory To Practice*. PhD thesis, Delft University Press, 1990.

COLOPHON

This thesis was typeset with LaTeX 2ε using Hermann Zapf's *Palatino* and *Euler* type faces (Type 1 PostScript fonts *URW Palladio L* and *FPL* were used). The listings are typeset in *Bera Mono*, originally developed by Bitstream, Inc. as "Bitstream Vera". (Type 1 PostScript fonts were made available by Malte Rosenau and Ulrich Dirr.)

The typographic style was inspired by Bringhurst's genius as presented in *The Elements of Typographic Style* [6]. It is available for LaTeX via CTAN as "`classicthesis`".

Final Version as of February 1, 2012 at 15:20.

DECLARATION

I hereby declare that this submission is my own work and that, to the best of my knowledge and belief, it contains no material previously published or written by another person nor material which to a substantial extent has been accepted for the award of any other degree or diploma of the university or other institute of higher learning, except where due acknowledgment has been made in the text.

Copenhagen, January 31, 2012

Matija Herceg